

**PHASE-MIXING SELF-INJECTION INTO
PLASMA-WAKEFIELD ACCELERATION STRUCTURES
DRIVEN IN A RISING DENSITY GRADIENT**

by

Aakash Ajit Sahai

Department of Physics,
Indiana University, Bloomington,
Indiana 47405, USA



Thesis submitted to the faculty of the University Graduate School
in partial fulfillment of the requirements for the degree

of

Master of Sciences
in the Department of Physics,
Indiana University, Bloomington,
Indiana 47405, USA

Indiana University

July 2015

Accepted by the Graduate Faculty, Indiana University,
in partial fulfillment of the requirements for the degree of Master of Sciences.

Master's Thesis Committee

Date: _____

Prof. S. Y. Lee, Supervisor

Prof. John Carini

Prof. William Michael Snow

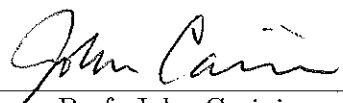
Accepted and Approved by the Graduate Faculty, Indiana University,
in partial fulfillment of the requirements for the degree of Master of Sciences.

Master's Thesis Committee

Date: 06/30/2015



Prof. S. Y. Lee, Supervisor



Prof. John Carini



Prof. William Michael Snow

Copyright © 2015 by **Aakash Ajit Sahai**

Anyone is free to copy, modify and reuse all the material presented here upon citing this
thesis.

PHASE-MIXING SELF-INJECTION INTO PLASMA-WAKEFIELD ACCELERATION STRUCTURES DRIVEN IN A RISING DENSITY GRADIENT

by

Aakash Ajit Sahai

Department of Physics,
Indiana University, Bloomington,
Indiana 47405, USA

We model the phase-mixing self-injection of electrons into plasma-wakefield acceleration structures driven in a longitudinally rising density gradient. Self-injection is a process where some of the plasma electrons lose coherence with the wave due to non-linearities. The non-linearity is inherently and intentionally induced in the plasma oscillations due to the variation of the restoring force along the rising density gradient. These electrons then get trapped and propagate with the accelerating phase of the plasma-wave. The electron oscillations driven by matched energy-sources are shown to get trapped in the wakefields similar in scaling to the phase-mixing of free oscillations. The onset of trapping is shown to scale with the gradient of rising density and the amplitude of oscillations. The planar longitudinal electron oscillations undergo trajectory crossing above a threshold amplitude or in a density inhomogeneity leading to phase-mixing and trapping of the oscillating electrons to a phase of the wave. In this thesis, we analyze the scaling of the phase-mixing based trapping of electron oscillations, independent of a threshold, in planar geometry driven by an electron beam in a rising density gradient. The cylindrical and spherical geometry electron oscillations undergo phase-mixing irrespective of the amplitude of oscillations. Here, driven radial electron oscillations in cylindrical geometry are shown to undergo phase-mixing leading to trapping of the plasma electrons in a longitudinally rising density gradient. We also present preliminary scaling results of phase-mixing based trapping of radially oscillating electrons in a rising density gradient.

Dedicated to the immeasurable support and sacrifices of



ahika
sha
jit
nkita &
nkur

Acknowledgements

I am indebted to my family for providing their constant support and encouragement for my endeavors. The spirit of learning has been instilled in me due to the enthusiasm, energy and respect with which scholarship and knowledge have been revered by the generations of my family.

I would like to acknowledge and take this opportunity to immensely thank all the help and support from Susan A. Winchester, Irina Y. Novitski of Fermi National Accelerator Laboratory, the United States Particle Accelerator School (USPAS) and Prof. William A. Barletta, the director of the USPAS. I would also like to extend my utmost gratitude to Prof. S. Y. Lee of the Department of Physics, Indiana University for his encouragement and so seamlessly running the program for a USPAS-affiliated degree. Also, I immensely thank all the instructors at various USPAS classes for stoking my interest in different particle accelerator technologies. I am really fortunate to have met so many interesting and talented classmates through my various courses and acknowledge their friendship.

It is the strong and deeply ingrained foundation of my family and friends in pursuit of knowledge that has always inspired me to strive for exploring science and technology unboundedly in my professional life while also keeping me firmly grounded in my personal life.

I am grateful to professor Thomas Katsouleas at Duke university who despite his full-time job as the dean of the engineering school provided guidance and funding for research.

I also acknowledge that it is because of his understanding of my interest in mastering conventional beam and accelerator physics that I was able to attend and teach at various USPAS courses.

Early in my doctoral career, my knowledge in this field of research got a boost due to the USPAS plasma acceleration theory course taught in January 2011 by Dr. Eric Esarey and Dr. Carl Schroeder, of the Lawrence Berkeley National Laboratory. Eric Esarey's enthusiasm and long experience of plasma acceleration theory was quite inspiring at that stage. I am yet to find an equivalent of this course which is refreshed every time I reference the now widely cited 2009 Reviews of Modern Physics paper[7] which was the main textbook for the course. I thank both Eric and Carl for letting me be a teaching assistant for this course in January 2013 at the Duke University session.

Finally, it is my humble duty to thank the welcoming and open-minded public and government of the United States of America for funding the basic sciences programs such as accelerator science and USPAS that helps several scientists and engineers like me to freely think about the abstract principles of nature. I am also grateful to the people of India for subsidizing my undergraduate education and hope that someday I will be able to payoff their investment in my career.

Preface

Plasma electron oscillations [1] which are the characteristic response of a collision-less [2] plasma were first detected based upon their energy modulating interactions with charged particle streams. These oscillations were later formalized into a theory of electron density waves with arbitrary relativistic phase velocities [3]. It was also formalized that such electron oscillations or density waves could grow to non-linear density perturbations and limiting electric field amplitudes [4]. A major breakthrough came when charged particle acceleration was proposed using the large electric fields and high phase velocities of plasma electron density waves. It was proposed to excite these waves in the wakefield of matched intense energy sources such as an ultra-short laser pulse [5] or a bunch of charged particles [6] propagating in a homogeneous plasma.

In this work, we study the scaling laws of the phase-mixing [4] based self-injection of plasma electrons into the plasma-wakefield acceleration structures [5][6] excited in a longitudinally rising plasma density gradient. Rising plasma density gradients, in the direction of propagation of the driving energy sources, which is also the direction of the plasma electron-wave wave-vector, are ubiquitous at the vacuum-plasma interfaces for confining the plasma particles within the plasma container walls.

The plasma-wakefields are high phase-velocity ($\beta_\phi \simeq 1$) driven electron density waves [3]. These waves are driven in the trail of appropriately shaped energy sources ($\beta_{es} \simeq 1 \approx \beta_\phi$) propagating in plasma of appropriate density, n_0 [6]. The driven plasma-oscillations are quite similar to the freely oscillating plasma electrons [1][2]. In a cold homogeneous plasma, the e^- undergoing oscillatory motion (β_e) to support the plasma waves may get

trapped in their potential-well due to the non-linearity [4] of the electron trajectories.

The non-linearities could be introduced by the driver intensity and shape, wave amplitude rising above a critical value or simply the geometry of electron oscillations. It is well known that cylindrical and spherical geometry oscillations always develop non-linearities independent of the wave amplitude. Phase-mixing of the plasma electrons results in trajectories that are nearly stationary in the wave frame, $\beta_e - \beta_\phi \simeq 0$. Under this condition, in the wave-frame, if these electrons do not have enough relative kinetic energy to escape the wave potential-well, they are trapped. If the electrons are trapped at the right phase of the wave, they co-propagate and also gain energy for an extended length.

In a rising density gradient ($d\omega_{pe}(x)/dx > 0$), intentional phase-mixing is introduced by the oscillation amplitude varying at different points along the density gradient. Therefore, phase-mixing between e^- trajectories always occurs. When phase-mixing results in accumulation of sufficient phase-difference between the individual oscillators, the electron trajectories are affected by the fields of adjacent oscillators, to an extent that they get trapped. We computationally verify the scaling laws of phase-mixing in 1-D driven oscillations. In the 1-D phase-mixing model, the mixing time depends both upon the gradient of the rising plasma density and the amplitude of the wake-potential.

However, 2D cylindrical plasma oscillations have plasma electrons executing cylindrical oscillations along the radial dimension. Thus, our analytical 1-D model of planar purely longitudinal oscillations is inadequate. We show that even in radial oscillations in a cylindrical geometry, phase-mixing is introduced due to a longitudinal density gradient. The phase-mixing of these radial oscillations also results in trapping of plasma electrons. In spite of the limitation of our theoretical model for 2D cylindrical geometry oscillations, we computationally find that the 1D scaling laws are still approximately valid.

The trapping of plasma- e^- in an up-ramp is critical for many applications such as controlling the trapped e^- energy-spectra, trapping electrons in sub-threshold plasma wake-fields, higher particle flux for high brightness radiation sources, understanding the energy dissipation from the excited plasmon train [16] etc.

Contents

Acknowledgements	3
Preface	5
List of Figures	9
1 Introduction	1
1.0.1 Conventional RF acceleration and its limitations	2
1.0.2 Lawson-Woodward theorem - Direct-Laser and Ponderomotive Acceleration	3
1.0.3 Plasma acceleration	5
1.0.4 Exciting plasma acceleration structures	8
1.1 Wave-breaking - self-steepening and trapping	9
1.2 Plasma model - Linearized Kinetic theory	12
1.3 Plasma excitation by energy sources	17
1.4 Acceleration structures in the plasma	24
1.5 Plasma-electron momentum equations - Fluid model	25
1.6 Plasma Instabilities driven by Laser	29
1.7 Particle-In-Cell simulations: short introduction	34
1.8 Linear vs. Non-linear plasma-waves	36
1.8.1 Linear plasma electron waves	37
1.8.2 Non-linear plasma electron waves	39

2 Phase-mixing, Trajectory-crossing and Trapping of Plasma Electrons	44
2.1 Non-linear plasma electron oscillations	45
2.1.1 Non-linear 1D plasma oscillations - Amplitude dependent	45
2.1.2 Non-linear Cylindrical and Spherical plasma oscillations	48
2.1.3 Inhomogeneous plasma - Planar oscillations	53
2.2 Warm-plasma - wave-breaking	56
2.3 Wave-breaking - multi-dimensional wake	57
2.4 Trapping condition - multi-dimensional wake	64
2.5 Phase-mixing of non-linear plasmons	65
3 1-D Planar geometry Sheet Oscillations in a Rising Density Gradient	68
3.1 Scaling of phase-mixing in 1D beam-driven planar wake	68
3.2 Phase-mixing scaling with drive-beam density, n_b/n_0	72
3.3 Phase-mixing scaling with rising gradient scale-length, L_Δ	76
4 2-D Cylindrical Geometry Radial Oscillations in a Rising Density Gradient	80
4.1 Trapping of electrons in 2D cylindrical geometry in a rising density gradient	81
4.2 2D scaling laws - trapping in cylindrical geometry oscillations	86
5 Conclusions & Future-work Directions	88
A Chirp Pulse Amplified Ultra-short Lasers	90
Bibliography	95
Biography	98

List of Figures

1.1	Competing laser plasma coupling processes	30
1.2	<i>Classification of plasma physics codes</i>	35
1.3	<i>PIC code computation loop - time-advance the simulations</i>	36
1.4	<i>Laser driven “linear” electron wake in 2D cartesian space using particle trapping simulations</i>	37
1.5	<i>Electron beam driven “linear” electron wake in 2D cylindrical space using particle tracking simulations</i>	40
1.6	<i>Laser driven “non-linear” electron wake in 2D cartesian space using particle-tracking simulations</i>	41
1.7	<i>Electron beam driven “non-linear” electron wake in 2D cylindrical space using particle-tracking simulations</i>	43
2.1	<i>Spatial profile of 1D electric field (normalized) vs. displacement amplitude, A [4]</i>	46
2.2	<i>Phase mixing of coupled oscillators with spatially increasing frequencies</i>	54
3.1	<i>1D planar - beam driven oscillations - phase-mixing scaling with the drive beam-density</i>	73
3.2	<i>Continued - 1D planar - beam driven oscillations - phase-mixing scaling with the drive beam-density</i>	74
3.3	<i>phase-mixing time scaling with the drive beam-density - 1D beam driven oscillations</i>	75
3.4	<i>1D planar - beam driven oscillations - phase-mixing scaling with rising density gradient scale-length</i>	77
3.5	<i>Continued - 1D planar - beam driven oscillations - phase-mixing scaling with the rising density gradient scale-length</i>	78

3.6	<i>phase-mixing time scaling with the density gradient scale-length - 1D beam driven oscillations</i>	79
4.1	<i>Rising plasma density gradient - line-out from simulations</i>	81
4.2	<i>Longitudinal momentum (p_{\parallel}) of trapped plasma e^- in 2-D wakefield PIC simulations</i>	82
4.3	<i>Time evolution of plasma e^- longitudinal momentum (p_{1x_1})</i>	83
4.4	<i>On-axis longitudinal electric field ($e1$) for the (a)laser and (b)beam excited plasma</i>	84
4.5	<i>Self-injected trapped plasma e^- in plasmon-buckets in real-space from 2-D PIC simulations</i>	85
4.6	<i>Scaling of onset of trapping in radial oscillations with density gradient scale-length - modeled using 2-D PIC simulations - comparison of the longitudinal momentum phase-space</i>	87
A.1	Schematic of Chirp Pulse Amplified laser - from Chirp Pulse Amplification - Wikipedia page	93
A.2	evolution of accessible physics regimes and applications with laser intensities, right hand side axis points to the electron quiver momentum imparted to electrons interacting with the fields [23]	94

Chapter 1

Introduction

Particle acceleration techniques require sustained interaction of electromagnetic fields with charged particles. The phase of the interacting electric field has to be “right” in the sense that the field-particle interaction force results in a continuous transfer of the electromagnetic field energy to the particle kinetic energy. Using this physical model we see that larger the force on the particles faster is the gain of kinetic energy by the particles. Higher magnitude forces require high power sources of electric, magnetic or electromagnetic energy. Technologically, static electric or static magnetic fields are hard to engineer thus electromagnetic fields sources are used. Another important aspect of charged particle acceleration is confining and maintaining the single-species plasma in the form of the charged particle beam. This requires transverse confinement over the entire length of particle acceleration. Thus transverse fields that focus the beam are also essential for particle acceleration.

The dominant modes of electromagnetic waves in free-space have electric and magnetic fields that are transverse to the direction of propagation of the wave. Hence, free-space electromagnetic wave cannot directly accelerate particles in the same direction as they propagate. The transverse modes are dominant in the sense that most of the power of the electromagnetic fields is distributed in these modes. Particle acceleration in directions transverse to the direction of propagation of electromagnetic fields does not allow sustained interaction of the right phase of electric field with the charged particles. This is because the fields change phase rapidly over the interaction length. Thus the net energy gain of the particles is small or zero in direct interaction of a free-space electromagnetic wave with

a particle. Note that in an idealized plane wave the net energy gain is zero and this is the so called *Lawson-Woodward theorem* [7].

However, when an electromagnetic wave interacts with boundaries which affect its electric fields the fraction of power in the free-space purely transverse modes is re-distributed. The boundaries enforce the electromagnetic waves to reconfigure to modes with significant longitudinal electric fields. Thus boundaries beyond which the fields cannot propagate freely are required to confine the electromagnetic fields and transfer power to modes which are useful for particle acceleration. This spatial confinement enables the transverse modes to couple to longitudinal modes due to the geometry of the confined space.

1.0.1 Conventional RF acceleration and its limitations

The reconfiguring of the spatial modes of an electro-magnetic wave is primarily the principle of Radio-frequency (RF) fields based charged particle acceleration used in almost all the particle accelerators worldwide. Mostly cylindrical metallic cavities are used to confine high power electromagnetic fields to create spatial modes in the cavity that have significant longitudinal electric field. When the charged particles pass through the cavities the right-phase of the electric fields can be made to interact continuously with the charged particles resulting in energy transfer to the charged particles.

Higher the power of the electromagnetic field confined in the cavities higher is the longitudinal electric field. Additionally, electromagnetic waves of higher frequencies have lower wavelength and thus allow the spatial confinement dimension to be smaller. So, confinement of electromagnetic fields with higher and higher frequencies requires smaller sized cavities. With simple extension of the chain of argument above one can imagine that higher and higher frequency electromagnetic fields with higher and higher power can allow to miniaturize the cavities while also increasing the accelerating field. Thus smaller and smaller accelerators can be built. Generally smaller also means lesser material costs thus driving the overall costs lower as the accelerators get smaller.

So, why do higher particle energies need building a larger particle accelerator ? Simple

answer to this is that mother nature imposes restrictions on confinement of electromagnetic waves.

The two major problems with the approach of using cavities of materials available in nature comes from - (a) confinement of high power and (b) confinement of high-frequency electromagnetic fields. As the power density or the power per unit area incident on the metallic walls used for confining the electromagnetic fields increases the electric fields can become high enough to ionize the material. Once the walls are ionized they can undergo an avalanche mechanism and be broken down completely and incapable of confining the fields. Secondly as the frequency of the electromagnetic fields increases their wavelengths get to the dimensions which can resonate with quantum-mechanical state of the material resulting in material undergoing ionization for much lower power of the electromagnetic fields. In the extreme cases for instances extreme ultra-violet frequencies the waves simply cannot be constrained or reflected by the metallic materials.

This is the reason that the peak accelerating longitudinal electric fields in standing-wave and traveling-wave RF cavity based accelerators are of the order of $E_{acc} = 100\text{MV/m}$. So, to accelerate an electron beam to 1GeV would need about 10 meters of cavities to interact with the beam.

1.0.2 *Lawson-Woodward theorem - Direct-Laser and Ponderomotive Acceleration*

As described in the App.[A](#), in relativistically high intensity laser systems, the electric fields can impart relativistic momentum to the electron. However, the nature of the momentum is oscillatory and electrons quiver around without gaining significant longitudinal momentum. So, the question naturally arises *is it possible to accelerate electrons in vacuum using laser electric fields?*. The answer to this lies in the *Lawson-Woodward (LW) theorem*.

The LW theorem states that *no net energy gain* is possible directly from the laser electric field in vacuum under the following assumptions:

1. the laser fields are in vacuum with no walls or boundaries present
2. the electron is highly relativistic ($v_e \simeq c$) along the acceleration path

3. no static electric or magnetic fields are present
4. the region of interaction is infinite
5. ponderomotive effects (nonlinear forces, e.g., the $\vec{v} \times \vec{B}$ force) are neglected

One or more of the assumptions of LW theorem must be violated in order to achieve a nonzero net energy gain by using laser fields in vacuum.

When trying to accelerate electrons by direct action of a laser field in vacuum and gases, the process is intrinsically limited by diffraction, electron slippage, ionization, and the smallness of the laser wavelength. In vacuum, the motion of an electron in a laser field is determined by the Lorentz force equation: $\frac{d\tilde{\vec{p}}}{dct} = \vec{E} + \vec{v} \times \vec{B} = \frac{\partial \vec{a}}{\partial ct} - \frac{\tilde{\vec{p}}}{\tilde{\gamma}} \times \vec{\nabla} \times \vec{a}$, where $\tilde{\vec{p}}$ is the electron momentum normalized to $m_e c$ and $\tilde{\gamma} = \sqrt{1 + \tilde{\vec{p}} \cdot \tilde{\vec{p}}}$ is the relativistic Lorentz factor.

1. Direct energy gain in laser field - linear response of the electron to the electric field E of the laser.
2. Ponderomotive laser acceleration - nonlinear response to the $v \times B$ force.

For any laser system there is always a finite laser focus spot size and this points towards the existence of an axial component of the electric field of the laser because $\vec{\nabla} \cdot \vec{E} = 0 \Rightarrow \frac{\partial}{\partial z} E_z = -\nabla_{\perp} \cdot E_{\perp} \simeq \frac{1}{kr_0} E_{\perp}$.

Therefore, this axial field can be very large, which suggests that this axial field could directly impart a net energy gain for a relativistic electron ($\tilde{\gamma} \gg 1$) co-propagating with laser pulse along the axis, with the energy gain scaling as $\int dz v_z E_z$. However, the phase velocity, of the optical field along the axis (z) is greater than c and is $\frac{v_{ph} h}{c} \simeq \left(1 + \frac{1}{kZ_R}\right)$ near the focus (since, the vacuum dispersion relation of the laser is $\frac{\omega^2}{c^2} = \left(k_z + \frac{2k_z}{Z_R}\right)$). And, if we have relativistic electrons co-propagating with the laser pulse then, $v_{ph} > c$, electrons with $v_z = c$ will phase slip with respect to the accelerating (laser axial) field and decelerate. This will occur over a dephasing length (z_{slip} over which phase slips by π), which for highly

relativistic electrons is $\pi Z_R (k_z z_{\text{slip}} | \frac{v_z}{c} - \frac{v_{ph}}{c} | = \pi \Rightarrow z_{\text{slip}} \simeq \pi Z_R)$, therefore, the dephasing length is of the order of diffraction length. Hence, interaction over an infinite length would cause the net acceleration to cancel out net deceleration. So, the interaction length has to be limited (region of length $2Z_R$ about the focus, violating LW), but this is practically hard to implement, due to the ionizing characteristic of high-intensity lasers.

Non-linear effect that can be associated with the high-intensity lasers is the action of nonlinear or ponderomotive forces associated with the laser-electron interaction. This effect (arising due to $\vec{v} \times \vec{B}$ force) can potentially violate the LW theorem to impart a net energy gain. Considering the equation with non-linear effects, $\frac{d\tilde{\vec{p}}}{dct}(\vec{v} \times \vec{B}) = -\frac{\tilde{\vec{p}}}{\gamma} \times \vec{\nabla} \times \vec{a} = -\vec{\nabla} \left(\frac{\tilde{\vec{p}}}{\gamma} \cdot \vec{a} \right) + \frac{\tilde{\vec{p}}}{\gamma} \left(\vec{\nabla} \cdot \vec{a} \right)^{\text{gauge}}$. The non-linear term is, $F_{pz} \simeq -\frac{m_e c^2}{\gamma} \nabla_z \left(\frac{a^2}{2} \right)$, is responsible for changes in the electron energy due to “ponderomotive” force. These ponderomotive forces can provide substantial energy gains even in the limit of an infinite interaction region. A major drawback to ponderomotive force acceleration scheme (including the Inverse Free Electron Laser acceleration) is that the force reduces as particles accelerate, $F_{pz} \propto \frac{1}{\gamma}$.

1.0.3 Plasma acceleration

Plasma acceleration is based on the fields excited in the plasma by appropriately shaped energy sources for charged particle acceleration. Plasma is a *quasi-neutral* fluid of freely moving charged particles that undergo collective oscillations [1]. There are at least two species of charged fluids - electrons and ions. When the energy sources couple to the plasma they excite density modulations of the particles in the plasma. The density modulations are different due to the difference in inertia of species. The difference in the density modulations results in charge separation between the electrons and the ions. The spatial charge-separation excites electric fields in the direction in which it is excited. As it will be shown below the charge-separation fields in the plasma are proportional to the square-root of the particle density, n_0 which is the number of particles per unit volume. The electric field can be as high as $E_{acc} = 96.2\sqrt{n_0(\text{cm}^{-3})}$ V/m which gives $E_{acc}(n_0 = 10^{18}\text{cm}^{-3}) =$

96.2GV/m. If a beam of charged particles is placed in the “right” phase of these charge-separation fields, continuous transfer of energy to the beam is possible. In comparison to RF fields, electron beam can be accelerated to 1GeV in a distance in the plasma of the order of a centimeter (10^{-2} m). Note that this acceleration length is 3 orders of magnitude smaller than the RF case.

Several questions may arise regarding the effect of the background plasma on the accelerated particles - (i) would the accelerated particle not scatter off the nuclei of the background ions by mechanisms such as *Coulomb scattering, bremsstrahlung, hadronic and nuclear interactions etc.* ? (ii) would the particles not lose energy by the radiation mechanisms such as *Cherenkov radiation, high-energy photons by $e^+ - e^-$ pair production, etc.* ? Since the plasma fields can rapidly accelerate the particles, the particles attain high energy in a short distance. Interaction cross-sections for scattering are inversely proportional to the square of the particle energy, $\sigma_{cs} \propto \mathcal{E}_{beam}^{-2}$. Thus, the scattering processes are only relevant in cases where the particle beam interacting with the plasma is low energy. On the other end, such processes become important when the beam density of a high energy beam exceeds some threshold. Such a situation may arise when the beam undergoes adiabatic damping at very high energies. Secondly, the radiation losses due to the interaction with the plasma are small because the radiation length are many orders of magnitude larger than the acceleration length.

The processes occurring in the plasma can be distinctly classified into two based upon their characteristic time-scales - *collision-less* [2] and *collisional*. It can be shown that the collisional mean-free path in a fully-ionized plasma is many orders of magnitude larger than the characteristic response distance of the plasma, the Debye wavelength. And, therefore the electron-ion collision frequency is many orders of magnitude smaller than the collective oscillation frequency. In a weakly-ionized plasma the collisions are dominated by the electron-neutral collisions and the dynamics can be different. In all the following analysis we consider only fully-ionized plasmas. This is a reasonable assumption because in plasma acceleration techniques often the intensity of the energy-sources used is high

enough to result in gas ionization by various processes like barrier-suppression, above the threshold, multi-photon ionization etc. Therefore the collision-less processes occur over time-scales that are much smaller than the mean-time between the probability of successive electron-ion collisions.

The large difference between the mass of electrons and ions results in separate characteristic time-scales of their collective motion. Hence, when the plasma is excited by energy coupling from the energy sources to the plasma, the first collective response is by the plasma electrons. The energy sources propagating in the plasma leave behind a wakefield in their trail. Due to the shorter time-scales of the electron plasma waves these are known and shown to be the dominant phenomenon in the wakefield [5]. A plasma electron density wave is characterized by its frequency [1],

$$\omega_{pe} = \sqrt{\frac{4\pi n_0 e^2}{m_e}} = 2\pi 8978.7 \sqrt{n_e(\text{cm}^{-3})} \text{ Hz} \quad (1.1)$$

(in cgs units) and its amplitude $\delta n(\vec{r}, t) = n(\vec{r}, t) - n_0$ where n_0 is the density of plasma at equilibrium, n is the perturbed electron density and δn is the net excessive electron charge at a point \vec{r} in space at a time, t .

Note that all the equations and theoretical formulation in the rest of the thesis is in c.g.s. (centimeter-gram-second) units as this is the system in which plasma physics is traditionally studied.

Another important point to note is that the plasma we considered is cold. The equilibrium Maxwell-Boltzmann velocity distribution of the electrons is completely randomized in space (6-D phase-space is reduced to 3-D velocity space) and the velocity distribution of

the thermalized electrons is, $f(v_e^{th}) = \mathcal{C} 4\pi (v_e^{th})^2 e^{-\frac{m(v_e^{th})^2}{2k_B T_e}}$ where $\mathcal{C} = \left(\frac{m}{2\pi k_B T_e}\right)^{3/2}$. The Boltzmann energy distribution in 3-D velocity space is $f_v(v_x, v_y, v_z) = \mathcal{C} \exp\left[-m\frac{v_x^2 + v_y^2 + v_z^2}{2k_B T_e}\right]$

where $\mathcal{C} = \left(\frac{m}{2\pi k_B T_e}\right)^{3/2}$. The velocity distribution is obtained by normalizing over the ve-

locity. The energy distribution function is normalized by multiplying with the surface area of the velocity sphere, $4\pi(v_e^{th})^2$. For the purpose of studying the motion of the plasma electrons in collective phenomenon like electron plasma waves we assume that the initial thermal velocities are negligible in comparison to the velocities excited as part of supporting the waves, $v_e^{th} \ll c\beta_e$.

1.0.4 Exciting plasma acceleration structures

The energy sources such as a bunch of photons or charged particles can propagate in the plasma at relativistic velocities. The relativistically propagating energy sources excite plasma waves with relativistic phase-velocities in their trail. It is well-known that relativistic phase-velocity electron plasma waves [3] are supported in the plasma. It is essential to control the phase velocity of the plasma waves because the distance over which the accelerating phase of wave electric fields interacts with the accelerated bunch decides the extension of acceleration length. If the accelerated bunch quickly outruns the accelerating phase of the plasma wave then the net average electric field over the interaction length may be negligible.

The electron plasma waves support large charge separation electric fields which are many times the RF fields of the conventional accelerators. So, the electric fields of the plasma waves can be used for accelerating charged particles. However, an acceleration mechanism must be capable of letting the acceleration structure and the accelerated beam interact over extended distances to constitute as a useful acceleration technique. The use of high phase-velocity plasma electron waves to accelerate electrons (e^-) [5] was first proposed in 1979 using a laser pulse. The coupling mechanism from the laser to the plasma-wave or a plasmon is the instability of interaction of the laser pulse with the plasma electrons referred to as the *Raman forward scattering*. The instability originates in the mixing between the electron momentum in the laser field and its momentum in the plasma wave. Such mixing leads to exchange of energy from the laser pulse to the longitudinal plasma density oscillations.

The proposal of the laser wakefield based plasma electron waves [5] realized and important aspect regarding the phase velocities of these wave. The phase-velocity of the electron plasma wave is shown to be nearly equal to the group velocity of the laser pulse. Thereby the phase velocity of the wake-wave could be controlled by controlling the laser pulse group velocity.

It was similarly shown that intense relativistic electron beams could be used to excite e^- plasma-waves used for acceleration [6]. The particle beams propagating in a plasma would interact with the plasma through their space-charge fields. In the beam-frame the electrostatic fields of the bunch would drive the plasma electrons away from the equilibrium. The energy coupling mechanism in this case is the *two-stream instability*. This instability is excited in the plasma due to the fact that the beam velocity can resonate with the phase velocity of the electron plasma wave and result in energy exchange.

The fields that are excited in the plasma electron wave are dependent upon its density. Following a back of the envelope approach to analyze the electrons oscillating in a plasma electron wave we use the Lorentz equation, $\frac{d\vec{p}_e^\parallel}{dt} = m_e c \frac{d\gamma_e \vec{\beta}_e^\parallel}{dt} = -e \vec{E}^\parallel$ in 1-D and assume a linear, $\gamma_e \simeq 1$ and non-relativistic, $\gamma_\phi = (1 - \beta_\phi^2)^{-1/2} \simeq 1$ plasma-wave with purely sinusoidal electron velocity, $\beta^\parallel = \max(\beta_e^\parallel) \cos(\omega_{pe} t)$. Under these assumptions $-m_e c \omega_{pe} \max(\beta_e^\parallel) \sin(\omega_{pe} t) = -e E^\parallel$. Then the amplitude of the field is

$$|E_{max}^\parallel| = \frac{m_e c \omega_{pe}}{e} \max(\beta_e^\parallel).$$

1.1 Wave-breaking - self-steepening and trapping

The wave is sustained only until the electron velocity is smaller than the phase velocity of the wave, $\max(\beta_e^\parallel) < \beta_\phi$.

As the particle velocity in the particle-density wave approaches the wave phase-velocity. The velocity of the particles gets higher as the potential of the wave get higher. In the wave-frame, the particles at small relative velocities interact with the wave-potential and

gain energy. The charged particles can be at a phase of the field or potential of the wave which accelerates them in the direction of the wave propagation. Since the density-wave has a direction of its phase-velocity, the particles with relative velocity in the same direction as the wave velocity get accelerated. Whereas, the particles with relative velocity in opposite direction get decelerated. As it can be seen from this qualitative picture, the particles start bunching close the accelerating phase of the wave. This process is referred to as wave-steepening or self-steepening. In later sections we observe this phenomenon in simulations.

Trajectory crossing is related to the ordering of the oscillating 1-D electron sheets and maintaining linearity of the trajectories that are driven as part of supporting the wave [4]. The electron density wave would break when $\max(\beta_e^{\parallel}) \geq \beta_{\phi}$ and this condition is referred to as *wave-breaking limit*. Thus, when $\max(\beta_e^{\parallel}) = \beta_{\phi}$ the maximum electric field sustainable by an electron density wave is $|E_{max}^{\parallel}| = \frac{m_e c \omega_{pe}}{e} \simeq 96 \sqrt{n_0 (\text{cm}^{-3})} \text{ V/m}$, n_0 is the plasma density in cm^{-3} . Technologically, for plasmas with densities of the order of 10^{18} cm^{-3} the fields are $E_{\parallel}^{max} \simeq 96.2 \text{ GV/m}$ [7].

Interestingly the electron bunch to be accelerated by the plasma structures could be generated by trapping plasma electrons and thereby external injector and tedious synchronizations mechanisms could be averted. In fact the initial experiments dealt with two major challenges - (i) driving a large amplitude plasma wave [7] (ii) controlling the unwanted trapping of plasma electrons. The unwanted trapping in earlier experiments lead to large energy spreads as the electrons were trapped in all the phases of the accelerating field and over the acceleration length gained a wide range of energies [10]. Experimental confirmation of the acceleration of electron beams as visualized in the original theoretical proposals with accelerating and focussing fields of the order of 10 GV/m were subsequently demonstrated for a laser-pulse driver in 2004 [9] and an electron-beam driver in 2014 [11]. These experiments showed the potential of plasma acceleration to excite and sustain fields predicted by theory. Secondly, they opened pathways towards the possibility of improv-

ing beam quality especially the energy-spread and emittance. Controlling the trapping of plasma electrons within the plasma acceleration structures is the topic of this thesis.

Plasma acceleration structures are excited by coherent motion of the plasma e^- driven in response to energy packets in the plasma. The plasma electrons oscillate within the potential well of the background ions, with time scales of oscillations at the plasma electron frequency, $\frac{2\pi}{\omega_{pe}}$. The excited oscillations are strong in amplitude only if the energy packet exciting the motion has spatial frequencies of the order of plasma spatial frequency, $k_p = c/\omega_{pe}$. This is important because drivers with length longer than $\frac{2\pi}{k_p}$ would be acted upon by the plasma oscillation fields created in their wake and thereby take away energy from the oscillations. Since the plasma e^- are within the potential well of the background ions, they are spatially limited to a single plasma spatial-oscillation bucket and do not co-propagate with the driver.

However, if the wake-potential exceeds the background ion-potential leading to wave-breaking or if the electron oscillations are not spatially confined to background ion-potential well by non-linear processes such as phase-mixing[4], the plasma electrons escape the potential well. Trapping is a mechanism of self-injection of plasma e^- into the plasma acceleration structure resulting in energy exchange (and acceleration) with the trapped plasma-electron beam. The trapped e^- co-propagate with the energy packet across many plasma-wavelengths locked to the crest of the wakefield. Therefore beam-loading of the acceleration structure potential leads to dissipation from the wakefields[16].

The highest field amplitude plasmon-bucket is just behind the driver. The buckets subsequent to the first have smaller fields as they dissipate energy to the surrounding plasma and also to the plasma ions[16]. Most optimized injection schemes like external injection, self-injection due to non-linear plasmon oscillations and returning trajectory crossing, ionization injection, down-ramp injection[18], colliding-pulse injection etc. inject into the first wakefield bucket to accelerate at the peak gradient.

Trapping plasma electrons within the plasma acceleration structures is challenging and tricky because it is constrains the bunch properties right at where the bunch is trapped

and thereby it is immensely interesting to study injection mechanisms. The primary bunch properties that need to be addressed at the source are - transverse emittances, bunch charge, energy spread, bunch length and number of bunches etc. In this thesis we show that by controlling certain plasma and driver (laser or e^- -beam) parameters the injection of plasma electrons into accelerating structures can be controlled.

1.2 Plasma model - Linearized Kinetic theory

The characteristic effects of the plasma state are based upon collective phenomenon. The plasma state once perturbed, unlike a gas does not relax to equilibrium state but continues to oscillate as suggested by eq.1.1. It is shown that for the presence of sustained oscillations it is crucial to introduce *long-range forces*. The collective phenomenon is characterized by the motion of a set of charges that are connected over long distances through the oscillating electric fields, \vec{E} . Such long-range interaction is very different from the stochastic collisional encounters dictating the dynamics in a gas. This field interaction of local oscillations is over distances much greater than the mean particle separation. However, such treatment of sustained oscillation is only partially complete to understand the full situation over all the different time-scales of the plasma state. The condition on the temperature and its effect on the plasma is not explicitly included in the equations such as eq.1.1, there is no explanation for the non-propagation of these density waves, the role of interactions at large distance are addressed by the Kinetic theory.

Just like in the conventional statistical mechanics the state of a fully ionized plasma is determined by 2 different 6D distribution functions: $f_\alpha(\vec{r}, \vec{p}, t)$ where $\vec{r} = x\hat{x} + y\hat{y} + z\hat{z}$ and $\vec{p} = p_x\hat{x} + p_y\hat{y} + p_z\hat{z}$ ($\vec{v} = m^{-1}\vec{p}$) and $\alpha = 1$ for electrons and $\alpha = 2$ for ions. A change in the number of particles within an element of the phase-space $dx dy dz dp_x dp_y dp_z$ due to the motion of the particle or external forces is taken into account by the methodology of kinetic theory. As the interaction of a charged particle and a neutral does not involve interaction mediated by fields it can be taken as a purely *collision interaction* and accounted for using

a sphere-of-action collisional approach. In plasma the interaction between charged particle mediated through fields is of much more importance. The *field interaction* can be divided into two different parts: (i) interaction at a distance less than or on the order of mean inter-particle separation (ii) interactions at distances greater than the mean particle separation. In the **equilibrium or the stationary state** it is assumed that macroscopically the number density of positive charges is equal to number density of negative charges implying *quasi-neutrality* i.e. neutrality at a macroscopic scale. The positive current $\vec{J}_+ = 0$ and the negative current $\vec{J}_- = 0$. The quasi-neutrality and zero net-current assumptions imply that $\vec{E}_0 = 0$ and $\vec{H}_0 = 0$. This also implies that the stationary or the equilibrium state is *collision-dominated* as the field-mediated interactions at the macroscopic scale are not possible with zero fields. Any excitation by external fields or currents can be accounted for by the long-range field-mediated approach.

The Kinetic theory of plasma electron dynamics can be studied using the Vlasov-Maxwell equations valid for the plasma properties over the electron timescales.

$$\begin{aligned} \partial f / \partial t + \vec{v} \cdot \partial f / \partial \vec{r} + (-e)(\vec{E} + m^{-1}c^{-1}[\vec{p} \times \vec{H}]) \cdot \partial f / \partial \vec{p} &= 0 \\ [\partial f_\alpha(\vec{r}, \vec{p}, t) / \partial t]_{coll}^{eq} &= 0 \\ \text{linearized : } \partial \phi / \partial t + \vec{v} \cdot \partial \phi / \partial \vec{r} + \frac{d\vec{p}(\Phi_0 + \phi)}{dt} \cdot \partial \Phi_0 / \partial \vec{p} &= 0 \\ \vec{\nabla} \times \vec{H} &= c^{-1} \partial \vec{E} / \partial t + 4\pi c^{-1} \int_{-\infty}^{+\infty} \vec{v} f d\vec{v} \\ \vec{\nabla} \cdot \vec{E} &= 4\pi \left(\int_{-\infty}^{+\infty} f \vec{v} d\vec{v} - n_0 \right) \\ \vec{\nabla} \times \vec{E} &= -c^{-1} \partial \vec{H} / \partial t \end{aligned} \tag{1.2}$$

Note an essential feature of the Vlasov equation is that it is linearized under perturbative expansion, $f = \Phi_0 + \phi^{(1)} + \mathcal{O}(\phi^{(2)})$ where Φ_0 is the equilibrium distribution function and $\phi^{(m)}$ are the higher order terms in the expansion of the perturbed distribution function. In the **linearized approximation** the dependencies on higher orders of the distribution

function,

$$f = \Phi_0 + \phi,$$

are approximated to be negligible and we represent $\phi^{(1)} = \phi$. We use the perturbative approximation

$$\frac{d\vec{p}(\Phi_0 + \phi)}{dt} \partial\phi/\partial\vec{p} \simeq 0$$

(separation of $\vec{p}(\Phi_0 + \phi)$ is not possible and terms of order ϕ^2 or higher are neglected). Also from the equilibrium condition,

$$\partial\Phi_0/\partial t + \vec{v} \cdot \partial\Phi_0/\partial\vec{r} + \frac{d\vec{p}(\Phi_0 + \phi)}{dt} \cdot \partial\Phi_0/\partial\vec{p} = 0.$$

Note also that when the excitation of the plasma cannot be perturbatively expanded due to large amplitude phenomenon a non-linear theory is required. Under this scenario the theory of Bernstein-Greene-Kruksal (BGK) is used as it incorporates the trapping of particles in large potential difference and the effect of these trapped particles on the potential.

We can now separate out the equations in eq.1.2 to describe the particular solutions of the two orthogonal dimensions using the two independent sets. The dimensions are chosen as $\hat{\parallel}$ along the wave-vector \vec{k} and $\hat{\perp}$ perpendicular to the wave-vector \vec{k} .

When there is only an irrotational (longitudinal) plasma field, $E_{\perp} = H_{\perp} = \vec{H} = 0$ and $E_{\parallel} \neq 0$. This implies $v_{\perp} = \phi_{\perp} = 0$. Correspondingly, $v_{\parallel} \neq 0$ and $\phi_{\parallel} \neq 0$. Upon substituting these conditions in the eq.1.2 we get the equation set describing a particular solution of the longitudinal waves, eq.1.2 $^{\parallel}$.

$$\begin{aligned} \partial\phi_{\parallel}/\partial t + \vec{v} \cdot \partial\phi_{\parallel}/\partial\vec{r} + e \vec{E}_{\parallel} \partial\Phi_0/\partial\vec{p} &= 0 \\ \vec{\nabla} \cdot \vec{E}_{\parallel} &= 4\pi e \int_{-\infty}^{+\infty} \phi_{\parallel} d\vec{v} \\ -\partial\vec{E}_{\parallel}/\partial t &= 4\pi e \int_{-\infty}^{+\infty} \phi_{\parallel} \vec{v} d\vec{v} \end{aligned} \quad (1.3)$$

When there is only a rotational (transverse) plasma field, $E_{\parallel} = H_{\parallel} = 0$, $E_{\perp} \neq 0$ and $H_{\perp} \neq 0$. This implies $v_{\parallel} = \phi_{\parallel} = 0$. Correspondingly, $v_{\perp} \neq 0$ and $\phi_{\perp} \neq 0$. Upon substituting these conditions in the eq.1.2 we get the equation set describing a particular solution of the transverse waves, eq.1.2⁺.

$$\begin{aligned} \partial\phi_{\perp}/\partial t + \vec{v} \cdot \partial\phi_{\perp}/\partial\vec{r} + e (\vec{E}_{\perp} + (\vec{v} \times \vec{H})_{\perp}) \partial\Phi_0/\partial\vec{p} &= 0 \\ \vec{\nabla} \times \vec{H} &= c^{-1} \partial\vec{E}/\partial t + 4\pi ec^{-1} \int_{-\infty}^{+\infty} \vec{v} \phi d\vec{v} \\ \vec{\nabla} \times \vec{E} &= -c^{-1} \partial\vec{H}/\partial t, \quad \vec{\nabla} \cdot \vec{E} = 0, \quad \vec{\nabla} \cdot \vec{H} = 0 \end{aligned} \quad (1.4)$$

The linearized equation along the orthogonal directions can be solved using spectral methods. The longitudinal dispersion relation for a collective phenomenon in the form of a longitudinal wave $(\omega, \vec{k}, \vec{v})$ in the plasma with the Boltzmann distribution at equilibrium Φ_0 and electron energy \mathcal{E} is,

$$4\pi e^2 \int_{-\infty}^{+\infty} d\vec{v} \frac{1}{\omega |\vec{k}|^2} \frac{(\vec{v} \cdot \vec{k})^2}{\vec{v} \cdot \vec{k} - \omega} \frac{\partial\Phi_0}{\partial\mathcal{E}} = 1 \quad (1.5)$$

Similarly, the transverse dispersion relation for a transverse wave is given by,

$$\frac{4\pi e^2}{c^2 |\vec{k}|^2 - \omega^2} \frac{\partial\Phi_0}{\partial\mathcal{E}} \int_{-\infty}^{\infty} d\vec{v} (\hat{e}_k \cdot \vec{v})^2 \frac{\omega}{\omega - \vec{k} \cdot \vec{v}} = 1 \quad (1.6)$$

Assuming a Maxwellian equilibrium distribution:

$$\Phi_0(\mathcal{E}(\vec{p})) = n_0 (2\pi \frac{k_B T_e}{m})^{-3/2} e^{-\mathcal{E}(\vec{p})/k_B T_e} \quad (1.7)$$

We can evaluate $\frac{\partial\Phi_0}{\partial\mathcal{E}} = n_0 \frac{-1}{k_B T_e} (2\pi \frac{k_B T_e}{m})^{-3/2} e^{-\mathcal{E}(\vec{p})/k_B T_e}$.

We can write the irrotational longitudinal dispersion relation for a Maxwellian.

$$\begin{aligned} \omega_{pe} \lambda_{De} &= \sqrt{\frac{4\pi ne^2}{m}} \sqrt{\frac{k_B T_e}{4\pi ne^2}} = \sqrt{\frac{k_B T_e}{m}} = v_{th} \\ \vec{v}/v_{th} &= v^*; \quad k \lambda_{De} = k^*; \quad \omega/\omega_{pe} = \omega^* \\ \int_{-\infty}^{+\infty} dv^* \frac{v^*}{(\omega^*/k^* - v^*)} e^{-v^* 2/2} &= \sqrt{2\pi} k^* 2 \end{aligned} \quad (1.8)$$

By using the Cauchy's principal value theorem around the pole at $\omega^*/k^* = v^*$ in the integral above, we can evaluate the dispersion relation for Maxwellian distribution.

$$\begin{aligned}\omega^2 &= \omega_{pe}^2 + 3k^2\omega_{pe}^2\lambda_{De}^2 \\ \omega^2 &= \omega_{pe}^2 + 3k^2v_{th}^2\end{aligned}\tag{1.9}$$

Similarly, using the Maxwellian distribution function

$$\begin{aligned}\omega^{*2} &= k^{*2} + \frac{1}{\sqrt{2\pi}} \int_{-\infty}^{\infty} dv^* e^{-v^{*2}/2} \frac{1}{1 - \frac{k^*}{\omega^*} \frac{v_{th}}{c} v^*} \\ v^* &= \frac{v}{(k_B T_e/m)^{1/2}}, \quad \omega_{pe}/k_0 = c \\ \text{Under, } \frac{\omega}{k} &\gg \frac{\vec{k} \cdot \vec{v}}{|\vec{k}|} \\ \omega^{*2} &= k^{*2} + 1 + \left(\frac{k^*}{\omega^*} \frac{v_{th}}{c} \right)^2 \\ \frac{v_{th}}{c} &\ll 1 : \omega^2 = c^2 k^2 + \omega_{pe}^2\end{aligned}\tag{1.10}$$

We note that $\frac{v_{th}}{c} \ll 1$ and under the condition that $\frac{k^*}{\omega^*} \frac{v_{th}}{c} \ll 1$, a perturbative expansion of $\frac{1}{1 - \frac{k^*}{\omega^*} \frac{v_{th}}{c} v^*}$ can be done. By writing this in the physical units and using $\omega_{pe}/k_0 = c$, we have, $\omega^2 = c^2 k^2 + \omega_{pe}^2$.

However, it is generally more convenient to analyze various phenomenon in the plasma using different moments of the linearized Vlasov equation. These moments lead to the fluid equations. The fluid equations are as follows, where α represents different species in the plasma, \mathcal{Q} is the heat flux, \hat{p} the thermal pressure (assumed to be isotropic) and other variables represent the familiar quantities.

$$\frac{\partial}{\partial t} n_\alpha + \vec{\nabla}_{\vec{r}} \cdot n_\alpha \langle \vec{v} \rangle = 0\tag{1.11}$$

$$n_\alpha \frac{\partial}{\partial t} \langle \vec{v} \rangle + n_\alpha \langle \vec{v} \rangle \vec{\nabla}_r \langle \vec{v} \rangle = \frac{n_\alpha q_\alpha}{m_\alpha} \left(\vec{E} + \frac{\langle \vec{v} \rangle \times \vec{B}}{c} \right) - \vec{\nabla}_r \frac{\hat{p}_\alpha}{m_\alpha} \quad (1.12)$$

$$\begin{aligned} \frac{\partial}{\partial t} \hat{p}_\alpha + 3\hat{p}_\alpha \frac{\partial \langle v \rangle}{\partial x} + \langle v \rangle \frac{\partial}{\partial x} \hat{p}_\alpha + 2 \frac{\partial}{\partial x} Q_\alpha &= 0 \\ \frac{\hat{p}}{n_\alpha^3} &= \text{constant in } 1-D \\ \frac{\hat{p}}{n_\alpha^\gamma} &= \text{constant, adiabatic index :} \gamma = 1 + \frac{2}{N}, \quad N = \text{degrees of freedom} \end{aligned} \quad (1.13)$$

1.3 Plasma excitation by energy sources

The laser-plasma interaction is modeled based upon the intensity that can be attained in the focal spot of the laser. Similarly, beam-plasma interaction is characterized by the peak beam density of the beam with respect to the background plasma density, $\frac{n_b}{n_0}$. The laser field is characterized by the *laser strength parameter* which is the normalized electromagnetic vector potential $a(x, r, t) = \frac{eA(x, r, t)}{m_e c^2}$ where, $\vec{B}(r, t) = \vec{\nabla} \times \vec{A}(r, t)$. The normalization helps quantify the momentum of an electron \vec{p}_e , interacting with the laser field in vacuum due to the conservation of the canonical momentum \vec{P} . When vorticity $\vec{\Lambda} = \nabla \times \vec{P}$ has no temporal variation, then in a plane-wave $\partial_t \vec{P}_e = 0 \Rightarrow \partial_t \left(\vec{p}_e - \frac{e\vec{A}}{c} \right) = 0$. Hence, it is desirable to represent the laser intensity with the normalized vector potential $\vec{a} = \frac{\vec{p}_e}{m_e c} = \frac{1}{m_e c} \frac{e\vec{A}}{c}$. This defines the laser electric field amplitude in terms of $\vec{a}(x, r, t)$, its monochromatic sinusoidal evolution in time (with angular frequency ω_0) and a radial focal spatial profile, $\vec{E}_{laser}(r, t) = -\frac{1}{c} \frac{\partial \vec{A}(r, t)}{\partial t} = -\frac{\omega_0}{c} \vec{A}(r, t) = \omega_0 \frac{m_e c}{e} \vec{a}(r, t)$. It should be noted that the laser pulse is not a plane wave and thereby the a_0 parameter characterizes the peak laser intensity I_0 (W/cm^2) and the peak power of the pulse $P_0 \propto I_0 \propto a_0^2$. When $a_0 = 1$ then $p_e = m_e c$ and thereby such a laser is capable of exciting relativistic-electron momentum such that the irradiated electron kinetic energy is of the order of the rest-mass energy ($I_0 > 2.1 \times 10^{18} \frac{W}{cm^2}$ for

Ti:Sapphire, $\lambda_0 \sim 800\text{nm}$). A TEM laser mode propagating in vacuum at such intensities has the following transverse electric field amplitude, where η is the free-space impedance,

$$E_{laser} = \sqrt{2\eta I_0} = 2\pi \frac{m_e c^2}{e \lambda_0} a_0 \simeq 4 \text{ TVm}^{-1} (\text{a}_0 = 1).$$

Thus it can be seen that in the relativistic regime, laser interacting with a free-space electron can quiver (transverse) it such that the electron kinetic energy is almost half the rest-mass energy, $a_0 \geq 1$. The transverse motion of a free-space electron (first order in \vec{a}) in the plane-wave transverse electromagnetic mode cannot impart any longitudinal momentum to the electrons. In a focussed field such as the laser with radial variation of the electric field, the Gauss's law $\vec{\nabla} \cdot \vec{E} = 0$ implies a small longitudinal field component due to field's radial gradients. As the phase velocity of the laser field in the focus is higher than the speed of light and electrons rapidly slip-off the accelerating phase of the axial field, therefore there is a negligible net momentum gain.

The laser packet is not a plane-wave and therefore the plasma electrons experience a longitudinal force. If the laser-electron interaction is not infinite or there is a time-varying field amplitude then the part $\frac{\vec{p}_\perp}{m_e \gamma_e} \times \vec{B}$ (it should be noted that \vec{p}_\perp is in phase with \vec{B} and $\pi/2$ out of phase with \vec{E}) of the Lorentz force causes a small longitudinal force which is second order in \vec{a} . The longitudinal ponderomotive force [13] is $F_z^{pond} \simeq m_e \frac{dp_e^\parallel}{dt} \simeq -e \frac{\vec{p}_\perp}{\gamma_e} \times \vec{B} = -\frac{m_e c^2}{2\gamma_e} \nabla_z a^2$. Therefore in vacuum $p_e^\parallel \propto \frac{a^2}{\gamma_e}$. It should be noted that because this force is a second order ($\propto a^2$) force its characteristic frequency is $2\omega_0$.

In relativistically intense laser propagation, the laser pulse envelope changes due to many effects. Effect such as self-focussing in the plasma due to the ponderomotively evacuated lower plasma density region creates an effective lensing on the laser. The large ponderomotive force also leads to front of the laser group velocity reducing and back of the pulse group velocity increasing, resulting in longitudinal pulse compression. Additionally, in relativistic intensity regime the phase velocity of the pulse is also affected. The front of the pulse undergoes a red-shift and the back of pulse a blue-shift.

The most efficient method of using the laser electric field is by ponderomotively exciting space-charge structures in the plasma such as plasma-electron waves. This is especially practical considering that the relativistic intensity lasers ionize any material into a plasma. Unlike the material breakdown limit of the accelerating fields in conventional accelerators, plasma cannot be broken (there are parasitic effects such as higher ionization of plasma-ions with higher magnitude fields in the plasma).

There is a limit of the plasma-wave field amplitude beyond which the plasma electrons are not just forming the density structures and their corresponding fields. In a plasma-wave with electric fields greater than the wave-breaking limit, the plasma electrons that escape the plasma-ion electrostatic field can be trapped in the propagating plasma waves and get accelerated. The plasma electrons trapped in the potential well of the accelerating phase of the wave are accelerated with the force of the plasma-wave electric field, until they reach energies high enough to exceed the acceleration structure velocity to this extent that they escape the well into the opposite phase (de-phasing limit).

The laser-plasma electron accelerators are high- β acceleration structures which use high- v_ϕ plasma waves. The high velocity acceleration structures of a laser-plasma electron accelerator need sufficiently high potentials to be created in the plasma to trap and accelerate relativistic electrons. The unavailability of a laser technology to create high enough ponderomotive potentials to trap and accelerate relativistic electron beams delayed the experimental demonstration of laser electron accelerators from their first theoretical proposal in 1979 [5] till 2004 [9]. The propagation of electromagnetic energy in an unmagnetized plasma is governed by the dispersion relations of the electromagnetic mode and the wave excited in the plasma. For monochromatic plane-wave electromagnetic field at ω_0 interacting with a homogeneous unmagnetized plasma of characteristic frequency ω_{pe} , the dispersion is governed by $\omega_0^2 = \omega_{pe}^2 + c^2 k^2$. The laser pulse electric field has a radial 2-D spatial variation and this simple 1-D dispersion characteristic equation does not describe the dispersion accurately. This dispersion relation is for the electromagnetic field exciting electron plasma wave and ignores the plasma ion dynamics and the corresponding dispersion relation of

the ions. When $\omega_0 \gg \omega_{pe}$, the group velocity of the laser pulse (and hence the speed of the laser created acceleration structure) in the plasma is very close to the speed of light in vacuum, $v_g = c\sqrt{1 - \omega_{pe}^2/\omega_0^2} \lesssim c$. The phase velocity of the electron plasma wave is equal to the group velocity of the laser pulse [5](p.267, eq.1),

$$\beta_{pe}^\phi \simeq v_{laser}^g/c.$$

In the beam-driven plasma wave the phase-velocity of the plasma-waves is nearly the beam velocity [6](p. 694),

$$\beta_{pe}^\phi \simeq v_{beam}/c.$$

Note that there is a small correction to the phase velocity of the plasma waves, β_{pe}^ϕ because the head of the driver is in general depleted or unguided in the plasma. Because of the energy loss at the head or because the head is not transversely confined the driver may appear to slowly drift behind the initial head position in the frame phase velocity front, $\beta_{pe}^\phi - \beta_{driver}(\text{head}) \neq 0$. Thus reducing the phase-velocity of the waves. If the head erosion is rapid then the phase-velocity is not nearly constant.

High plasma wave phase velocity implies that the plasma wave is relativistic with $\gamma_{pe} = \omega_0/\omega_{pe}$. However, if the plasma frequency is nearly equal to the laser frequency $\omega_{pe} \simeq \omega_0$, the group velocity is very low, $v_g \ll c$ and depends upon the ratio of the plasma frequency to the laser frequency $\frac{\omega_{pe}}{\omega_0}$. The propagation is possible only if $\omega_0 > \omega_{pe}$. It should be noted that when the plasma is cold, the dynamics of the plasma is described by the plasma density ($n_e(x, t)$) and full description using the distribution function ($f(x, p, t)$) is not necessary. The properties of collective coherent particle oscillations in a plasma is characterized by the density distribution. Plasma waves and other coherent structures in the plasma do not constitute thermal plasma. When the plasma equilibrates through mode mixing into randomness with maximum entropy then it is considered thermal.

The space-charge electric fields that is excited in a plasma depend upon the plasma density, in addition to the magnitude of charge displacement force. It is the charge displacement from equilibrium between the plasma electrons and ions which creates the fields.

Therefore larger the electron density (assuming high enough force and energy of the perturbation) higher the number of electrons that can be displaced from equilibrium. It should be noted that the electron plasma frequency ignoring the plasma-ion dynamics ($\omega_{pe}^2(x, t) = \frac{4\pi n_e(x, t)e^2}{m_e}$) is determined by the plasma density, $n_e(x, t)$ (directly from Gauss' law and Newton's second law of motion). It is this plasma field which has a significant longitudinal component to provide a high acceleration gradient in addition to the transverse focussing fields. We now look at the space charge fields excited in the rest-frame of the laser. If the force acting on the plasma electrons is below the electrostatic force of the background plasma-ions, they remain within the electrostatic potential well of the plasma ions. External energy coupled into the plasma excites motion of the electrons (electron gas neutralized by ions) to the leading order at the plasma electron frequency ω_{pe} .

The space-charge force equation on a representative laser excited plasma electron oscillating in the space charge Langmuir or plasma-electron wave is $d\vec{p}_e/dt = -e\vec{E}_{pe} = e\vec{\nabla}\phi_{pm}$. Where ϕ_{pm} is the acceleration structure potential created in the electron plasma wave (in the rest-frame of the wave). This potential is also referred to as ponderomotive potential because it is excited by the ponderomotive force of a laser pulse envelope. We can infer the plasma space-charge field, oscillating at ω_{pe} , based upon the electron momentum in the rest-frame of the plasma wave, $|\vec{E}_{pe}| = \left(\frac{m_e c \omega_{pe}}{e}\right) \gamma_{pm} \beta_{pm}$. With the relativistic correction (in the rest-frame of the propagating plasma-wave) to the electron plasma frequency, $|\vec{E}_{pe}| = \left(\frac{m_e c \omega_{pe}^{\gamma_e=1}}{e}\right) \frac{\gamma_{pm} \beta_{pm}}{\sqrt{\gamma_e}}$. We can further reduce $\gamma_{pm} \beta_{pm} = \sqrt{\gamma_{pm}^2 - 1}$ thereby $|\vec{E}_{pe}| = \left(\frac{m_e c \omega_{pe}^{\gamma_e=1}}{e}\right) \sqrt{\frac{\gamma_{pm}^2 - 1}{\gamma_e}}$. The free-space electron in laser field has transverse momentum at the laser frequency ω_0 . Hence, the plasma electron momentum in the direct irradiation of the laser field is $\vec{\beta}_e \gamma_e$ equal to the laser field $\vec{a}(x, t)$ in the plasma (when $\omega_0 \gg \omega_{pe}$). However, if the interacting laser pulse is short and the plasma electrons creating the fields are not collocated with the laser field, $\gamma_e \approx 1$ and $|\vec{E}_{pe}| \approx \left(\frac{m_e c \omega_{pe}^{\gamma_e=1}}{e}\right) \gamma_{pm}$.

When the laser field is collocated, in addition to quivering the electrons in the plasma

wave crest, it also ponderomotively accelerates them. The plasma electrons oscillating longitudinally have momentum corresponding to the ponderomotive force $\vec{\beta}_{pm}\gamma_{pm}$ in the rest-frame of the laser. The maximum amplitude of the electron plasma-wave is therefore dependent upon the magnitude of the ponderomotive force. The limit of the maximum longitudinal field while the plasma electrons are still bound to the background ions is referred to as the wave-breaking limit. As the plasma field approaches the wave-breaking limit the ponderomotively driven plasma-electron density is bunched into a tighter volume. At wave-breaking the electrons in the wave-crest are all at the same location leading to the limit of density steepening.

If some of the plasma electrons can attain velocities on the order of the phase velocity of the plasma wave, in the rest-frame of the plasma wave they experience the plasma wave-fields. Generally, it is assumed that the fraction of such fast electrons is very small compared to the background plasma density. Such considerations are important in terms of the energy balance, that is, if the plasma electrons extract the field energy then the plasma wave will collapse. Plasma electrons creating the plasma electron density wave can also be trapped in the potential ϕ_{pm} of the wave and get accelerated if $|e\phi_{pm}| > (\gamma_e^{trap} - 1)m_e c^2$. Where $|\gamma_e^{trap}\beta_e^{trap}|$ is the trapped electron momentum in the rest-frame of the laser, relative to the plasma wave momentum. It should also be noted that the potential ϕ_{pm} is in the rest-frame of the laser or the frame co-moving with the plasma-wave. Making a coordinate transform from the rest-frame of the driver to the lab-frame, $\phi_{lab-frame} = \frac{1}{\gamma_\phi}\phi_{pm}$. Thus the trapping condition for an electron in the lab-frame is $-\phi_{lab-frame} > (\frac{\gamma_e^{trap}}{\gamma_\phi} - \frac{1}{\gamma_\phi})\frac{m_e c^2}{e}$. The electrons that are locked with a phase of the potential in a limiting condition have $\beta_e^{trap} = \beta_\phi$. Thus at the onset of trapping the Lorentz factors are, $\gamma_e^{trap} = \gamma_\phi$. The trapping condition can be written as,

$$\phi_{lab-frame} < \left(\frac{1}{\gamma_\phi} - 1\right) \frac{m_e c^2}{e} \quad (1.14)$$

More detailed analysis is provided in the later chapters.

The plasma electrons are oscillating in the plasma wave and thereby the phase of the plasma-wave relative to the plasma electrons decides the magnitude of the relative momentum of the electrons. The laser is at the head of the electron plasma wave (the wave is in the wake of the laser) of relativistic phase velocity which equals the group velocity of the laser. The electron density trapped in the plasma wave is subject to the total energy equation depending on the number density of the ponderomotive electrons. The trapping of plasma electrons and the transfer of energy from the space-charge plasma fields leads to effective lowering of the fields. This is referred to as beam-loading. Similarly, in laser-plasma ion accelerators the transfer of energy from the acceleration structure to the trapped ions is a mechanism of energy loss through beam-loading. However, in the ion accelerators the ions to be trapped are initially at rest. Therefore only the amplitude of the snowplow potential and not the relative phase of the ion velocity to the potential is important. The long term energy dissipation of the plasma fields and deconstruction of the density structures is through mode mixing, collisions, kinetic effects such as Landau damping etc.

The wave-breaking limit is estimated by the length of the trajectory of the the oscillating plasma electron (with speed v_{pe}) in the frame of reference of the plasma wave. For the plasma electrons breaking the electrostatic pull of the plasma ions, the trajectory length in the time duration of $2\pi/\omega_{pe}$ exceeds the plasma wavelength λ_{pe} . It can also be estimated from the Gauss's law in a plasma, $\vec{k}_p \cdot \vec{E}_{pe} = 4\pi n_e e$. The maximum electric field of a plasma wave in the non-relativistic excitation of plasma electrons is $|\vec{E}_{pe}| = \omega_{pe} (\frac{m_e c}{e})$. Therefore in the non-relativistic regime the limit of the plasma electric field is $E_{pe} \propto \omega_{pe} \propto \sqrt{n_e}$. So the maximum longitudinal electric field that can be excited by a laser in the plasma is when $\omega_{pe} = \omega_0$. When $\omega_{pe} > \omega_0$ the laser frequency is below the plasma electron characteristic frequency and driver is detuned. This is opposite to the case when $\omega_0 \gg \omega_{pe}$. More details of the trajectory crossing is provided below.

1.4 Acceleration structures in the plasma

In plasma-based electron acceleration mechanisms the acceleration structure is a propagating plasma electron density wave. The plasma wave is excited by electromagnetic energy or particle beams in their wake. The energy coupled into the plasma can be used to create traveling density structures with longitudinal and transverse space-charge fields in the frame of the propagating energy. These fields are used to transport and accelerate beams.

In laser-plasma electron accelerators the acceleration structure is created by the ponderomotively driven electron density displacement relative to the stationary background plasma-ions[5]. Higher the ponderomotive force larger the electron density displacement. The density accretion in the plasma density wave is limited by the displacement of all the plasma electrons. However, the fields are limited by the amplitude of the spatial charge separation from the equilibrium. The acceleration structure is sustained until the laser can propagate in the plasma. This is limited by the depletion of laser to low enough energy until it is too weak (its ponderomotive force is weak) to excite a large amplitude electron-plasma wave. Since the laser pulse excites an electron plasma wave, it is guided in the rarer electron density region (lower refractive index channel) enclosed by the higher electron densities surrounding it. The laser velocity can be controlled by varying the plasma density. However, the plasma electrons that are driven ponderomotively gain significant momentum to get trapped in the plasma electron wave and as a result get accelerated.

In particle beam-plasma interactions the plasma density structures are created by the beam fields interacting with the plasma [6]. Beam density spatial distribution governs the beam fields. The electron plasma wave is driven by the force of the self-fields of the particle beam on the plasma electrons. An intense relativistic beam with density comparable to the plasma loses significant energy to the plasma, but does not slow down. So, the electron-plasma waves propagate at an almost constant beam velocity in the plasma. However, the plasma fields created by the beam fields can affect the beam transversely such as by focussing it or longitudinally by modulating the beam particle velocity. Thereby the beam

density distribution can be significantly modified inside the plasma. The plasma electron density accretion driven in the frame of the wave by the beam is of the order of the beam density $\delta n \simeq n_b$. Hence if the beam fields can drive a high enough density accretion then the plasma fields are limited by the plasma density. For beam density exceeding the plasma density plasma electron waves in the wake of the beam can have large enough electron accretion to lead to bared ion regions where electrons are evacuated. However, it is possible to create spatial beam profiles that have higher self-fields and can thereby create higher magnitude space charge wave in the plasma.

Also, it is noted that relativistic beam is desirable for beam-excited plasma electron wave. It is well-known that it is easier to focus a relativistic beam because the beam's electrostatic self-fields are compensated by the magnetic pinch force which grows with velocity. Additionally a highly relativistic beam has a large beta-function and can be transported over a larger length without expanding transversely, $\beta = \sigma_r/\sigma_\theta$ and can propagate for longer distances.

1.5 Plasma-electron momentum equations - Fluid model

We start with the Maxwell's equations (in microscopic form in Gaussian units) governing an electromagnetic wave propagating in a plasma, $\vec{\nabla} \times \vec{E} = -\frac{1}{c} \frac{\partial \vec{B}}{\partial t}$, $\vec{\nabla} \times \vec{B} = \frac{4\pi \vec{J}}{c} + \frac{1}{c} \frac{\partial \vec{E}}{\partial t}$, $\vec{\nabla} \cdot \vec{E} = 4\pi\rho = 0$, $\vec{\nabla} \cdot \vec{B} = 0$, with the electric field of light evolving in time-space as, $\vec{E} = E_0 \cos(kz - wt)\hat{z}$. The sources in these equations are $\vec{J} = \sum_j q_j n_j \vec{v}_j$, $\rho = \sum_j q_j n_j$. We use the fluid equations to describe the plasma. The zeroth-order moment - continuity equation is $\frac{\partial n_j}{\partial t} - \vec{\nabla} \cdot (n_j \vec{v}_j) = 0$. The first-order moment - the equation of motion is, $\frac{d\vec{p}_j}{dt} = \left(\frac{\partial}{\partial t} + \vec{v}_j \vec{\nabla} \right) \vec{p}_j = q_j \left(\vec{E} + \frac{1}{c} \vec{v}_j \times \vec{B} \right) - \vec{\nabla} \overset{\text{cold}}{\cancel{\mathbf{P}_j}}$, where, $\vec{p}_j = \gamma \beta m_j \vec{v}_j$ and \mathbf{P}_j is the thermal pressure.

Now taking curl on both the sides of the force balance equation for electron, $\frac{\partial}{\partial t} \vec{\nabla} \times \vec{p} - \vec{\nabla} \times \vec{v} \times \vec{\nabla} \times \vec{p} = q \left(\vec{\nabla} \times \vec{E} + \frac{1}{c} \vec{\nabla} \times \vec{v} \times \vec{B} \right) \Rightarrow \frac{\partial}{\partial t} \vec{\nabla} \times (\vec{p} + \frac{q}{c} \vec{A}) = \frac{q}{c} \vec{\nabla} \times \vec{v} \times \vec{B} + \vec{\nabla} \times \vec{v} \times \vec{\nabla} \times \vec{p}$.

Simplifying we obtain the equation of the canonical momentum, $\vec{P} = \vec{p} + \frac{q}{c} \vec{A}$,

$$\frac{\partial}{\partial t} \vec{\nabla} \times \left(\vec{p} + \frac{q}{c} \vec{A} \right) = \vec{\nabla} \times \vec{v} \times \left(\vec{\nabla} \times \left(\frac{q}{c} \vec{A} + \vec{p} \right) \right) \quad (1.15)$$

Defining *relativistic vorticity*, as $\vec{\Lambda} = \nabla \times \vec{P}$, where, $\vec{\nabla} \times \vec{P} = \vec{\nabla} \times \vec{p} + \frac{q}{c} \vec{B} = \vec{\nabla} \times \left(\frac{q}{c} \vec{A} + \vec{p} \right)$.

We know that, for relativistic vorticity $\frac{\partial}{\partial t} \vec{\Lambda} - \vec{\nabla} \times \vec{v} \times \vec{\Lambda} = 0$. If, $\Lambda(\vec{r}) = 0$ at any point space then it is zero always, $\partial_t \Lambda(\vec{r}) = 0$. In 1-D considerations, this leads to the conservation of canonical momentum,

$$\partial_t P_{\perp} = 0 \Rightarrow \partial_t \left(p_{\perp} - \frac{e A_{\perp}}{c} \right) = 0 \quad (1.16)$$

$$\vec{p}_{\perp} = \frac{e \vec{A}_{\perp}}{c} \rightarrow \frac{\vec{p}_{\perp}}{m_e c} = \vec{a} \quad (1.17)$$

In higher dimensions it can be shown that the canonical momentum is conserved in lower orders.

We also get the equation for *ponderomotive force* of the laser from this using the vector calculus identity, $mc^2 \vec{\nabla} \gamma = -\vec{v} \times \vec{\nabla} \times \vec{p} - \vec{v} \cdot \vec{\nabla} \vec{p}$, which gives us the force balance as,

$$\begin{aligned} \partial_t \vec{p} &= -e \vec{E} - m_e c^2 \vec{\nabla} \gamma \\ &= e \vec{\nabla} \Phi - m_e c^2 \vec{\nabla} \gamma \\ \partial_t \frac{\vec{p}}{m_e c} &= c \vec{\nabla} (\phi - \gamma) \end{aligned} \quad (1.18)$$

This equation is differentiated in time, we have, $\partial_t^2 \vec{p} = -e \partial_t \vec{E} - mc^2 \partial_t \vec{\nabla} \gamma$. Taking the vorticity, $\Lambda = 0 \Rightarrow \vec{\nabla} \times \vec{p} = \frac{e}{c} \vec{B}$, and using the Ampere's law with Maxwell's corrections, $c \vec{\nabla} \times \vec{\nabla} \times \vec{p} = \partial_t \vec{E} + 4\pi \vec{J}$, $\vec{J} = -en \vec{v} = -en \frac{\vec{p}}{\gamma}$.

$$\partial_t^2 \vec{p} + c^2 \vec{\nabla} \times \vec{\nabla} \times \vec{p} = -\frac{4\pi e^2 n}{m_e} \frac{\vec{p}}{\gamma} - mc^2 \partial_t \vec{\nabla} \gamma \quad (1.19)$$

Using the Gauss' law, $\vec{\nabla} \cdot \vec{E} = -4\pi en$, we obtain the density perturbation,

$$n = n_0 + \frac{1}{4\pi e^2} \vec{\nabla} \cdot (\partial_t \vec{p} + mc^2 \vec{\nabla} \gamma) \quad (1.20)$$

Using the density perturbation in the equation we get the Master equation for the plasma waves in a cold-collision-less plasma,

$$\partial_t^2 \vec{p} + c^2 \vec{\nabla} \times \vec{\nabla} \times \vec{p} = - \left[\omega_{p0}^2 + \frac{1}{m} (\partial_t \vec{p} + mc^2 \vec{\nabla} \gamma) \right] \frac{\vec{p}}{\gamma} - mc^2 \partial_t \vec{\nabla} \gamma \quad (1.21)$$

From this we get the *longitudinal waves*,

$$\vec{\nabla} \times \vec{p} = 0 \Rightarrow (\partial_t^2 + \omega_{p0}^2) \vec{p} = 0$$

and *transverse waves*,

$$\vec{\nabla} \cdot \vec{p} = 0 \Rightarrow \left(\partial_t^2 - \nabla^2 + \frac{\omega_{p0}^2}{\gamma} \right) \vec{p} = 0.$$

Using Ampere-Maxwell's equation, $\vec{\nabla} \times \vec{B} = \frac{1}{c} \partial_t \vec{E} + \frac{4\pi}{c} \vec{J} \Rightarrow \vec{\nabla} \times \vec{\nabla} \times \vec{A} = \frac{1}{c} \partial_t \left(\frac{-1}{c} \partial_t \vec{A} - \vec{\nabla} \phi \right) + \frac{4\pi}{c} \vec{J} \Rightarrow \frac{1}{c^2} \partial_t^2 \vec{A} + \vec{\nabla} \times \vec{\nabla} \times \vec{A} = \frac{4\pi}{c} \vec{J} - \frac{1}{c} \partial_t \vec{\nabla} \phi$. This gives us, $\frac{1}{c^2} \partial_t^2 A_\perp - \partial_\parallel^2 A_\perp = \frac{4\pi}{c} J_\perp = -\frac{4\pi}{c} e n \frac{p_\perp}{\gamma} = -\frac{4\pi}{c} e n \frac{e A_\perp}{\gamma} = -\frac{4\pi e^2}{mc^2 \gamma} (n_0 + \delta n) A_\perp$. Replacing for the plasma frequency, $\frac{1}{c^2} \partial_t^2 A_\perp - \partial_\parallel^2 A_\perp = -\frac{4\pi e^2}{mc^2 \gamma} (n_0 + \delta n) A_\perp = -\frac{\omega_{p0}^2}{c^2} \left(1 + \frac{\delta n}{n_0} \right) \frac{1}{\gamma} A_\perp$. The Lorentz factor is, $\gamma = \sqrt{1 + \frac{p_\parallel^2}{m^2 c^2} + \frac{e^2 A_\perp^2}{m^2 c^4}}$. The vector potential evolution follows,

$$\left(\frac{1}{c^2} \partial_t^2 - \partial_\parallel^2 \right) A_\perp \simeq -\frac{\omega_{p0}^2}{c^2} \left(1 + \frac{\delta n}{n_0} - \frac{e^2 A_\perp^2}{2m^2 c^4} \right) A_\perp \quad (1.22)$$

From the continuity eq., $\partial_t \delta n + n_0 \vec{\nabla} \delta \vec{v} = 0$, we have, $\partial_t^2 \frac{\delta n}{n_0} + \vec{\nabla} \delta \partial_t \vec{v} = 0$. The change in velocity is, $\partial_t \vec{v} = -\frac{e}{m} \delta \vec{E} - c^2 \nabla \left(1 + \frac{e^2 A_\perp^2}{2m^2 c^4} \right)$. The equation of motion of the density perturbation is thus,

$$\partial_t^2 \frac{\delta n}{n_0} + \frac{4\pi e^2 n_0}{m_e} \frac{\delta n}{n_0} = c^2 \nabla^2 \frac{e^2 A_\perp^2}{2m^2 c^4} \quad (1.23)$$

When the electric fields of the wake are less than the cold-plasma wave-breaking limit, $E_0 = \frac{m_e c \omega_p}{e}$, the waves are linear sinusoidal oscillations with frequency ω_p and a phase velocity $v_p (\simeq c)$. This *non-relativistic* wave-breaking limit can be derived by assuming that this linear sinusoidal field has the form $\vec{E} = E_0 \sin(\omega_p(z/v_p - t))\hat{z}$. Then from Gauss's law, $\vec{\nabla} \cdot \vec{E} = -4e\pi(n_e - n_0)$. But, the spatial variation of the electric field is at $\vec{k}_p = \frac{\omega_p}{c}\hat{z}$, hence, $k_p E_0 = \frac{\omega_p}{c} E_0 = -4e\pi(n_e - n_0) \Rightarrow E_0 = \frac{m_e c \omega_p}{e}$. Similarly, *relativistic* cold-plasma wave-breaking limit can be derived as, $E_{wb} = \sqrt{2(\gamma_p - 1)}E_0$. Cold-plasma theory holds good in the limit, $\gamma_p \beta_{th} \ll \beta_p$, where $c\beta_{th} = \sqrt{\frac{k_B T_0}{m}}$. For *relativistic warm plasma*, $\gamma_p \beta_{th} \gg 1$, we have, $E_{WB} = \frac{E_0}{\beta_p}$.

The wave-breaking limit in cold plasma for electron plasma waves of relativistic phase-velocity can be derived by starting with the equations for purely longitudinal oscillations in the z-direction [3],

$$\frac{d^2 \gamma_z^e (1 - \beta_\phi \beta_z^e)}{d\tau^2} = \omega_{pe}^2 \beta_\phi^2 \left(\frac{\beta_z^e}{\beta_\phi - \beta_z^e} \right) \quad (1.24)$$

Upon integrating this equation with $d\tau$ we obtain,

$$\frac{1}{2} \left(\frac{d\gamma_z^e (1 - \beta_\phi \beta_z^e)}{d\tau} \right)^2 = \omega_{pe}^2 \beta_\phi^2 \left(-(1 - \beta_{ez}^2)^{-1/2} + \mathcal{C} \right) \quad (1.25)$$

The constant of integration can be found using the fact that at the velocity amplitude of longitudinal oscillation, $\max(\beta_{ez})$ the left hand side is zero, so $\mathcal{C} = (1 - \beta_m^2)^{-1/2}$. We obtain the integrated equation as,

$$\frac{1}{2} \left(\frac{d\gamma_z^e (1 - \beta_\phi \beta_z^e)}{d\tau} \right)^2 = \omega_{pe}^2 \beta_\phi^2 \left(-(1 - \beta_{ez}^2)^{-1/2} + (1 - \beta_m^2)^{-1/2} \right) \quad (1.26)$$

The electric field can be obtained in the plasma-wave frame $\hat{r} \cdot \vec{r} - V_\phi t$ using the Lorentz equation, $m_e c \left(\frac{\beta_z^e}{\beta_\phi} - 1 \right) \frac{d\gamma_z^e \beta_z^e}{d\tau} = -e E_z$. We use the relation in eq.1.26, $\frac{1}{\beta_\phi} \frac{d\gamma_z^e}{d\tau} - \frac{\gamma_z^e \beta_z^e}{d\tau} = \pm \sqrt{2} \omega_{pe} \left((1 - \beta_m^2)^{-1/2} - (1 - \beta_{ez}^2)^{-1/2} \right)^{1/2}$. We have used $d\tau = -\frac{1}{V_\phi} d(\hat{r} \cdot \vec{r} - V_\phi t)$.

$$\beta_z^e \frac{d\gamma_z^e \beta_z^e}{d\tau} = \frac{1}{2\gamma_z^e} \frac{d(\gamma_z^e \beta_z^e)^2}{d\tau} = \frac{1}{2\gamma_z^e} \frac{d(\gamma_z^e)^2 - 1}{d\tau} = \frac{d\gamma_e}{d\tau} \quad (1.27)$$

We use the identity in eq.1.27 to obtain the longitudinal electric field, E_z .

$$\begin{aligned} eE_z &= m_e c \left(\frac{\beta_z^e}{\beta_\phi} \frac{d\gamma_z^e \beta_z^e}{d\tau} - \frac{d\gamma_z^e \beta_z^e}{d\tau} \right) \\ &= m_e c \left(\frac{1}{\beta_\phi} \frac{d\gamma_z^e}{d\tau} - \frac{d\gamma_z^e \beta_z^e}{d\tau} \right) \\ E_z &= \pm \frac{m_e c \omega_{pe}}{e} \sqrt{2} \left((1 - \beta_m^2)^{-1/2} - (1 - \beta_{ez}^2)^{-1/2} \right)^{1/2} \\ E_z &= \pm \frac{m_e c \omega_{pe}}{e} \sqrt{2} (\gamma_m - \gamma_{ez})^{1/2} \end{aligned} \quad (1.28)$$

The maximum of the longitudinal electric field in purely longitudinal oscillations would occur when the oscillating electron trajectory is at its extremum. During the extremum the oscillating electron velocity is zero, $\beta_{ez} = 0$.

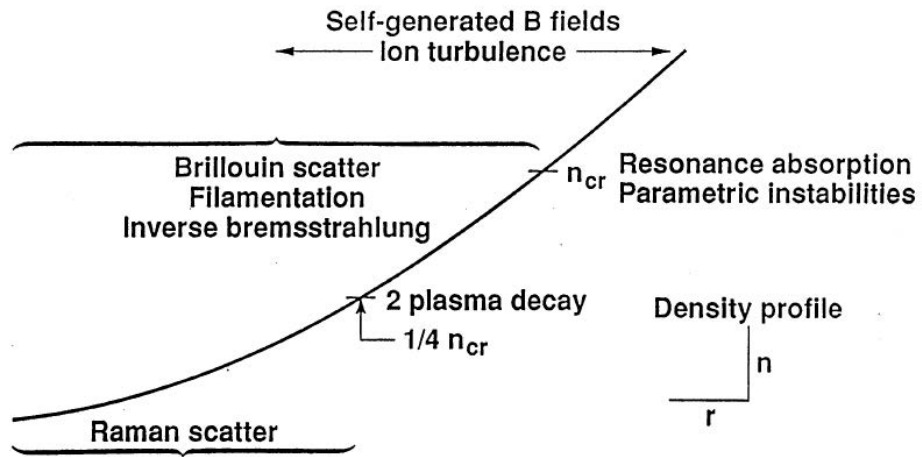
$$E_z^{max} = \frac{m_e c \omega_{pe}}{e} \sqrt{2(\gamma_m - 1)} \quad (1.29)$$

In the low amplitude longitudinal momentum regime, $\gamma_m \simeq 1$, and therefore $\gamma_m = (1 - \beta_m^2)^{-1/2} = 1 + \frac{1}{2}\beta_m^2$. Using this in eq.1.29, we have $E_z^{max} = \frac{m_e c \omega_{pe}}{e} \sqrt{2(1 + \frac{1}{2}\beta_m^2 - 1)}$. So, $E_z^{max}(\gamma_m \sim 1) = \frac{m_e c \omega_{pe}}{e} \beta_m$.

1.6 Plasma Instabilities driven by Laser

The main scattering processes in laser-plasma interaction are as follows and are also shown in Fig.1.1 corresponding to the plasma density at which they have a significant growth rate [8]:

- Ion Acoustic decay instability $\omega_0 \rightarrow \omega_p + \omega_i$ at $n \simeq n_{cr}$
- Raman instability $\omega_0 \rightarrow \omega_p + \omega_{sc}$ at $n \leq \frac{n_{cr}}{4}$



**Many processes compete to determine the coupling.
The mix of these processes depends on the plasma conditions.
The plasma conditions depends on the mix of the processes.**

FIGURE 1.1: Competing laser plasma coupling processes

- Brillouin instability $\omega_0 \rightarrow \omega_p + \omega_{sc}$ at $n \leq n_{cr}$
- Two plasmon decay instability $\omega_0 \rightarrow \omega_p + \omega_{sc}$ at $n \simeq \frac{n_{cr}}{4}$

There are also *kinetic* version of all these processes such as Stimulated Compton scattering. Also other instabilities play a role in coupling energy from laser to plasma, these instabilities are such as filamentation instabilities which occur at $n \leq n_{cr}$.

A feedback process is established during the laser-plasma interactions such that it couples the energy of the plasma modes in density fluctuations back into the laser as a modulation. This further reinforces laser to couple into the modes that dominate the density fluctuations. This feedback loop can be visualized as follows:

- *initial fluctuations* - The laser radiation pressure or ponderomotive forces generate a current by imparting oscillating momentum to the electrons, $\delta J = -e \delta n_e v_{osc} \propto \delta n E_{laser}$.
- *plasma wave excitation* - The current δJ which is a source term in the wave-equation generates a wave whose amplitude is δE .
- *laser field modulation* - This electric field of the plasma can modulate the laser field

$$E_{laser} \rightarrow \delta E. E_{laser}.$$

- *Feedback* - The modulated laser field then modulates the radiation pressure or the ponderomotive force at the same spatial scale as the δE , leading to a mode further reinforcing its own density fluctuations at δn .

Considering the light waves in a plasma and starting with the Ampere's law, $\vec{\nabla} \times \vec{B} = \frac{4\pi\vec{J}}{c} + \frac{1}{c} \frac{\partial \vec{E}}{\partial t}$ and working in terms of the magnetic vector potential, $\vec{B} = \vec{\nabla} \times \vec{A}$ with Coulomb gauge $\vec{\nabla} \cdot \vec{A} = 0$, we have, the Faraday's law in the presence of a potential ϕ as, $\vec{E} = -\vec{\nabla}\phi - \frac{1}{c} \frac{\partial \vec{A}}{\partial t}$. Substituting, $\vec{\nabla} \times \vec{\nabla} \times \vec{A} = \frac{4\pi\vec{J}}{c} + \frac{1}{c} \frac{\partial(-\vec{\nabla}\phi - \frac{1}{c} \frac{\partial \vec{A}}{\partial t})}{\partial t} \Rightarrow \vec{\nabla}(\vec{\nabla} \cdot \vec{A}) + (-\nabla^2 + \frac{1}{c^2} \frac{\partial^2}{\partial t^2}) \vec{A} = \frac{4\pi\vec{J}}{c} - \frac{\partial \vec{\nabla}\phi}{\partial t}$. Considering, the Poisson equation, $\nabla^2\phi = -4e\pi n_e$ and the Continuity equation, $\vec{\nabla} \cdot \vec{J} = -e \frac{\partial n_e}{\partial t}$.

Combining these two we have, $\cancel{\vec{\nabla}} \vec{J}_{longitudinal} = \frac{\partial}{\partial t} \frac{\nabla^2 \phi}{4\pi}$. And, transverse component of the current drives the wave, thereby, $(-\nabla^2 + \frac{1}{c^2} \frac{\partial^2}{\partial t^2}) \vec{A} = \frac{4\pi}{c} \vec{J}_{transverse} + \cancel{\frac{4\pi}{c} \vec{J}_{longitudinal}} - \cancel{\frac{\partial \vec{\nabla}\phi}{\partial t}}$. If it is assumed that $\vec{A} \cdot \vec{\nabla} n_e = 0$, then the transverse current simplifies as $\vec{J}_{transverse} = en_e \vec{v}_e^\perp$. When $v_e^\perp \ll c$, $m_e \frac{\partial \vec{v}_e^\perp}{\partial t} = -e \vec{E}_\perp = -\frac{e}{cm_e} \left(-\frac{\partial \vec{A}}{\partial t} \right) \Rightarrow \vec{v}_e^\perp = \frac{e}{cm_e} \vec{A}$. Thereby, $J_{transverse} = en_e \left(\frac{e}{cm_e} \vec{A} \right)$ and when replaced into the transverse wave equation, $(-\nabla^2 + \frac{1}{c^2} \frac{\partial^2}{\partial t^2}) \vec{A} = \frac{4\pi e^2 n_e}{c^2 m_e} \vec{A}$.

Since, the magnetic vector potential has two contributing terms, one from the Laser field itself and the other *scattered component* from the plasma density fluctuations being excited by the interaction with the laser, $\vec{A} = \vec{A}_{laser} + \vec{A}_{scattered}$. We have the wave equation where there is interaction of laser field and the density fluctuations (modeled as a current), $(-c^2 \nabla^2 + \frac{\partial^2}{\partial t^2} - \omega_{pe}^2) \vec{A}_{scattered} = \frac{4\pi e^2 n_e}{m_e} \vec{A}_{laser}$. The left hand side of the equation has only the scattered component because we know the dispersion relation of the transverse component of the laser field, $(-c^2 \nabla^2 + \frac{\partial^2}{\partial t^2} - \omega_{pe}^2) \vec{A}_{laser} = 0$.

Raman instability is due to an electron plasma wave coupling with the incident laser

field and modulating it. Hence, considering a warm electron fluid (n_e, u_e, p_e) with fixed background ions, we have, the Continuity equation, $\vec{\nabla} \cdot \vec{J} = -e \frac{\partial n_e}{\partial t} \Rightarrow \vec{\nabla} \cdot n_e \vec{u}_e = \frac{\partial n_e}{\partial t}$.

And, the Vlasov equation is, $\frac{\partial \vec{u}_e}{\partial t} + \vec{u}_e \vec{\nabla} \cdot \vec{u}_e + \frac{e}{m_e} \left(\vec{E} + \frac{\vec{u}_e \times \vec{B}}{c} \right) = -\frac{\vec{\nabla} \vec{p}_e}{n_e m_e} \Rightarrow \frac{\partial \vec{u}_e}{\partial t} + \frac{1}{2} \vec{\nabla} \cdot \vec{u}_e^2 + \frac{e}{m_e} \left(\vec{E} + \frac{\vec{u}_e \times \vec{B}}{c} \right) = -\frac{\vec{\nabla} \vec{p}_e}{n_e m_e}$. Now, the hot electron velocity can be expressed as, $\vec{u}_e = \vec{u}_L + \vec{a} \left(= \frac{e \vec{A}}{m_e c} \right)$. The Vlasov equation then gives us the dispersion relation for the warm plasma,

$$\frac{\partial \vec{u}_L}{\partial t} + \cancel{\frac{\partial \vec{A}}{\partial t} \frac{e \vec{A}}{m_e c}} = -\frac{1}{2} \vec{\nabla} \cdot \left(\vec{u}_L + \frac{e \vec{A}}{m_e c} \right)^2 - \frac{e}{m} \left(-\vec{\nabla} \phi - \cancel{\frac{1}{c} \frac{\partial \vec{A}}{\partial t}} + \frac{(\vec{u}_L + \frac{e \vec{A}}{m_e c}) \times (\vec{\nabla} \times \vec{A})}{c} \right) - \frac{\vec{\nabla} \vec{p}_e}{n_e m_e} \Rightarrow \frac{\partial \vec{u}_L}{\partial t} =$$

$$\frac{e}{m_e} \vec{\nabla} \phi - \frac{1}{2} \vec{\nabla} \cdot \left(\vec{u}_L + \frac{e \vec{A}}{m_e c} \right)^2 - \frac{e}{m_e c} \left(\vec{\nabla} \cdot \left[\left(\vec{u}_L + \frac{e \vec{A}}{m_e c} \right) \cdot \vec{A} \right] - \vec{A} \left[\vec{\nabla} \cdot \left(\vec{u}_L + \frac{e \vec{A}}{m_e c} \right) \right] \right) - \frac{\vec{\nabla} \vec{p}_e}{n_e m_e} \Rightarrow$$

$$\frac{\partial \vec{u}_L}{\partial t} = \frac{e}{m_e} \vec{\nabla} \phi - \frac{1}{2} \vec{\nabla} \cdot \left(\vec{u}_L + \frac{e \vec{A}}{m_e c} \right)^2 - \frac{\vec{\nabla} \vec{p}_e}{n_e m_e}. \text{ Linearizing the equations, we have, } n_e = n_i +$$

$$\tilde{n}_e, \vec{A} = \vec{A}_{laser} + \vec{A}_{scattered}, \phi = \tilde{\phi}. \text{ We obtain, } n_0 \vec{\nabla} \cdot \vec{u}_e + \frac{\partial \tilde{n}_e}{\partial t} = 0, \frac{\partial \vec{u}_L}{\partial t} = \frac{e}{m_e} \vec{\nabla} \tilde{\phi} -$$

$$\frac{e^2}{m_e^2 c^2} \vec{\nabla} \cdot \vec{A}_L \cdot \vec{A}_{scattered} - \frac{3v_e^2 \vec{\nabla} \tilde{n}_e}{n_0} \text{ and, } \nabla^2 \phi = 4\pi e \tilde{n}_e. \text{ Taking time derivative of the linearized}$$

$$\text{Continuity equation, } n_0 \vec{\nabla} \cdot \frac{\partial \vec{u}_e}{\partial t} + \frac{\partial^2 \tilde{n}_e}{\partial t^2} = 0, \text{ and taking the divergence of the dispersion}$$

$$\text{relation for the warm plasma, } \frac{\partial \vec{\nabla} \vec{u}_L}{\partial t} = \frac{e}{m_e} \vec{\nabla}^2 \tilde{\phi} - \frac{e^2}{m_e^2 c^2} \nabla^2 \vec{A}_L \cdot \vec{A}_{scattered} - \frac{3v_e^2 \nabla^2 \tilde{n}_e}{n_0}. \text{ Using the}$$

Poisson equation, we get, the dispersion relation due to the density fluctuations modulating

$$\text{the laser field, } \left(\frac{\partial^2}{\partial t^2} + \omega_{pe}^2 - 3v_e^2 \nabla^2 \right) \tilde{n}_e - \frac{n_0 e^2}{m_e^2 c^2} \nabla^2 \vec{A}_L \cdot \vec{A}_{scattered}.$$

Fourier analyzing the dispersion relation by taking the harmonic excitation of the laser field, $\vec{A}_L = \vec{A}_0 \cos(k_0 z - \omega_0 t)$, we get, fourier domain dispersion of the scattered light,

$$(\omega^2 - k^2 c^2 - \omega_{pe}^2) \vec{A}_{scattered}(\vec{k}, \omega) = \frac{4\pi e^2}{2m_e} \vec{A}_0 [\tilde{n}_e(k - k_0, \omega - \omega_0) - \tilde{n}_e(k + k_0, \omega + \omega_0)] \text{ and,}$$

the fourier domain dispersion relation of the density fluctuations, $(\omega^2 - \omega_{ek}^2) \tilde{n}_e(\vec{k}, \omega) =$

$$\frac{k^2 e^2}{2m_e^2 c^2} A_0 \left[\vec{A}_{scat}(k - k_0, \omega - \omega_0) - \vec{A}_{scat}(k + k_0, \omega + \omega_0) \right], \text{ where } \omega_{ek} = (\omega^2 + 3v_e^2 k^2)^{\frac{1}{2}}. \text{ Eliminating } A_0 \text{ from the equation, with } \omega_0 = \omega_{pe} \text{ and neglecting the higher frequency difference}$$

non-resonant terms $\tilde{n}_e(k - 2k_0, \omega - 2\omega_0), \tilde{n}_e(k + 2k_0, \omega + 2\omega_0)$, we get the Fourier do-

$$\text{main dispersion, } (\omega^2 - \omega_{ek}^2) = \frac{\omega_{pe}^2 k^2 v_{osc}^2}{4} \left[\frac{1}{D(k - k_0, \omega - \omega_0)} + \frac{1}{D(k + k_0, \omega + \omega_0)} \right], \text{ where, } D(k, \omega) =$$

$$\omega^2 - c^2 k^2 - \omega_{pe}^2.$$

For back or side scattered light, we can neglect the *upshifted*, $D(k + k_0, \omega + 2\omega_0) \Rightarrow D^+$ wave, $(\omega^2 - \omega_{ek}^2) D^- = \frac{\omega_{pe}^2 k^2 v_{osc}^2}{4}$, and take $\omega = \omega_{ek} + \delta\omega$ & $\delta\omega \ll \omega_{ek}$. The maximum side or back-scatter growth occurs when the frequency of these waves is *resonant* with the frequency of the exciting laser, $(\omega_{ek} - \omega_0)^2 - c^2(k - k_0)^2 - \omega_{pe}^2 = 0$. Then $\delta\omega = i\gamma$, the instability growth rate is, $\gamma = \frac{kv_{osc}}{4} \left[\frac{\omega_{pe}^2}{\omega_{ek}(\omega_0 - \omega_{ek})} \right]$, for $k = k_0 + \frac{\omega}{c} \left(1 - \frac{2\omega_{pe}}{\omega_0} \right)^{\frac{1}{2}}$.

The *Raman instability* on a linear density profile with scale length α , has the threshold condition of $\frac{v_{osc}}{c} \geq \frac{2}{k_0\alpha} \left(\frac{v_{gs}}{c} \right)$, where, v_{gs} is the group velocity of the scattered light. Raman scattering can change the light absorption (*efficiency*) into the medium due to backscatter or changing the location (*symmetry*) of the maximum absorption. The electron plasma wave generated can result in hot electrons that change the plasma characteristics.

The *Brillouin instability* has both the electron and the ion thermal velocity. The dispersion relation, $\omega^2 - k^2 c_s^2 = \frac{k^2 v_{osc}^2 \omega_{pi}^2}{4} \left[\frac{1}{D(k-k_0, \omega-\omega_0)} + \frac{1}{D(k+k_0, \omega+2\omega_0)} \right]$, where, $c_s = \sqrt{\frac{ZT_e}{M}}$ and $\omega_{pi} = \omega_{pe} \sqrt{\frac{Zm_e}{M_i}}$.

The *Filamentation instability* can also be obtained from the same dispersion relation as the Brillouin instability. In this instability the modulation in the density fluctuations are amplified. In *Ponderomotive filamentation*, there is high enough density fluctuations and depletion due to the light pressure. In *Thermal filamentation*, there is density fluctuations due to collisional heating and plasma expansion.

From experiments and computer simulations it has been found that the collective plasma effects due to the plasma waves have the following scaling laws:

- effects are more potent in *long scale-length* plasmas
- reduce with *shorter laser wavelength* light
- reduce with laser beam *incoherence*

There is also observation of *supra-thermal* electrons being generated.

1.7 Particle-In-Cell simulations: short introduction

For a deeper understanding of the structure and magnitude of the linear and non-linear plasma wake, visualization with Particle-in-Cell (PIC) simulations results is very useful. It is also quite useful to verify analytical models developed using fluid and kinetic equations, as we will show later in this thesis.

We briefly introduce PIC particle tracking simulation in this section. For further exploration into this subject, extensive literature is available, most significantly the textbook titled “Plasma Physics via Computer Simulation” by CK Birdsall and AB Langdon [22].

Particle-in-Cell computational method

Analytically solving for the exact motion of all the plasma electrons using the governing equations - the Maxwell equations for fields and the equations of motion for electrons, is not possible when describing wakes in higher dimensions or under non-linear density perturbation. The Maxwell’s equations describe the electric and magnetic fields generated by spatial configuration and velocities of the individual particles and the equations of motion of plasma electron use these fields to provide a description of the motion of particles.

Under approximations regarding the “time-scales” and “spatial-scales” of the problem under consideration - certain terms in the plasma physics equations are negligible. These terms in plasma physics equation represent different physical effects that become relevant or irrelevant in accordance to the scales of the problem. There are two important classifications of the plasma physics effects - (i) time-scales: collisional and collision-less effects and (ii) spatial-scales: averaged (fluid) and individual particles (Kinetic).

Fortunately, computers can be used to solve the set of equations for field and particle motion for individual electrons while also taking into account the effect spatial configuration and velocities of other electrons having an effect on the electron under consideration. It is well known that time-domain methods for solving Maxwell’s equation use a spatial grid to discretize the space that has to be modeled and step in time to advance the fields in time over the entire space. The most common method to implement this scheme is

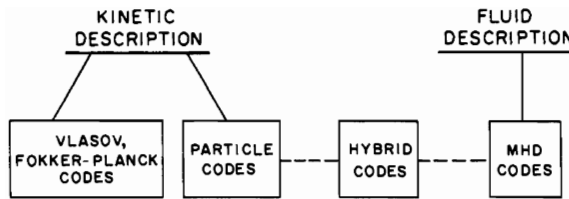


FIGURE 1.2: *Classification of plasma physics codes based upon different time and spatial scales.* Different spatial and time-scales of the problem leading to different codes (reproduced from [22]).

Finite-Difference Time-Domain (FDTD) method [17]. This method uses a staggered grid for electric and magnetic fields to allow the curls to align in space. It also uses the time leapfrog method to advance the time-step.

Particle-In-Cell (PIC) is a time-domain method and it ignores full calculations of collision terms. It inherently provides the kinetic description. The algorithm uses a time-domain electromagnetic solver in conjunction with particle pushers to implement the Lorentz force equation. However, when particles are involved - it is important to conserve total particle number and several other constraints are imposed on the computational formulations. One may imagine that using this solver all the particles in a problem could be simulated using the computer. However, this is not possible as it would lead to currently unreachable memory demands or equivalently require unattainable computational power. Even if the problem is parallelized several million individual processors may be required to work in conjunction to track all the particles over the simulation volume of the problem. As an example a plasma of dimensions ten times the Ti:Sapphire laser wavelength - $100 \mu\text{m} \times 100 \mu\text{m} \times 100 \mu\text{m}$ with a plasma of density $n_0 = 10^{18}\text{cm}^{-3}$ about 10^{12} -Trillion particles have to be tracked. To overcome this particle number requirement a *macro-particle* is chosen out of a set of particle that are together in the phase-space.

The Lorentz force equation is applied onto the macro-particle at every half-time step. Once the particles have been pushed fields are recalculated using the Maxwell's equation. To model reasonable interaction between the particles in real-space and grid at discretized space, the particle density is deposited onto the grid using a charge distribution method,

where the grid points that are nearest neighbors get deposited with charge weighted by its distance from the point.

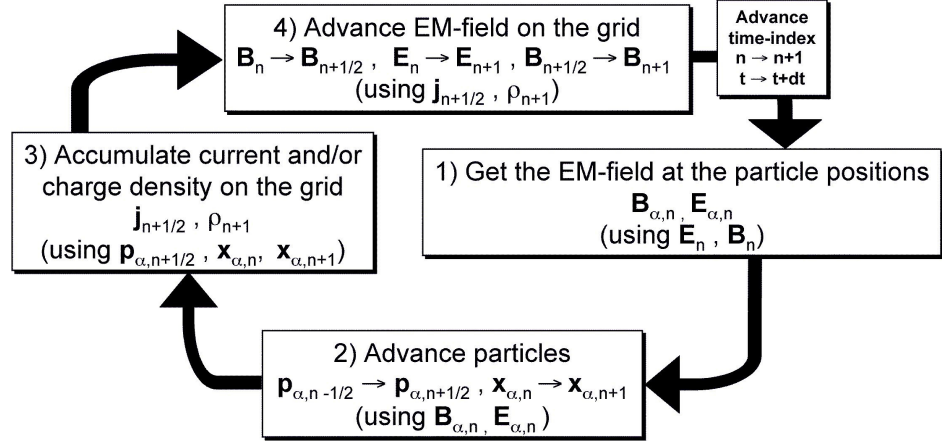


FIGURE 1.3: *Time advance loop for the Particle in Cell codes.* Time-advance of PIC simulations used for computationally solving the set of Maxwell, Lorentz and fluid equations in the time-domain for a set of particles used to represent the plasma. (reproduced from [15]). This shows the sequence in which the Maxwell's equations are solved on a grid to obtain the fields. Subsequently, these fields are used to calculate the force on each of the particle from the fields. The particle position and momentum are updated in accordance with the Lorentz equation. The updated source terms in the Maxwell's equations namely, particle density and particle current, are now used to calculate the fields.

1.8 Linear vs. Non-linear plasma-waves

Linear wake with small density perturbation are shown in Fig.1.6 for a laser driver and Fig.1.7 for an electron beam driven wake.

When the density perturbation $\delta n = n - n_0$ where n is the electron density in a perturbation is such that $\delta n \ll 1$ then the fluid equations can be linearized in the first-order of perturbation δ . However, as the energy sources coupling into the plasma becomes more intense (power density) they can drive larger density perturbations. Under the strong perturbation condition $\mathcal{O}(\delta^2)$ terms are not negligible and the equations have to retain all the higher-order terms. In the quasi-non-linear and the non-linear regime generally full analytical solutions are not possible and numerical solutions are used to characterize them.

1.8.1 Linear plasma electron waves

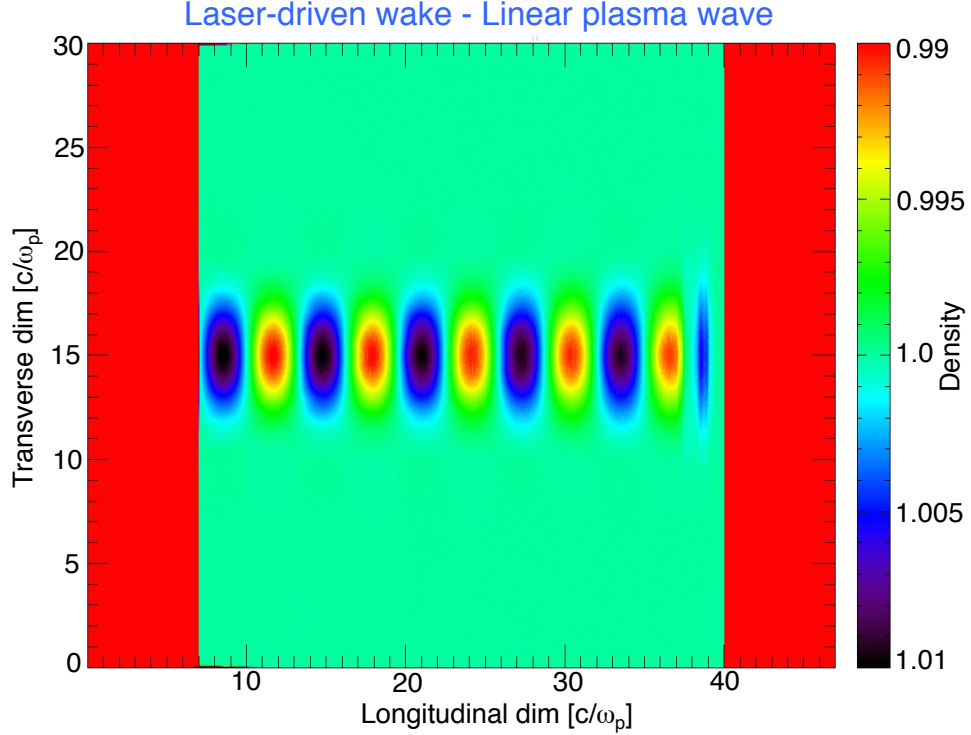


FIGURE 1.4: *The spatial profile and on-axis line-out of normalized plasma electron density in 2D cartesian space for a linear laser wake from Particle-in-Cell (PIC) simulations.* The laser pulse has Gaussian radial profile of full-width at half maximum (FWHM) radius of $4\frac{c}{\omega_{pe}}$ launched at the transverse dimension of $15\frac{c}{\omega_{pe}}$. The peak normalized laser vector potential is $a_0 = 0.1$ and the FWHM pulse length is about $2\frac{c}{\omega_{pe}}$. The laser frequency to plasma frequency ratio of $\frac{\omega_0}{\omega_{pe}} = 10$. The density perturbation in this case is $\delta n = 0.01$. Importantly note that $\delta n \propto a_0^2 = 0.01$.

Upon expanding the perturbed density in terms of δ or the wave potential Φ ,

$$n = n^{(0)} + n^{(1)} + n^{(2)} + \mathcal{O}(n^{(3)})$$

and noting that $n^{(1)} \propto \frac{\partial}{\partial r} n = 0$. The Poisson equation up to the second-order under this perturbative expansion is

$$\nabla^2 \phi = k_{pe}^2 \left(1 + \frac{n^{(2)}}{n_0} - 1 \right) = k_{pe}^2 \frac{n^{(2)}}{n_0}$$

under the fact that $n^{(0)} = n_0$.

The second-order continuity equation is $\frac{1}{c} \frac{\partial}{\partial t} \frac{n^{(2)}}{n_0} + \vec{\nabla}_r \cdot \vec{\beta}^{(2)} = 0$.

Upon taking the divergence of the longitudinal momentum eq.1.18, $\vec{\nabla} \cdot \vec{\nabla} \phi = \frac{1}{c} \frac{\partial}{\partial t} (\vec{\nabla} \cdot \hat{\|}) \gamma \beta_{\parallel} + \vec{\nabla} \cdot \vec{\nabla} \gamma$.

For *linear density perturbation* and *linear plasma-waves* we make some important approximations. The first approximation is the intensity is small, $\langle a \rangle^2 \ll 1$ then $\gamma = \sqrt{1 + [\gamma \beta_{\perp}]^2 + [\gamma \beta_{\parallel}]^2} = \sqrt{1 + a_{\perp}^2 + \left(\frac{1}{2\gamma} \nabla a_{\perp}^2\right)^2} \simeq 1$. Using this we can write $\vec{\nabla} \gamma \beta_{\parallel} \hat{\|} = \gamma \nabla \beta_{\parallel} + \beta_{\parallel} \nabla \gamma = \gamma \nabla \beta_{\parallel}$.

The second approximation we make is the 1-D approximation assuming that the linear plasma waves have no transverse gradient and are perfectly planar. Under this approximation $\nabla_{\perp}(\phi - \gamma) = 0$ and $\vec{\beta}^{(2)} = \beta_{\parallel} \hat{\|}$. Also, the ponderomotive force $\nabla \gamma = \frac{1}{2\gamma} \nabla a_{\perp}^2 \simeq \frac{1}{2} \nabla a_{\perp}^2$.

Under these approximations we obtain the linear plasma-wave equations as follows,

$$\begin{aligned} \left(\frac{1}{c^2} \frac{\partial^2}{\partial t^2} + k_{pe}^2 \right) \frac{n^{(2)}}{n_0} &= \nabla^2 \frac{a_{\perp}^2}{2} \\ \left(\frac{1}{c^2} \frac{\partial^2}{\partial t^2} + k_{pe}^2 \right) \phi &= k_{pe}^2 \frac{a_{\perp}^2}{2} \\ \left(\frac{1}{c^2} \frac{\partial^2}{\partial t^2} + k_{pe}^2 \right) [\gamma \beta_{\parallel}] &= -\frac{1}{c} \frac{\partial}{\partial t} \nabla \frac{a_{\perp}^2}{2} \end{aligned} \quad (1.30)$$

In the case of linear plasma-waves driven by an electron beam of density n_b the equations are as follows,

$$\begin{aligned} \left(\frac{1}{c^2} \frac{\partial^2}{\partial t^2} + k_{pe}^2 \right) \frac{n^{(2)}}{n_0} &= -k_{pe}^2 \frac{n_b}{n_0} \\ \left(\frac{1}{c^2} \frac{\partial^2}{\partial t^2} + k_{pe}^2 \right) \phi &= 0 \\ \left(\frac{1}{c^2} \frac{\partial^2}{\partial t^2} + k_{pe}^2 \right) [\gamma \beta_{\parallel}] &= k_{pe}^2 \int_{-\infty}^{\infty} \frac{1}{c} \frac{\partial}{\partial t} \frac{n_b(z)}{n_0} dz \end{aligned} \quad (1.31)$$

Using the Green's function method of solving in-homogenous equations, we can obtain analytical solutions to equations eq.1.30. The solution to the longitudinal momentum equation in the frequency form using the well known Green's function solution is,

$$[\gamma(t)\beta_{\parallel}(t)] = -\frac{c}{\omega_{pe}} \int_0^{\infty} ds \sin(\omega_{pe}[t-s]) \nabla \frac{\partial}{\partial s} \frac{a_{\perp}^2}{2} \quad (1.32)$$

Similarly the solution for the linear plasma-wave equation for the potential in the frequency form using the Green's function method is

$$\phi(t) = \omega_{pe} \int_0^{\infty} ds \sin(\omega_{pe}[t-s]) \frac{a_{\perp}^2(s)}{2}.$$

The electric field can thus be obtained by taking the gradient of the scalar potential, $E = -\nabla\Phi = -\frac{m_e c^2}{e} \nabla\phi$ and using the definition of the wave-breaking electric field limit for a non-relativistic plasma-wave in cold-plasma, $E_{wb} = \frac{m_e c \omega_{pe}}{e}$. Therefore,

$$E = -c E_{wb} \int_0^{\infty} ds \sin(\omega_{pe}[t-s]) \nabla \frac{a_{\perp}^2(s)}{2}.$$

1.8.2 Non-linear plasma electron waves

Non-linear waves cannot be analyzed using the perturbation theory. They are thus analyzed just behind the drive and the coordinate used is the distance behind the plasma-wave phase-velocity front, $v_{\phi}^p t$.

An important assumption is made for the energy-source driving the wake - the shape of the driver does not vary at short-distances behind the driver. For instance, it is known that the laser pulse undergoes longitudinal compression and frequency shifts while also undergoing transverse self-focussing over scale-lengths much longer than the plasma wavelength. Similarly an electron-beam is known to lose particles at its head from energy loss and due to lack of transverse forces just at the head. A beam may also undergo transverse oscillations of its tail while the head is stable. However, it is assumed that such process

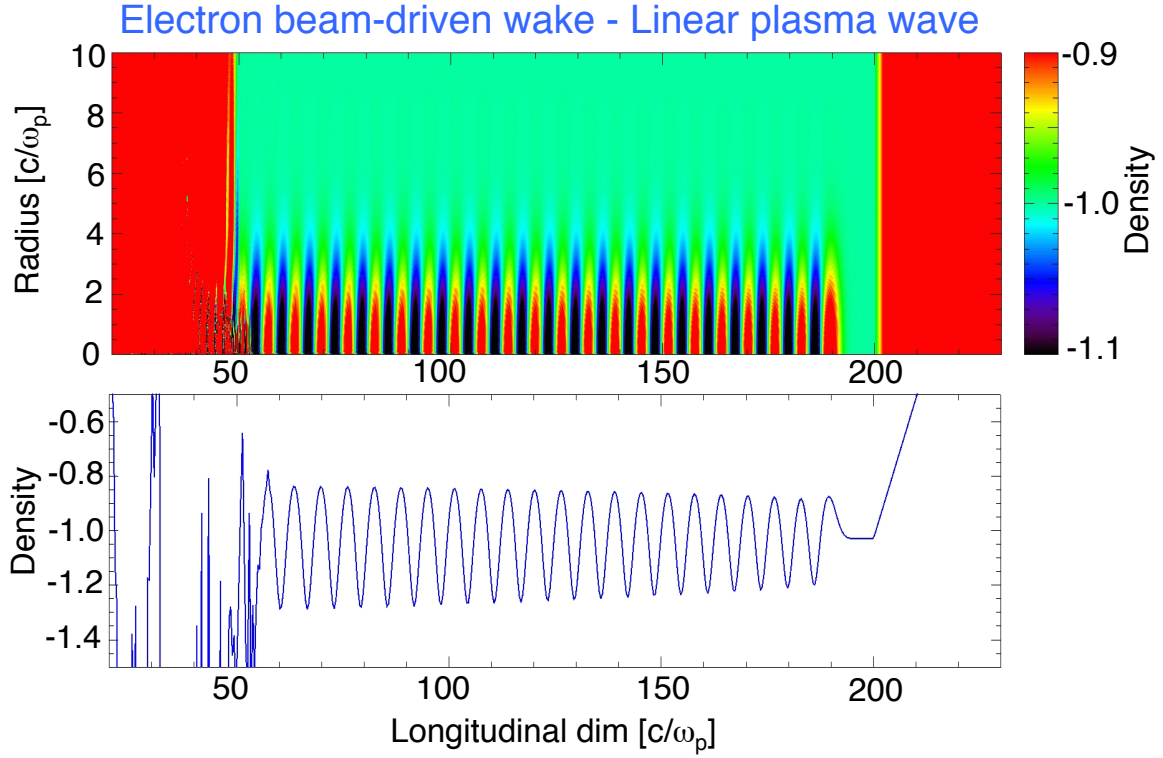


FIGURE 1.5: *The spatial profile of normalized plasma electron density in 2D cylindrical space for a linear electron-beam driven wake from Particle-in-Cell (PIC) simulations.* The electron beam has Gaussian radial and longitudinal profile of $\sigma_r = 2.0 \frac{c}{\omega_{pe}}$ and $\sigma_z = 1.5 \frac{c}{\omega_{pe}}$. The peak beam density is $\frac{n_b}{n_0} = 0.1$. The density perturbation in this case is $\delta n = 0.1$. Importantly note that $\delta n \propto n_b = 0.1$.

occur over several plasma wavelengths. Thus, the dynamics of the driving energy-sources is of time-scales about an order of magnitude longer than the plasma wavelength. So, under time-scale considerations the driver shape is assumed to be constant. This approximation is referred to as *quasi-static approximation*.

$$\begin{aligned}
 z - v_\phi^p t &= \xi \\
 \frac{\partial}{\partial z} &= \frac{\partial}{\partial \xi} \\
 \frac{\partial}{\partial t} &= -v_\phi^p \frac{\partial}{\partial \xi}
 \end{aligned} \tag{1.33}$$

Using this coordinate transform the fluid equations can be transformed as,

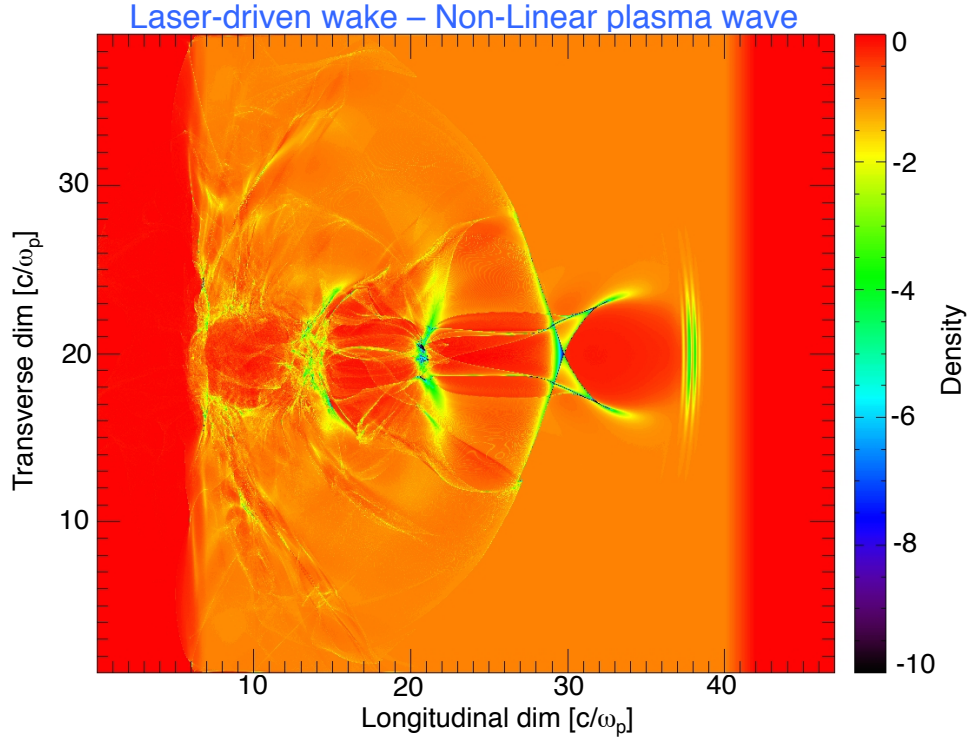


FIGURE 1.6: *Non-linear laser wake spatial profile of plasma electron density in 2D cartesian space from Particle-in-Cell (PIC) simulations.* The laser-pulse has Gaussian radial profile of FWHM radius of $2\frac{c}{\omega_{pe}}$ launched at the transverse dimension of $20\frac{c}{\omega_{pe}}$. The peak normalized laser vector potential is $a_0 = 1.0$ and the FWHM pulse length is about $14\frac{c}{\omega_{pe}}$. The laser frequency to plasma frequency ratio of $\frac{\omega_0}{\omega_{pe}} = 10$.

$$n = \frac{\beta_\phi^p n_0}{(\beta_\phi^p - \beta_\parallel)}$$

$$\gamma = \sqrt{1 + [\gamma\beta_\perp]^2 + [\gamma\beta_\parallel]^2}$$

$$= \sqrt{1 + a_\perp^2 + [\gamma\beta_\parallel]^2}$$

$$\gamma = 1 + \phi + \beta_\phi^p [\gamma\beta_\parallel]$$

$$\gamma = \frac{1 + \phi}{(1 - \beta_\phi^p \beta_\parallel)} \quad (1.34)$$

We can determine the longitudinal momentum in terms of the scalar, ϕ and vector potential, a_\perp using the Lorentz factor and its dependence on ϕ and a_\perp in eq.1.34.

$$\begin{aligned}
[\gamma \beta_{\parallel}] &= \frac{p_{\parallel}}{m_e c} \\
&= \gamma_{\phi}^2 \left[\beta_{\phi}^p (1 + \phi) - \sqrt{(1 + \phi)^2 - \gamma_{\phi}^{p-2} (1 + a_{\perp}^2)} \right]
\end{aligned} \tag{1.35}$$

Using the longitudinal momentum to determine the density perturbation in eq.1.34, n/n_0 as,

$$\begin{aligned}
\gamma &= \gamma_{\phi}^{p-2} (1 + \phi) \left(1 - \beta_{\phi}^p \sqrt{1 - \frac{\gamma_{\phi}^{p-2} (1 + a_{\perp}^2)}{(1 + \phi)^2}} \right) \\
\frac{n}{n_0} &= \beta_{\phi}^p \gamma_{\phi}^{p-2} \left(\left\{ 1 - \frac{(1 + a_{\perp}^2)}{\gamma_{\phi}^{p-2} (1 + \phi)^2} \right\}^{-1/2} - \beta_{\phi}^p \right)
\end{aligned} \tag{1.36}$$

Substituting the density perturbation into the transformed 1-D Poisson equation we obtain,

$$\begin{aligned}
\frac{\partial^2}{\partial \xi^2} \phi &= k_{pe}^2 \left(\frac{n}{n_0} - 1 \right) \\
&= k_{pe}^2 \gamma_{\phi}^{p-2} \left[\beta_{\phi}^p \left\{ 1 - \frac{(1 + a_{\perp}^2)}{\gamma_{\phi}^{p-2} (1 + \phi)^2} \right\}^{-1/2} - 1 \right]
\end{aligned} \tag{1.37}$$

Under the plasma density driven by an electron beam we include the beam density, n_b in the perturbed density equation,

$$\begin{aligned}
\frac{\partial^2}{\partial \xi^2} \phi &= k_{pe}^2 \left(\frac{n}{n_0} + \frac{n_b}{n_0} - 1 \right) \\
&= k_{pe}^2 \frac{n_b}{n_0} + k_{pe}^2 \gamma_{\phi}^{p-2} \left[\beta_{\phi}^p \left\{ 1 - \frac{(1 + a_{\perp}^2)}{\gamma_{\phi}^{p-2} (1 + \phi)^2} \right\}^{-1/2} - 1 \right]
\end{aligned} \tag{1.38}$$

Numerical solutions and special-case analytical solutions to eq.1.38 show that as the non-linearity of the excitation of plasma electron density increases (and the amplitude of

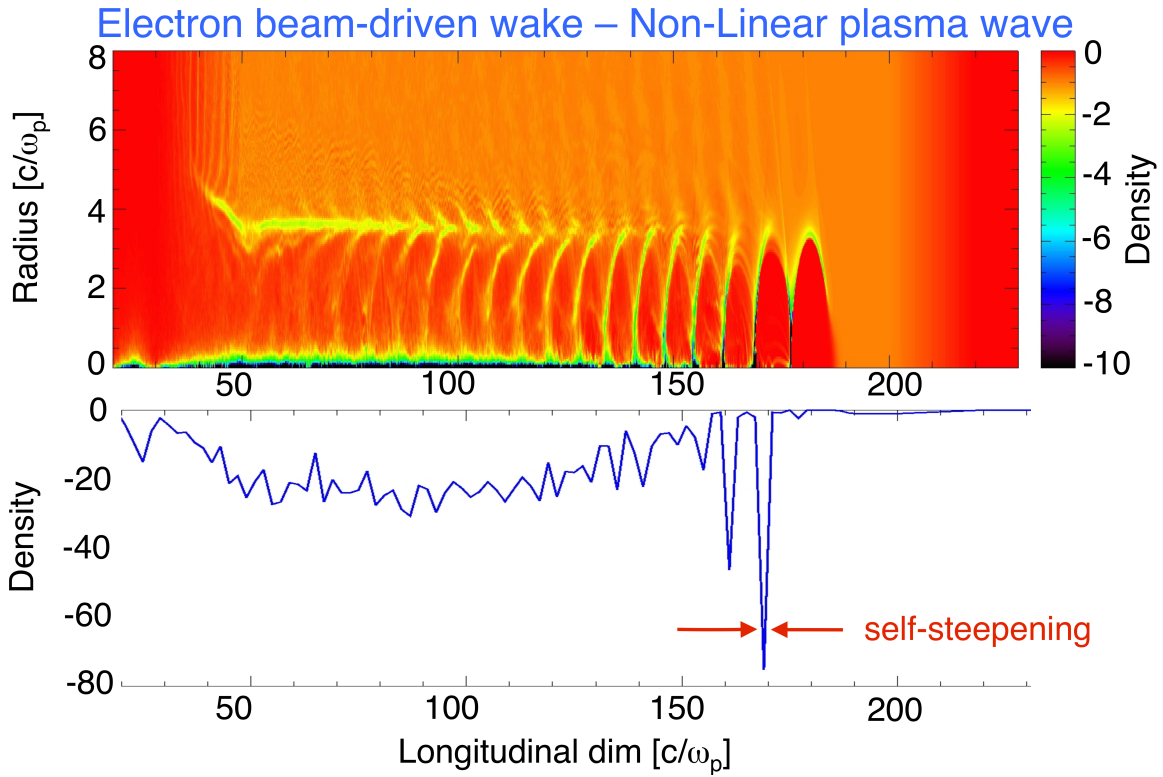


FIGURE 1.7: The spatial profile and on-axis line-out of normalized plasma electron density in 2D cylindrical space for a linear electron-beam driven wake from Particle-in-Cell (PIC) simulations. The electron beam has Gaussian radial and longitudinal profile of $\sigma_r = 2.0 \frac{c}{\omega_{pe}}$ and $\sigma_z = 1.5 \frac{c}{\omega_{pe}}$. The peak beam density is $\frac{n_b}{n_0} = 10$.

plasma-wave) with $a_\perp > 1$ the plasma-wave steepens and its period increases. Under the non-linear plasma wave density condition the electric-field and potential wave-forms are not sinusoidal but exhibit “wave-steepening” and take the form of asymmetric spikes. The non-linear plasma wavelength is longer than the sinusoidal plasma wavelength, $\lambda_{Np} > \lambda_{pe}$.

Chapter

2

Phase-mixing, Trajectory-crossing and Trapping of Plasma Electrons

As outlined in the introduction section there are non-linear wave phenomenon which cause a fraction of electrons oscillating in the plasma electron wave to lose coherence with the wave. Such electrons are then subject to fields excited by the electrons oscillating within the plasma wave. It is also importantly noted that any equations or inferences based upon the fluid equations are inaccurate once there is onset of effects associated with the non-linearities.

The non-linear phenomenon can be classified broadly into two types: (a) non-linearity of the excited plasma wave (b) non-linear effects induced by the driver. Non-linearity of the first-type are - trajectory crossing which could be due to the wave geometry, density inhomogeneity or amplitude, wave steepening due to the modulation of particle velocities by the potential, sufficiently high potential of the wave trapping the background electrons etc. The second-type effects are - driver induced spatial profile of the potential and particle velocities, driven electrons overshooting, the wave phase velocities etc.

In this section we study the non-linear phenomenon associated with electron oscillations and try to understand the time duration it takes for these effects to manifest their effect on the wave.

However, when some of the electrons get out-of-phase with the electron-plasma-wave

and experience the potential of the wave they can be trapped to a phase-node of the wave. And the electrons that are trapped within the potential well of the wave can continuously experience the electric field and gain energy.

2.1 Non-linear plasma electron oscillations

2.1.1 Non-linear 1D plasma oscillations - Amplitude dependent

It is interesting to better understand the non-linearity of planar 1-D electron oscillations in a cold plasma. Considering the displacement $\xi(x_0, t)$ of the electron sheet from its equilibrium position, x_0 then the position of the displaced electron sheet is $x = x_0 + \xi$. The displacement of electron sheet leaves behind a net positive charge of $n_+ = en_0\xi$. Ahead of the displaced electron sheet there is a net negative electron charge, $n_- = -en_0\xi$. Thus from the Gauss's law we can determine the electric field on the electron sheet due to the unshielded positive charge, $\vec{\nabla}E = en_0\xi$. Since the problem is purely planar and 1-D the electric field at the location of the electron sheet is $E = 4\pi en_0\xi$. The equation of motion of the electron sheet is $\frac{d^2\xi}{dt^2} = -\frac{e}{m_e}E = -\frac{4\pi e^2 n_0}{m_e}\xi = -\omega_{pe}^2\xi$. In a familiar form the equation of motion is, $\left(\frac{d^2}{dt^2} + \omega_{pe}^2\right)\xi = 0$. The general solutions are $\xi(x_0, t) = \Xi_1(x_0) \cos(\omega_{pet}t) + \Xi_2(x_0) \sin(\omega_{pet}t)$ where Ξ_1, Ξ_2 depend upon the initial or boundary conditions and are arbitrary functions of x_0 .

So, under the linear approximation where the displaced electron sheets maintain their initial ordering, each of the electron sheets executes independent simple harmonic oscillations. In other words the oscillations do not depend upon the amplitude and are independent of the motion of other electron sheets. With this simple behavior under the linear approximation we can build a physical picture of the break-down of the approximation and onset of non-linearity. We consider another electron sheet whose equilibrium position is at a distance $\Delta x_0 > 0$ away from x_0 . Its amplitude of oscillation is $x_2 = x_0 + \Delta x_0 + \xi_2$. If $\xi_2 = \xi$ then the sheets are perfectly ordered. However, if its amplitude is such $\xi_2 < \xi - \Delta x_0$ then the second sheet would be out of order. This is because the second displaced sheet would

be ahead of the first one which is reverse order of their initial positions. Using this very simple picture originally presented in [4] we can write a very simple condition under which the linear approximation holds, $\lim_{\Delta \rightarrow 0} \frac{\Delta\xi}{\Delta x_0} = \frac{\xi_2 - \xi}{(x_0 + \Delta x_0) - x_0} > \frac{\xi - \Delta x_0 + \xi}{(x_0 + \Delta x_0) - x_0} = \frac{-\Delta x_0}{\Delta x_0} = -1$ giving,

$$\frac{\partial\xi}{\partial x_0} > -1 \quad (2.1)$$

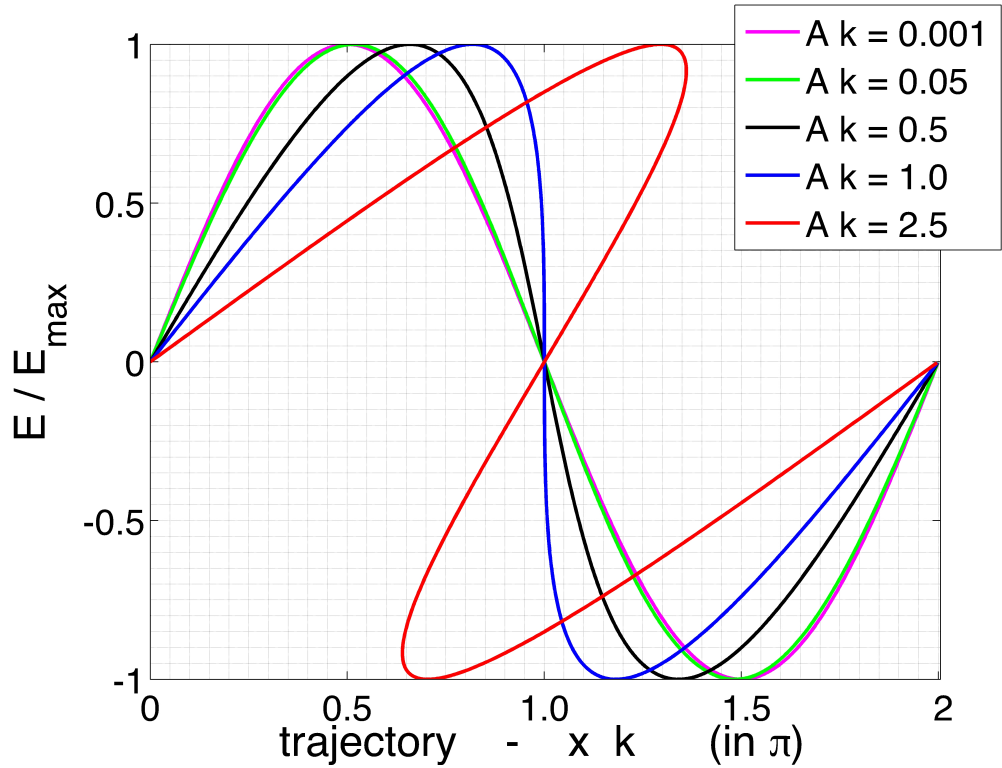


FIGURE 2.1: *The spatial profile of 1D normalized electric field in a plasma of planar electron sheets with respect to instantaneous displacement of a sheet x from its equilibrium position x_0 . The amplitude of the displacement of an electron sheet is $\xi(x_0) = A$ is plotted in units of $\frac{1}{k}$. The instantaneous displacement of a sheet $x = x_0 + \xi$ is assumed to be periodic and plotted in units of spatial frequency $\frac{1}{k}$. It can be seen that when $A \geq \frac{1}{k}$ the electric field is multi-valued in space and thereby unphysical. This breaks down the linear picture of an oscillator.*

This condition can be expressed interestingly in terms of the total energy of the oscillations. We first partially differentiate the equation of motion of an electron sheet with

respect to the initial equilibrium position and obtain, $\left(\frac{d^2}{dt^2} + \omega_{pe}^2\right) \frac{\partial\xi}{\partial x_0} = 0$. We integrate the equation of motion with respect to the displacement to obtain the total energy or the Hamiltonian, $\int d\xi \frac{d}{dt} \frac{d\xi}{dt} + \omega_{pe}^2 \int d\xi \xi = \mathcal{E}$. Simplifying, $\int dt \frac{d\xi}{dt} \frac{d}{dt} \frac{d\xi}{dt} + \frac{1}{2}\omega_{pe}^2 \xi^2 = \int dt \frac{1}{2} \frac{d}{dt} \left(\frac{d\xi}{dt}\right)^2 + \frac{1}{2}\omega_{pe}^2 \xi^2 = \mathcal{E}$. Thus the total energy is $\frac{1}{2} \left(\frac{d\xi}{dt}\right)^2 + \frac{1}{2}\omega_{pe}^2 \xi^2 = \mathcal{E}$. Since the quantity $\frac{\partial\xi}{\partial x_0}$ satisfies the same equation of motion, it also leads to

$$\frac{1}{2} \left(\frac{\partial}{\partial x_0} \frac{d\xi}{dt}\right)^2 + \frac{1}{2}\omega_{pe}^2 \left(\frac{\partial\xi}{\partial x_0}\right)^2 = \mathcal{E}.$$

Initially when the velocity of the displacement, $\frac{d\xi}{dt}|_{t=0} = 0$, then the whole energy is in $\frac{1}{2}\omega_{pe}^2 \left(\frac{\partial\xi}{\partial x_0}\right)^2|_{t=0} = \mathcal{E}$. Using the condition $\frac{\partial\xi}{\partial x_0} > -1$ above, we simplify $\frac{1}{2}\omega_{pe}^2 \left(\frac{\partial\xi}{\partial x_0}\right)^2|_{t=0} = \mathcal{E}$ to $\sqrt{\frac{2\mathcal{E}}{\omega_{pe}^2}} = \frac{\partial\xi}{\partial x_0} > -1$. This relation can be expressed as $\sqrt{2\mathcal{E}} > -\omega_{pe} \rightarrow \sqrt{2\mathcal{E}} < \omega_{pe}$ which implies $\mathcal{E}|_{t=0} < \frac{\omega_{pe}^2}{2}$. So, if the initial energy is less than $\frac{\omega_{pe}^2}{2}$ then the ordering of the sheets is maintained for all time.

To further understand the non-linear solutions to the equation of motion we study a solution under the special condition, $\Xi_1(x_0) = A \sin(kx_0)$ and $\Xi_2(x_0) = 0$; then the solution is, $\xi(x_0, t) = A \sin(kx_0) \cos(\omega_{pe}t)$. Using the solution, $E = 4\pi e n_0 A \sin(kx_0) \cos(\omega_{pe}t)$ and the instantaneous position of the sheet is $x = x_0 + A \sin(kx_0) \cos(\omega_{pe}t)$. At time $t = 0$ or an integer multiple of 2π , $t = 2m\pi$ the expression for the electric field, $E = 4\pi e n_0 A \sin(kx_0)$ and the trajectory $x = x_0 + A \sin(kx_0)$. We numerically solve and obtain $E(x)$, it is plotted for different values of A in Fig.2.1. It is shown that when

$$A \geq \frac{1}{k}$$

, the electric field solution is not physical. Substituting this condition into the electric field expression, $E = 4\pi e n_0 \frac{1}{k} \sin(kx_0) \cos(\omega_{pe}t)$ and using $k = \frac{c}{\omega_{pe}}$, the electric field expression simplifies to, $E = \frac{4\pi e^2 n_0}{m_e} \frac{m_e}{e} \frac{c}{\omega_{pe}} \sin(kx_0) \cos(\omega_{pe}t) = \frac{m_e c \omega_{pe}}{e} \sin(kx_0) \cos(\omega_{pe}t)$. Thus, the amplitude of electric field for the onset of trajectory crossing in planar electron sheet

oscillations is,

$$E = \frac{m_e c \omega_{pe}}{e}.$$

So, after the amplitude exceeds this critical amplitude there is an *onset of trajectory crossing*. As a result of trajectory crossing there is fine-scale phase-mixing of various regions of the oscillations which destroy the oscillations. After trajectory crossing starts $\frac{\partial \xi}{\partial x_0} > -1$ is not satisfied.

2.1.2 Non-linear Cylindrical and Spherical plasma oscillations

In cylindrical and spherical geometry the plasma electrons oscillate inwards and outwards along the radial dimension of either a cylinder or a sphere. The equation of motion of the displacement in these geometry under the condition that the ordering of the electron rings along the radii is maintained.

Cylindrical Oscillations - Considering plasma oscillations in a cylindrical geometry with a cylindrical shell of electrons (can be visualized as a ring of electrons due to the symmetry along the length) displaced from its equilibrium radius, r_0 by a displacement radius $\mathcal{R}(r_0)$, so that the instantaneous radius of the displaced ring is $r(r_0, t) = r_0 + \mathcal{R}(r_0, t)$. The positive charge left behind by the displacement of an electron ring is $en_0 \pi [(r_0 + \mathcal{R}(r_0))^2 - r_0^2]$. The negative charge in the ring of electrons is $-en_0 2\pi r dr$ where the ring of electrons is infinitesimally thin with thickness dr . The net negative charge still left within the cylinder is $-en_0 \pi r_0^2$. The electric field at the displaced cylindrical shell of electrons using the Gauss's law in its Integral form is $\int d\vec{S} \cdot \vec{E}(r) = 4\pi \int_V dV n(r)$. We can simplify this integral under the consideration that the cylinder has perfect uniformity along its length, so the surface integral becomes a line integral over the circumference and the volume integral is simply the geometric formulation of the net positive just inside the cylindrical shell. So, $2\pi r E(r) = 4\pi en_0 \pi [(r_0 + \mathcal{R}(r_0))^2 - r_0^2]$. Therefore,

$$E(r) = \frac{2\pi en_0}{(r_0 + \mathcal{R}(r_0))} [(r_0 + \mathcal{R}(r_0))^2 - r_0^2].$$

Using this the cylindrical shell equation of motion of the displacement along the radial dimensions is,

$$m \frac{d^2 R}{dt^2} = -eE(r) = -\frac{2\pi e^2 n_0}{(r_0 + \mathcal{R}(r_0))} [(r_0 + \mathcal{R}(r_0))^2 - r_0^2].$$

Spherical Oscillations - Spherical plasma oscillations occur with the expansion and collapse of the spherical electron shells of infinitesimal thickness. So, the radius of a shell with equilibrium radius r_0 is undergoing a displacement $\mathcal{R}(r_0, t)$ resulting in an instantaneous radius of the spherical shell of $r(r_0, t) = r_0 + \mathcal{R}(r_0, t)$. When the displacement is outwards and the spherical shell moves outwards a net positive charge is left behind in the plasma. This net positive charge is $en_0 \frac{4\pi}{3} [(r_0 + \mathcal{R}(r_0))^3 - r_0^3]$. The negative charge of the spherical shell of electrons that is displaced is $-en_0 4\pi r^2 dr$. The negative charge that is left-over inside the sphere is $-en_0 \frac{4\pi}{3} r_0^3$. The electric field at a location just inside the spherical shell is given by the Gauss's law in its integral form $\int d\vec{S} \cdot \vec{E}(r) = 4\pi \int_V dV n(r)$. Performing the simple integrals $4\pi r^2 E(r) = 4\pi en_0 \frac{4\pi}{3} [(r_0 + \mathcal{R}(r_0))^3 - r_0^3]$. So, the electric field is

$$E(r) = \frac{en_0}{(r_0 + \mathcal{R}(r_0))^2} \frac{4\pi}{3} [(r_0 + \mathcal{R}(r_0))^3 - r_0^3].$$

Using this we can write the spherical shell equation of motion of the radial displacement as,

$$m \frac{d^2 R}{dt^2} = -eE(r) = -\frac{4\pi e^2 n_0}{3(r_0 + \mathcal{R}(r_0))^2} [(r_0 + \mathcal{R}(r_0))^3 - r_0^3].$$

By normalizing the radial displacement \mathcal{R} to its initial radial position r_0 the equations can be written in a single radial variable,

$$\rho = \frac{R}{r_0}.$$

The equation of motion in the cylindrical geometry is,

$$\frac{d^2 \rho}{dt^2} = -\frac{1}{2} \omega_{pe}^2 \frac{(1 + \rho)^2 - 1}{(1 + \rho)} \quad (2.2)$$

The equation of motion in spherical coordinates is,

$$\frac{d^2 \rho}{dt^2} = -\frac{1}{3} \omega_{pe}^2 \frac{(1+\rho)^3 - 1}{(1+\rho)^2} \quad (2.3)$$

These are equations of motion of *anharmonic oscillators*. As it is seen from the equation of motion, the period of the oscillation of such radially symmetric oscillators depends upon the amplitude of oscillations, $\rho_{max} = \frac{R_{max}}{r_0}$. In a case where R_{max} is a constant for all the cylindrical or spherical shells, the oscillators at different equilibrium radial positions r_0 have a different ρ and hence a different period of oscillation. The only condition under which the periods of oscillations of each radial oscillator is same is when ρ is a constant.

Now we can understand the physical picture of trajectory crossing of con-centric cylindrical shells or spherical shells of electrons. The trajectory crossing in these geometries is shown to be independent of the amplitude of displacement. This is unlike the physical picture in a 1D planar electron sheet where the *onset of trajectory crossing* occurs only when the amplitude A of the displacement ξ is higher than a critical amplitude. At equilibrium the two concentric shells under consideration are located at a distance between radial positions, $r_0^{(2)} - r_0^{(1)} < R_{max}$ with $r_0^{(2)} > r_0^{(1)}$, that is less than the oscillation amplitude, R_{max} . Then since $\rho^{(2)} < \rho^{(1)}$ the period of oscillation of the two shells is different. Hence, after a certain period of time of oscillations the slower outer ring would be collapsing radially inwards while the inner ring being faster would be moving outwards. This will result in spatial overlap of the two shells with the two shells being momentarily located at the same radius. This crossing of the trajectories of the shells would lead to reversing of the initial ordering. As a result of this there would be fine-scale phase-mixing and the radial oscillations would destroy themselves.

Since the anharmonic oscillator equation is a non-linear second-order differential equation of the special form (Autonomous ODE), $\rho''(t) = f(\rho, \rho')$ it can be solved analytically.

Substituting, $v = \frac{d\rho}{dt}$. Then $\frac{d^2 \rho}{dt^2} = \frac{dv}{dt} = \frac{dv}{d\rho} \frac{d\rho}{dt} = v \frac{dv}{d\rho}$.

The cylindrical equation transforms as $v \frac{dv}{d\rho} = -\frac{1}{2} \omega_{pe}^2 \frac{(1+\rho)^2 - 1}{(1+\rho)}$. Integrating the equa-

tion, $v^2 = -\omega_{pe}^2 \int d\rho \frac{(1+\rho)^2-1}{(1+\rho)} = -\omega_{pe}^2 \left[\frac{\rho^2}{2} + \rho - \ln(1+\rho) \right] + \mathcal{C}$. At the amplitude of the oscillation the velocity is momentarily 0 when the trajectory is undergoing reversal that is $v = \frac{d\rho}{dt} = 0$ when $\rho = \rho_{max}$. Therefore, $\mathcal{C} = \omega_{pe}^2 \left[\frac{\rho_{max}^2}{2} + \rho_{max} - \ln(1+\rho_{max}) \right]$. So, the integrated equation is, $v^2 = -\omega_{pe}^2 \left[\frac{\rho^2}{2} + \rho - \ln(1+\rho) \right] + \omega_{pe}^2 \left[\frac{\rho_{max}^2}{2} + \rho_{max} - \ln(1+\rho_{max}) \right]$.

Taking the square-root on both the sides, $v = \frac{d\rho}{dt} = \omega_{pe} \sqrt{\frac{\rho_{max}^2 - \rho^2}{2} + (\rho_{max} - \rho) + \ln \left(\frac{1+\rho}{1+\rho_{max}} \right)}$.

We can integrate and obtain a solution for the period of oscillations as a function of amplitude, $\int_0^{\rho_{max}} \frac{d\rho}{\sqrt{\frac{\rho_{max}^2 - \rho^2}{2} + (\rho_{max} - \rho) + \ln \left(\frac{1+\rho}{1+\rho_{max}} \right)}} = \int_0^{\pi/2} d\omega_{pe} t$. The amplitude dependent period of oscillations of cylindrical shell of electrons is,

$$\mathcal{T}_{cyl} = \frac{2\pi}{\omega_{pe}} \left(1 - \frac{\rho_{max}^2}{12} + \mathcal{O}(\rho_{max}^3) \right) \quad (2.4)$$

The spherical equation transforms as $v \frac{dv}{d\rho} = -\frac{1}{3} \omega_{pe}^2 \frac{(1+\rho)^3 - 1}{(1+\rho)^2}$. Integrating the equation, $v^2 = -\frac{2}{3} \omega_{pe}^2 \int d\rho \frac{(1+\rho)^3 - 1}{(1+\rho)^2} = -\frac{2}{3} \omega_{pe}^2 \left[\frac{\rho^2}{2} + \rho + \frac{1}{(1+\rho)} \right] + \mathcal{C}$. At the amplitude of the oscillation the velocity is momentarily 0 when the trajectory is undergoing reversal that is $v = \frac{d\rho}{dt} = 0$ when $\rho = \rho_{max}$. Therefore, $\mathcal{C} = \omega_{pe}^2 \left[\frac{\rho_{max}^2}{2} + \rho_{max} + \frac{1}{(1+\rho_{max})} \right]$. So, the integrated equation is, $v^2 = -\omega_{pe}^2 \left[\frac{\rho^2}{2} + \rho + \frac{1}{(1+\rho)} \right] + \omega_{pe}^2 \left[\frac{\rho_{max}^2}{2} + \rho_{max} + \frac{1}{(1+\rho_{max})} \right]$. Taking the square-root on both the sides, $v = \frac{d\rho}{dt} = \omega_{pe} \sqrt{\frac{\rho_{max}^2 - \rho^2}{2} + (\rho_{max} - \rho) + \frac{1}{(1+\rho_{max})} - \frac{1}{(1+\rho)}}$. We can integrate and obtain a solution for the period of oscillations as a function of amplitude, $\int_0^{\rho_{max}} \frac{d\rho}{\sqrt{\frac{\rho_{max}^2 - \rho^2}{2} + (\rho_{max} - \rho) + \frac{1}{(1+\rho_{max})} - \frac{1}{(1+\rho)}}} = \int_0^{\pi/2} d\omega_{pe} t$. The amplitude dependent period of oscillations of spherical shell of electrons is,

$$\mathcal{T}_{sph} = \frac{2\pi}{\omega_{pe}} \left(1 - \frac{7\rho^2}{48} + \mathcal{O}(\rho_{max}^3) \right) \quad (2.5)$$

The time duration for fine-scale mixing and trajectory crossing is the time required for two shells separated by twice the amplitude $r_0^{(2)} - r_0^{(1)} = 2R_{max}$ to be out-of-phase by π or

half-of-the-period. Under this condition the two shells cross at the instant when the shell at the lower radius or the inner shell is at $r^{(1)} = r_0^{(1)} + R_{max}$ and the shell at the larger radius or the outer shell is at $r^{(2)} = r_0^{(2)} - R_{max}$. This condition can also be stated in terms of the periods of oscillations of the individual shells. The two shells start their oscillations at the same instant. Then the trajectory crossing starts at a time t_{mix} when

$$n_1 = n_2 \pm \frac{1}{2}.$$

Where the number of oscillations of the individual oscillators during the t_{mix} period is $n_1 = \frac{t_{mix}}{\mathcal{T}_1}$ and $n_2 = \frac{t_{mix}}{\mathcal{T}_2}$. Thus in terms of the periods of oscillations,

$$t_{mix} = \pm \frac{\mathcal{T}_1 \mathcal{T}_2}{2(\mathcal{T}_1 - \mathcal{T}_2)}.$$

A relation between \mathcal{T}_1 and \mathcal{T}_2 can be determined assuming R_{max} is constant. Assume that the concentric shells are close to each other along the radial dimension and it is given that $r^{(1)} < r^{(2)}$. Then the relation is of the form $\mathcal{T}_1 < \mathcal{T}_2$ and we write, $\mathcal{T}_2 = \mathcal{T}_1 + \Delta\mathcal{T}$. Since for fixed R_{max} the amplitude of oscillations $\rho_{max} = \frac{1}{\rho}R_{max}$ and $\mathcal{T} = f(\rho_{max}) = f(r_0)$. Thus $\Delta\mathcal{T} = \frac{d\mathcal{T}}{dr_0}\Delta r_0$ and using $\Delta r_0 = 2R_{max}$ from the problem statement above, $\Delta\mathcal{T} = \frac{d\mathcal{T}}{dr_0}2R_{max}$. So, the period of oscillation of the sheets are related as,

$$\mathcal{T}_2 = \mathcal{T}_1 + \frac{d\mathcal{T}}{dr_0}2R_{max}.$$

Using the above equation for the mixing time t_{mix} and the relation between \mathcal{T}_2 and \mathcal{T}_1 we can simplify the expression for the mixing time. $t_{mix} = \pm \frac{\mathcal{T}_1(\mathcal{T}_1 + \frac{d\mathcal{T}}{dr_0}2R_{max})}{2\frac{d\mathcal{T}}{dr_0}2R_{max}}$. Simplifying,

$$t_{mix} = \pm \left(\frac{\mathcal{T}_1^2}{2\frac{d\mathcal{T}}{dr_0}2R_{max}} + \frac{\mathcal{T}_1}{2} \right).$$

Therefore the mixing time duration is,

$$\Delta t_{mix} = \pm \left(\frac{\mathcal{T}^2}{4\frac{d\mathcal{T}}{dr_0}R_{max}} \right) \quad (2.6)$$

The mixing time can be determined for cylindrical and spherical oscillations using the above expression for the period of oscillations. In the cylindrical case up to the second-order in amplitude, $\mathcal{T}_{cyl} = \frac{2\pi}{\omega_{pe}} \left(1 - \frac{R_{max}^2}{12r_0^2}\right)$. Evaluating, $\frac{d\mathcal{T}}{dr_0} = \frac{d\mathcal{T}}{dR_{max}} \frac{dR_{max}}{dr_0} = -\left(\frac{\pi}{\omega_{pe}} \frac{R_{max}}{3r_0^2}\right) \frac{dR_{max}}{dr_0}$. Substituting this in the mixing time expression, $\Delta t_{mix} = \left(\frac{2\pi}{\omega_{pe}}\right)^2 \left(1 - \frac{\rho_{max}^2}{12}\right)^2 \left(4 \frac{\pi}{\omega_{pe}} \frac{R_{max}^2}{3r_0^2} \frac{dR_{max}}{dr_0}\right)^{-1}$. Simplifying and neglecting $\frac{\rho_{max}^2}{6}$ and $\mathcal{O}(\rho_{max}^3)$ term in the numerator,

$$\text{Cyl : } \Delta t_{mix} = \frac{\pi}{\omega_{pe}} \frac{3r_0^2}{R_{max}^2 \frac{dR_{max}}{dr_0}}.$$

In the spherical case up to the second-order in amplitude, $\mathcal{T}_{sph} = \frac{2\pi}{\omega_{pe}} \left(1 - \frac{7\rho^2}{48}\right)$. Evaluating, $\frac{d\mathcal{T}}{dr_0} = \frac{d\mathcal{T}}{dR_{max}} \frac{dR_{max}}{dr_0} = -\left(\frac{\pi}{\omega_{pe}} \frac{7R_{max}}{12r_0^2}\right) \frac{dR_{max}}{dr_0}$. Substituting this in the mixing time expression, $\Delta t_{mix} = \left(\frac{2\pi}{\omega_{pe}}\right)^2 \left(1 - \frac{7\rho^2}{48}\right)^2 \left(4 \frac{\pi}{\omega_{pe}} \frac{7R_{max}^2}{12r_0^2} \frac{dR_{max}}{dr_0}\right)^{-1}$. Simplifying and neglecting $\frac{7\rho_{max}^2}{24}$ and $\mathcal{O}(\rho_{max}^3)$ term in the numerator,

$$\text{Sph : } \Delta t_{mix} = \frac{\pi}{\omega_{pe}} \frac{12r_0^2}{7R_{max}^2 \frac{dR_{max}}{dr_0}}.$$

2.1.3 Inhomogeneous plasma - Planar oscillations

Phase-mixing and trajectory crossing of planar oscillations is not limited to the condition of amplitude exceeding a critical amplitude. Phase-mixing and trajectory crossing also occurs in an inhomogeneous density such as a density gradient. Considering planar plasma electron sheets oscillating along the x -direction with the equilibrium position at x_0 and the displacement being $\xi(x_0, t)$. The plasma density over which the sheet is displaced is $n_0(x)$. The total ion density which is left behind by the electron sheet at x_0 displaced to $x_0 + \xi(x_0, t)$ is $e \int_{x_0}^{x_0+\xi} dx n_0(x)$. Thus the electric field at the electron sheet due to the ions is $E = 4\pi e \int_{x_0}^{x_0+\xi} dx n_0(x)$. The equation of motion of the electron-sheet in this inhomogeneous plasma is

$$m \frac{d^2 \xi}{dt^2} = -eE = -4\pi e^2 \int_{x_0}^{x_0+\xi} dx n_0(x).$$

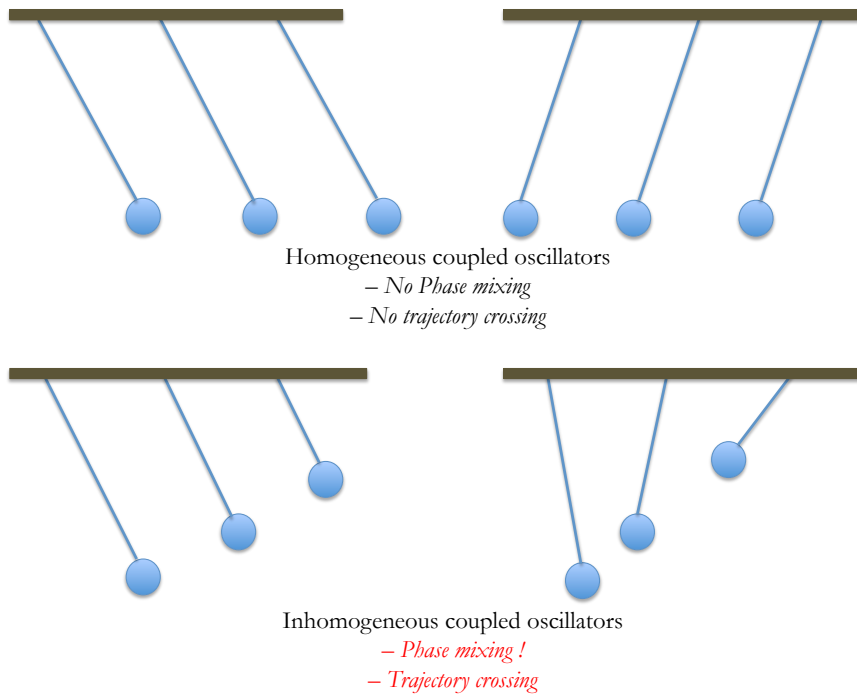


FIGURE 2.2: *Phase mixing of coupled oscillators with spatially increasing frequencies.* Individual plasmons excited in the wake of a driver in a homogeneous plasma are coupled together and undergo in-phase or synchronous-phase oscillations. However, in an inhomogeneous rising density plasma (common at the vacuum-plasma interface of plasma sources), the individual plasmons have increasing characteristic frequency. Hence there is phase-mixing and trajectory crossing.

This equation shows that in a plasma with inhomogeneous density the frequency of the oscillations of an electron sheet depends upon the amplitude of oscillations. This is because as the integral over the density suggests the net charge exciting the restoring force is a function of the displacement, ξ . And the net charge also depends upon the initial position, x_0 . Phase-mixing will always occur under these conditions.

The regions of plasma that are separated by distances over which the plasma density significantly varies have plasma frequencies which are significantly different. As a result of this coherent oscillations are not supported over this region with significantly different plasma frequency.

We can write a general solution to the equation for planar plasma oscillations in an inhomogeneous plasma as a *Fourier series* of different frequencies excited at different densities,

$n_0(x)$. Thus the general solution is,

$$\xi(x_0, t) = \operatorname{Re} \left\{ \sum_{m=1}^{\infty} \xi_m(x_0) \exp(im\omega_{pe}(x_0)t) \right\}.$$

Taking the partial derivative of the general solution with time,

$$\frac{\partial \xi(x_0, t)}{\partial t} = \operatorname{Re} \left\{ i\omega_{pe}(x_0) \sum_{m=1}^{\infty} m \xi_m(x_0) \exp(im\omega_{pe}(x_0)t) \right\}.$$

Taking the partial derivative of the general solution with spatial variable for equilibrium position,

$$\frac{\partial \xi(x_0, t)}{\partial x_0} = \operatorname{Re} \left\{ \sum_{m=1}^{\infty} \frac{\partial \xi_m(x_0)}{\partial x_0} \exp(im\omega_{pe}(x_0)t) + i t \frac{\partial \omega_{pe}(x_0)}{\partial x_0} \sum_{m=1}^{\infty} m \xi_m(x_0) \exp(im\omega_{pe}(x_0)t) \right\}.$$

We can find the ratio of the spatial derivative with the time derivative, $\frac{\partial \xi(x_0, t)}{\partial x_0} \left(\frac{\partial \xi(x_0, t)}{\partial t} \right)^{-1}$.

$$\begin{aligned} & \frac{\partial \xi(x_0, t)}{\partial x_0} \left(\frac{\partial \xi(x_0, t)}{\partial t} \right)^{-1} \\ &= \frac{\operatorname{Re} \left\{ \sum_{m=1}^{\infty} \frac{\partial \xi_m(x_0)}{\partial x_0} \exp(im\omega_{pe}(x_0)t) + i t \frac{\partial \omega_{pe}(x_0)}{\partial x_0} \sum_{m=1}^{\infty} m \xi_m(x_0) \exp(im\omega_{pe}(x_0)t) \right\}}{\operatorname{Re} \left\{ i\omega_{pe}(x_0) \sum_{m=1}^{\infty} m \xi_m(x_0) \exp(im\omega_{pe}(x_0)t) \right\}} \\ &= \operatorname{Re} \left\{ -i \frac{\sum_{m=1}^{\infty} \frac{\partial \xi_m(x_0)}{\partial x_0} \exp(im\omega_{pe}(x_0)t)}{\omega_{pe}(x_0) \sum_{m=1}^{\infty} m \xi_m(x_0) \exp(im\omega_{pe}(x_0)t)} \right\} + \frac{t}{\omega_{pe}(x_0)} \frac{\partial \omega_{pe}(x_0)}{\partial x_0} \\ &= \frac{t}{\omega_{pe}(x_0)} \frac{\partial \omega_{pe}(x_0)}{\partial x_0} \end{aligned} \quad (2.7)$$

We can use the condition in eq.2.1, $\frac{\partial \xi}{\partial x_0} > -1$ to determine an expression for the mixing time in an inhomogeneous plasma. We also use the fact that the trajectory traverse a path to the maximum and back to equilibrium in half the period, $\frac{\partial \xi(x_0, t)}{\partial t} \simeq \frac{2\xi_m}{T_0/2} = 4\frac{\xi_m}{T}$.

Therefore, the expression is $\frac{t}{\omega_{pe}(x_0)} \frac{\partial \omega_{pe}(x_0)}{\partial x_0} \frac{\partial \xi(x_0, t)}{\partial t} > -1$. Therefore, $\Delta t_{mix} = \frac{\omega_{pe}(x_0)}{\frac{\partial \omega_{pe}(x_0)}{\partial x_0} 4 \frac{\xi_m}{T_0}}$.

Further simplifying using $\omega_{pe}(x_0) = \frac{2\pi}{T_0}$,

$$\Delta t_{mix} = \frac{\pi}{2 \frac{\partial \omega_{pe}(x_0)}{\partial x_0} \xi_m} \quad (2.8)$$

From this expression for the 1D mixing time of planar electron sheets we can determine the scaling laws. Firstly, the mixing time depends inversely on the spatial gradient of the plasma frequency varying in the density inhomogeneity. Secondly, the mixing time depends upon the amplitude of the planar oscillation. The dependence on the planar oscillation amplitude is similar to the homogenous density sheet crossing.

2.2 Warm-plasma - wave-breaking

Since the cold-plasma approximation is quite a valid one, the wave-breaking limits assuming no thermal velocities of plasma electrons is sufficient to describe trajectory-crossing or phase-mixing between individual oscillator trajectories. However, when non-linear density perturbations are excited in a large amplitude plasma wave, thermal effects may become important as the electron thermal pressure may not allow the density compression to build up as predicted by the simple fluid model where thermal effects are ignored.

In the warm-plasma limit fluid description may still be used because the leading order motion is still due to oscillations with minor correction from the thermal motion through the pressure term in the second-order and third-order fluid equations. Thus to include the effect of thermal motion of electrons it is important to choose the correct equation of state which links the pressure and temperature, $\mathbf{P} \propto f(n_e, T_e)$. The only constraint on the equation of state is that the wave phase-velocity be much higher than the average thermal velocity. If this constraint is not met then the thermal motion of electrons in the wave-frame become important and a non-linear wave model such as the BGK (Bernstein-Greene-Kruskal) model has to be used to complete the physical picture. A non-linear wave model is important because due to thermal motion of electrons some of the electrons are trapped in the wave potential. Therefore, it is important to assume $v_{th}^e \ll v_\phi$.

Under a warm plasma assumption wave breaking in large amplitude plasma density waves can be shown to originate earlier than in the case of cold-plasma. Importantly unlike in the cold-plasma case where the wave-breaking limit is defined by trajectory crossing in

the case of warm plasma it is defined by trapping of plasma electron in the wave potential. As a result of trapping of the electrons in the tail of the thermal distribution the plasma wave cannot be described by averaged behavior as expected for the application of the fluid model.

In essence as the wave amplitude gets larger a higher number of plasma electrons are trapped in the wave. The trapping of electron leads to the transfer of the wave field energy to trapped particle energy. The loss of field energy implies that the wave is damped behind the trapped particles. The transition from a high amplitude wave to a weak wave is abrupt and this distortion leads to wave-breaking. The physical phenomenon described above has been modeled using the water-bag velocity distribution function [12].

2.3 Wave-breaking - multi-dimensional wake

Most of the above analysis for trajectory crossing is for 1-D oscillations except for the cylindrical and spherical geometry. The amplitude dependence of the trajectory crossing in the 1-D oscillations allows us to establish a critical value of the electric field where trapping may begin.

The phenomenon of trajectory crossing in cylindrical oscillations is relevant as such oscillations occur in ultra-short $l_{energy} < \lambda_{pe}$, laser and beam-plasma interactions. But, the phenomenon of trajectory crossing in such oscillations is not dependent upon the amplitude ξ_m of oscillations unlike in planar oscillations but depends upon the gradient of the oscillation amplitude, $\frac{dR_{max}}{r_0}$.

The 1-D model does not model the trapping of particles in wakes whose transverse shape depends upon the shape of the driver. In the case of a plasma wave that is driven in the wake of an energy source the exact definition of trajectory crossing and particle trapping is not easy to obtain analytically. To determine the multi-dimensional expression for the potential of the plasma wave is not trivial. The multi-dimensional waves also have to trap the particles in other dimensions and hence the relation between the particle energy

in the wave-frame and wave-potential in the transverse dimensions have to be determined.

To further analyze the trapping of particles we turn to the Hamiltonian formalism for the plasma electron dynamics in a wake. Below, we follow the analysis given in [14].

The canonical momentum is $\vec{P} = \vec{p}_e - \frac{e}{c}\vec{A}$ and the conjugate canonical coordinate is the space variable, \vec{r} . We note that the mechanical momentum is $\vec{p}_e = \vec{P} + \frac{e}{c}\vec{A}$. Therefore writing the Hamiltonian,

$$\mathcal{H} = \gamma_e m_e c^2 - e\Phi = \left(\sqrt{1 + \vec{p}_e \cdot \vec{p}_e / (m_e c)^2} \right) m_e c^2 - e\Phi.$$

Thus, the Hamiltonian equations are

$$\frac{d\vec{r}}{dt} = \frac{\partial \mathcal{H}}{\partial \vec{P}}$$

and

$$\frac{d\vec{P}}{dt} = -\frac{\partial \mathcal{H}}{\partial \vec{r}}.$$

$$\text{We can use } \frac{\partial \vec{p}_e}{\partial \vec{P}} = \frac{\partial \vec{P} + \frac{e}{c}\vec{A}}{\partial \vec{P}} = \frac{\partial \vec{P}}{\partial \vec{P}} + \frac{e}{c} \frac{\partial \vec{A}}{\partial \vec{P}} = 1.$$

Considering the first equation,

$$\frac{d\vec{r}}{dt} = \frac{\partial \mathcal{H}}{\partial \vec{P}} = \frac{\partial \mathcal{H}}{\partial \vec{p}_e} \frac{\partial \vec{p}_e}{\partial \vec{P}} = \frac{m_e c^2}{2\gamma_e} 2 \frac{\vec{p}_e}{m_e^2 c^2} = \vec{v}_e.$$

Considering the second equation, $\frac{d\vec{P}}{dt} = -\frac{\partial \mathcal{H}}{\partial \vec{r}} = -m_e c^2 \frac{\partial (\sqrt{1 + \vec{p}_e \cdot \vec{p}_e / (m_e c)^2})}{\partial \vec{r}} + e \frac{\partial \Phi}{\partial \vec{r}} = -\frac{\partial \vec{p}_e}{\partial \vec{r}} \cdot 2 \frac{m_e c^2}{m_e^2 c^2} \frac{\vec{p}_e}{m_e^2 c^2} + e \vec{\nabla} \Phi = -\frac{\partial \vec{p}_e}{\partial \vec{r}} \cdot \frac{\vec{p}_e}{m_e \gamma_e} + e \vec{\nabla} \Phi$. The gradient of the mechanical momentum is $\frac{\partial}{\partial \vec{r}} (\vec{P} + \frac{e}{c}\vec{A}) = \frac{e}{c} \frac{\partial}{\partial \vec{r}} \vec{A} = \frac{e}{c} \vec{\nabla} \vec{A}$. Substituting, $\frac{d\vec{P}}{dt} = \frac{e}{c} \vec{\nabla} \vec{A} \cdot \vec{v}_e - e \vec{\nabla} \Phi$.

$$\frac{d\vec{P}}{dt} = \frac{e}{c} \vec{\nabla} \vec{A} \cdot \vec{v}_e - e \vec{\nabla} \Phi \quad (2.9)$$

Using the vector calculus identity, $\vec{\nabla} \vec{A} \cdot \vec{v}_e = (\vec{v}_e \cdot \vec{\nabla}) \vec{A} - \vec{v}_e \times \vec{\nabla} \times \vec{A}$. Substituting it in the second equation, $\frac{d\vec{p}_e}{dt} - \frac{e}{c} \frac{d\vec{A}}{dt} = -\frac{e}{c} (\vec{v}_e \cdot \vec{\nabla}) \vec{A} - \frac{e}{c} \vec{v}_e \times \vec{\nabla} \times \vec{A} + e \vec{\nabla} \Phi$. Simplifying,

$\frac{d\vec{p}_e}{dt} = \frac{e}{c} \left(\frac{d\vec{A}}{dt} - (\vec{v}_e \cdot \vec{\nabla}) \vec{A} \right) - \frac{e}{c} \vec{v}_e \times \vec{\nabla} \times \vec{A} + e \vec{\nabla} \Phi$. Also, using the convective derivative, $\frac{d\vec{A}}{dt} = \frac{\partial \vec{A}}{\partial t} + (\vec{v}_e \cdot \vec{\nabla}) \vec{A}$ which implies that $\frac{\partial \vec{A}}{\partial t} = \frac{d\vec{A}}{dt} - (\vec{v}_e \cdot \vec{\nabla}) \vec{A}$. Using this, $\frac{d\vec{p}_e}{dt} = \left(e \vec{\nabla} \Phi + \frac{e}{c} \frac{\partial \vec{A}}{\partial t} \right) - \frac{e}{c} \vec{v}_e \times \vec{\nabla} \times \vec{A}$. From the definition of the electric field above,

$$\frac{d\vec{p}_e}{dt} = -e \vec{E} - \frac{e}{c} \vec{v}_e \times \vec{\nabla} \times \vec{A} = -e \vec{\nabla} \Phi - \frac{e}{c} \vec{v}_e \times \vec{\nabla} \times \vec{A}.$$

So, we recover the equation of motion, $\frac{d\vec{p}_e}{dt} = -e \vec{E} - \frac{e}{c} \vec{v}_e \times \vec{B}$. Thus we have shown a self-consistent Hamiltonian formulation.

Poisson bracket - Poisson bracket is defined in canonical coordinates $(\vec{r}, \vec{\mathcal{P}})$ on the phase space. Let us say we are given two functions $g_1(\vec{r}, \vec{\mathcal{P}}, t)$ and $g_2(\vec{r}, \vec{\mathcal{P}}, t)$. Note $f(\vec{r}, \vec{\mathcal{P}}, t)$ means f is a function of the $2N + 1$ independent variables $2N$ from the degrees of freedom of the canonical variable space and time, t . The Poisson bracket between the two function is defined as,

$$\{g_1, g_2\} = \sum_{i=1}^N \left(\frac{\partial g_1}{\partial \vec{r}_i} \frac{\partial g_2}{\partial \vec{\mathcal{P}}_i} - \frac{\partial g_1}{\partial \vec{\mathcal{P}}_i} \frac{\partial g_2}{\partial \vec{r}_i} \right).$$

Noting that by definition the conjugate coordinate variables follow $\frac{\partial \vec{\mathcal{P}}}{\partial \vec{r}} = 0$ and $\frac{\partial \vec{r}}{\partial \vec{\mathcal{P}}} = 0$. The Hamilton equations of motion can be expressed in terms of the Poisson bracket as follows, $\dot{\vec{\mathcal{P}}} = -\frac{\partial \mathcal{H}}{\partial \vec{r}} = \{\vec{\mathcal{P}}, \mathcal{H}\} = \frac{\partial \vec{\mathcal{P}}}{\partial \vec{r}} \frac{\partial \mathcal{H}}{\partial \vec{\mathcal{P}}} - \frac{\partial \vec{\mathcal{P}}}{\partial \vec{\mathcal{P}}} \frac{\partial \mathcal{H}}{\partial \vec{r}} = -\frac{\partial \mathcal{H}}{\partial \vec{r}} = \frac{d\vec{\mathcal{P}}}{dt}$. Similarly the second equation, $\dot{\vec{r}} = -\frac{\partial \mathcal{H}}{\partial \vec{\mathcal{P}}} = \{\vec{r}, \mathcal{H}\}$. Suppose that $f(\vec{r}, \vec{\mathcal{P}}, t)$ is a function on the manifold. Then from the multivariable chain rule, we obtain $\frac{d}{dt} f(\vec{r}, \vec{\mathcal{P}}, t) = \frac{\partial f}{\partial \vec{\mathcal{P}}} \frac{d\vec{\mathcal{P}}}{dt} + \frac{\partial f}{\partial \vec{r}} \frac{d\vec{r}}{dt} + \frac{\partial f}{\partial t}$. Using the Hamiltonian equation of motion, $\frac{d\vec{r}}{dt} = \frac{\partial \mathcal{H}}{\partial \vec{\mathcal{P}}}$ and $\frac{d\vec{\mathcal{P}}}{dt} = -\frac{\partial \mathcal{H}}{\partial \vec{r}}$. We thus write, $\frac{d}{dt} f(\vec{r}, \vec{\mathcal{P}}, t) = -\frac{\partial f}{\partial \vec{\mathcal{P}}} \frac{\partial \mathcal{H}}{\partial \vec{r}} + \frac{\partial f}{\partial \vec{r}} \frac{\partial \mathcal{H}}{\partial \vec{\mathcal{P}}} + \frac{\partial f}{\partial t} = \{f, \mathcal{H}\} + \frac{\partial f}{\partial t}$.

$$\frac{d}{dt} f(\vec{r}, \vec{\mathcal{P}}, t) = \{f, \mathcal{H}\} + \frac{\partial f}{\partial t} \quad (2.10)$$

Using the Poisson bracket formulation to represent the evolution of a function f in the conjugate coordinate phase-space we can study the time dependence of any quantity.

We start with letting $f = \mathcal{H}$. In this case, $\frac{d}{dt}\mathcal{H}(\vec{r}, \vec{\mathcal{P}}, t) = \{\mathcal{H}, \mathcal{H}\} + \frac{\partial \mathcal{H}}{\partial t}$. Thus, $\frac{d}{dt}\mathcal{H}(\vec{r}, \vec{\mathcal{P}}, t) = \frac{\partial \mathcal{H}}{\partial t}$. Taking the partial time derivative of the Hamiltonian, $\frac{d}{dt}\mathcal{H}(\vec{r}, \vec{\mathcal{P}}, t) = \frac{\partial \mathcal{H}}{\partial t} = m_e c^2 \frac{\partial}{\partial t} \gamma_e - e \frac{\partial}{\partial t} \Phi$.

We known from above that the mechanical momentum, $\vec{p}_e = \vec{\mathcal{P}} + \frac{e}{c} \vec{A}$ thus in case the canonical momentum is conserved quantity (a 1-D planar assumption) then the time evolution of the Hamiltonian does not depend upon the canonical momentum. So, Hamiltonian evolves in time as,

$$\frac{d}{dt}\mathcal{H}(\vec{r}, \vec{\mathcal{P}}, t) = m_e c^2 \frac{\partial}{\partial t} \gamma_e - e \frac{\partial}{\partial t} \Phi \quad (2.11)$$

For the ease of analysis of trapping of plasma electrons in the wake we can transform its motion to the frame of reference of the wave. The plasma wave has the phase velocity of v_ϕ^p . Plasma quantities in the wave-frame can be represented in the coordinate representing distance just behind the phase-front ($r_\perp, \xi = z - v_\phi^p t$). Transforming the energy of the electron to the wave frame, $\mathcal{H}_\phi^p = \gamma_\phi (\mathcal{H} - v_\phi^p p_z)$. In the transformed coordinate system, $\frac{\partial}{\partial t} = -v_\phi \frac{\partial}{\partial \xi}$. Thus the evolution of Hamiltonian in the transformed coordinates is,

$$\frac{d}{dt}\mathcal{H}(\vec{r}, \vec{\mathcal{P}}, t) = v_\phi^p \left(-m_e c^2 \frac{\partial}{\partial \xi} \gamma_e + e \frac{\partial}{\partial \xi} \Phi \right) \quad (2.12)$$

Using the eq.1.18 in its 1-D limit, $\partial_t \frac{p_{\parallel}}{m_e c} = c \vec{\nabla}_{\parallel} (\phi - \gamma)$. The conservation of transverse momentum always holds in 1-D as shown in eq.1.17. Using the longitudinal component of the eq.2.9, $\frac{d\mathcal{P}_{\parallel}}{dt} = \frac{e}{c} \nabla A_{\parallel} v_{e-\parallel} - e \nabla_{\parallel} \Phi$. in the right-hand side of eq.2.12, $v_\phi^p \left(-m_e c^2 \frac{\partial}{\partial \xi} \gamma_e + e \frac{\partial}{\partial \xi} \Phi \right) = v_\phi^p \left(-\frac{e}{c} \frac{\partial}{\partial \xi} \vec{v}_e \cdot \vec{A} + e \frac{\partial}{\partial \xi} \Phi \right) = v_\phi^p \frac{d\mathcal{P}_{\parallel}}{dt}$. Thus, $\frac{d}{dt} (\mathcal{H}(\vec{r}, \vec{\mathcal{P}}, t) - v_\phi^p \mathcal{P}_{\parallel}) = 0$. So, the conserved quantity is,

$$\begin{aligned} \frac{d}{dt} (\mathcal{H}(\vec{r}, \vec{\mathcal{P}}, t) - v_\phi^p \mathcal{P}_{\parallel}) &= 0 \\ \mathcal{H}(\vec{r}, \vec{\mathcal{P}}, t) - v_\phi^p \mathcal{P}_{\parallel} &= \text{constant} \end{aligned} \quad (2.13)$$

Expanding the terms of the conserved quantity, $\mathcal{H}(\vec{r}, \vec{\mathcal{P}}, t) - v_\phi^p \mathcal{P}_\parallel = \gamma_e m_e c^2 - e\Phi - v_\phi^p (p_{e-\parallel} - \frac{e}{c} A_\parallel)$. Normalizing the conserved quantity with the rest-mass energy, $\gamma_e - \phi + \beta_\phi^p a_\parallel - \beta_\phi^p \hat{p}_{e-\parallel}$ = constant. Where we have used, $a = \frac{eA}{m_e c^2}$, $\phi = \frac{e\Phi}{m_e c^2}$ and $\hat{p} = \frac{p}{m_e c}$. So, normalized expression for the conserved quantity is,

$$\gamma_e - \phi + \beta_\phi^p a_\parallel - \beta_\phi^p \hat{p}_{e-\parallel} = \text{constant} \quad (2.14)$$

Defining, $\phi - \beta_\phi^p a_\parallel = \psi$. The constant of motion can be determined using the initial conditions, when $\phi = \phi_0$ and $a_\parallel = a_\parallel^0$ then $\phi^0 - \beta_\phi^p a_\parallel^0 = \psi_0$. Denoting the initial condition as, $\gamma_e = \gamma_0$ and $\hat{p}_{e-\parallel} = \hat{p}_{e-\parallel}^0$ and $\gamma_0 - \beta_\phi^p \hat{p}_{e-\parallel}^0 = \Lambda_0$. Thus the constant of motion using the initial conditions is $\Lambda_0 - \psi_0 = \text{constant}$. Using the constants as defined, $\gamma_e - \beta_\phi^p \hat{p}_{e-\parallel} - (\phi - \beta_\phi^p a_\parallel) = \Lambda_0 - \psi_0$. Simplifying, $\gamma_e - \beta_\phi^p \hat{p}_{e-\parallel} - \psi = \Lambda_0 - \psi_0$. Further simplifying, $\gamma_e - \beta_\phi^p \hat{p}_{e-\parallel} = \Lambda_0 + \psi - \psi_0$. Thus the constant of motion using the initial conditions can be written as,

$$\begin{aligned} \phi - \beta_\phi^p a_\parallel &= \psi, & \gamma_0 - \beta_\phi^p \hat{p}_{e-\parallel}^0 &= \Lambda_0 \\ \gamma_e - \beta_\phi^p \hat{p}_{e-\parallel} &= \Lambda_0 + \Delta\psi \end{aligned} \quad (2.15)$$

As we are studying the trapping of electron and wave-breaking in the wave potential, it is desirable to obtain a relation between the longitudinal momentum, $\hat{p}_{e-\parallel}$ to the effective potential, ψ and the transverse momentum, $\hat{p}_{e-\perp}$ to analyze the trapping condition. Rearranging the eq.2.15, $\gamma_e = \Lambda_0 + \Delta\psi + \beta_\phi^p \hat{p}_{e-\parallel}$ and using $\gamma_e = 1 + \hat{p}_{e-\parallel}^2 + \hat{p}_{e-\perp}^2$. Upon squaring the equation it is, $1 + \hat{p}_{e-\parallel}^2 + \hat{p}_{e-\perp}^2 = \Lambda_0^2 + \Delta\psi^2 + \beta_\phi^p^2 \hat{p}_{e-\parallel}^2 + 2\Lambda_0 \Delta\psi + 2\Lambda_0 \beta_\phi^p \hat{p}_{e-\parallel} + 2\beta_\phi^p \hat{p}_{e-\parallel} \Delta\psi$. Simplifying and re-arranging in the format for a quadratic equation in $\hat{p}_{e-\parallel}$,

$$(1 - \beta_\phi^p)^2 \hat{p}_{e-\parallel}^2 - 2\beta_\phi^p (\Lambda_0 + \Delta\psi) + [(1 + \hat{p}_{e-\perp}^2) - (\Lambda_0 + \Delta\psi)^2] = 0 \quad (2.16)$$

Solving the quadratic equation, we can determine the *discriminant*, $\mathcal{D} = 4\beta_\phi^p^2 (\Lambda_0 + \Delta\psi)^2 +$

$4(1 - \beta_\phi^p)^2(\Lambda_0 + \Delta\psi)^2 - 4(1 - \beta_\phi^p)^2(1 + \hat{p}_{e-\perp}^2)$. Simplifying,

$$\mathcal{D} = 4 \left[(\Lambda_0 + \Delta\psi)^2 - (1 - \beta_\phi^p)^2 (1 + \hat{p}_{e-\perp}^2) \right].$$

We use eq.2.15, $\mathcal{D} = 4 \left[\gamma_e^2 + \beta_\phi^p \hat{p}_{e-\parallel}^2 - 2\gamma_e \beta_\phi^p \hat{p}_{e-\parallel} - (1 + \hat{p}_{e-\perp}^2) + \beta_\phi^p (1 + \hat{p}_{e-\perp}^2) \right]$.

Upon expanding the Lorentz factor, $\mathcal{D} = 4 \left[\hat{p}_{e-\parallel}^2 + \beta_\phi^p \hat{p}_{e-\parallel}^2 - 2\gamma_e \beta_\phi^p \hat{p}_{e-\parallel} + \beta_\phi^p (1 + \hat{p}_{e-\perp}^2) \right]$.

Thus, the discriminant of the equation is,

$$\mathcal{D} = 4(\gamma_e \beta_\phi^p - \hat{p}_{e-\parallel})^2$$

. Using this we determine that $\mathcal{D} \geq 0$.

So, there is always a real solution for the longitudinal momentum. The solution for the longitudinal momentum from these considerations is, $\hat{p}_{e-\parallel} = \gamma_\phi^p \left(\beta_\phi^p (\Lambda_0 + \Delta\psi) \pm \sqrt{\mathcal{D}/4} \right)$.

Simplifying, $\hat{p}_{e-\parallel} = \gamma_\phi^p \left(\beta_\phi^p (\Lambda_0 + \Delta\psi) \pm \sqrt{\mathcal{D}/4} \right) \times \frac{(\beta_\phi^p (\Lambda_0 + \Delta\psi) \mp \sqrt{\mathcal{D}/4})}{(\beta_\phi^p (\Lambda_0 + \Delta\psi) \mp \sqrt{\mathcal{D}/4})}$. This gives the

longitudinal momentum as,

$$\hat{p}_{e-\parallel} = \frac{1 + \hat{p}_{e-\perp}^2 - (\Lambda_0 + \Delta\psi)^2}{\beta_\phi^p (\Lambda_0 + \Delta\psi) \mp \sqrt{[(\Lambda_0 + \Delta\psi)^2 - (1 - \beta_\phi^p)^2 (1 + \hat{p}_{e-\perp}^2)]}} \quad (2.17)$$

We can determine the $\beta_{e-\parallel}$ using $\hat{p}_{e-\parallel}$ if γ_e is known. We can obtain the Lorentz factor using the longitudinal momentum $\hat{p}_{e-\parallel}$ in eq.2.17 and eq.2.15, $\gamma_e = \beta_\phi^p \hat{p}_{e-\parallel} + (\Lambda_0 + \Delta\psi)$.

Substituting, we obtain,

$$\gamma_e = \frac{\beta_\phi^p (1 + \hat{p}_{e-\perp}^2) \mp \sqrt{\mathcal{D}/4} (\Lambda_0 + \Delta\psi)}{\beta_\phi^p (\Lambda_0 + \Delta\psi) \mp \sqrt{\mathcal{D}/4}} \quad (2.18)$$

The longitudinal velocity is thus obtained using eq.2.17 and eq.2.19, $\beta_{e-\parallel} = \frac{\hat{p}_{e-\parallel}}{\gamma_e} = \frac{1 + \hat{p}_{e-\perp}^2 - (\Lambda_0 + \Delta\psi)^2}{\beta_\phi^p (\Lambda_0 + \Delta\psi) \mp \sqrt{\mathcal{D}/4}} \times \frac{\beta_\phi^p (\Lambda_0 + \Delta\psi) \mp \sqrt{\mathcal{D}/4}}{\beta_\phi^p (1 + \hat{p}_{e-\perp}^2) \mp \sqrt{\mathcal{D}/4} (\Lambda_0 + \Delta\psi)}$. Simplifying the expression for the longitudinal velocity of the electron,

$$\beta_{e-\parallel} = \frac{\hat{p}_{e-\parallel}}{\gamma_e} = \frac{1 + \hat{p}_{e-\perp}^2 - (\Lambda_0 + \Delta\psi)^2}{\beta_\phi^p(1 + \hat{p}_{e-\perp}^2) \mp \sqrt{\mathcal{D}/4}(\Lambda_0 + \Delta\psi)} \quad (2.19)$$

For a background plasma electron to get trapped in the plasma wave it must gain a longitudinal velocity which is equal to or greater than the plasma wave phase velocity,

$$\beta_{e-\parallel} \geq \beta_\phi^p.$$

To analyze this we evaluate the quantity, $\beta_{e-\parallel} - \beta_\phi^p$. By analyzing this expression we can determine the trapping condition. Substituting the expressions, $\beta_{e-\parallel} - \beta_\phi^p = \frac{\hat{p}_{e-\parallel}}{\gamma_e}$. We

use, $|\beta_\phi^p - \beta_{e-\parallel}| = \pm \frac{\sqrt{\mathcal{D}}}{2\gamma_e} = \frac{-\mathcal{D}/2 \pm \sqrt{\mathcal{D}}\beta_\phi^p(\Lambda_0 + \Delta\psi)}{\beta_\phi^p(1 + \hat{p}_{e-\perp}^2) \mp \sqrt{\mathcal{D}/4}(\Lambda_0 + \Delta\psi)}$. We use the expression $\Lambda_0 + \Delta\psi = \gamma_e(1 - \beta_\phi^p \beta_{e-\parallel})$. Substituting, $\beta_\phi^p - \beta_{e-\parallel} = \frac{-\gamma_e^2(\beta_\phi^p - \beta_{e-\parallel})^2 \pm \beta_\phi^p \gamma_e^2 |\beta_\phi^p - \beta_{e-\parallel}| (1 - \beta_\phi^p \beta_{e-\parallel})}{\beta_\phi^p(1 + \hat{p}_{e-\perp}^2) \mp \gamma_e^2 |\beta_\phi^p - \beta_{e-\parallel}| (1 - \beta_\phi^p \beta_{e-\parallel})}$. From the definition of Lorentz factor, $1 + \hat{p}_{e-\perp}^2 = \gamma_e^2 - \gamma_e^2 \beta_{e-\parallel}^2$. Substituting the Lorentz factor,

$$\beta_\phi^p - \beta_{e-\parallel} = \gamma_e^2 \frac{- (\beta_\phi^p - \beta_{e-\parallel})^2 \pm \beta_\phi^p |\beta_\phi^p - \beta_{e-\parallel}| (1 - \beta_\phi^p \beta_{e-\parallel})}{\gamma_e^2 (\beta_\phi^p(1 - \beta_{e-\parallel}^2) \mp |\beta_\phi^p - \beta_{e-\parallel}| (1 - \beta_\phi^p \beta_{e-\parallel}))}. \text{ We find the trapping condition as,}$$

$$\begin{aligned} \beta_\phi^p - \beta_{e-\parallel} &= \frac{- (\beta_\phi^p - \beta_{e-\parallel})^2 \pm \beta_\phi^p |\beta_\phi^p - \beta_{e-\parallel}| (1 - \beta_\phi^p \beta_{e-\parallel})}{\beta_\phi^p(1 - \beta_{e-\parallel}^2) \mp |\beta_\phi^p - \beta_{e-\parallel}| (1 - \beta_\phi^p \beta_{e-\parallel})} \\ &= |\beta_\phi^p - \beta_{e-\parallel}| \left(\frac{-|\beta_\phi^p - \beta_{e-\parallel}| \pm \beta_\phi^p (1 - \beta_\phi^p \beta_{e-\parallel})}{\beta_\phi^p(1 - \beta_{e-\parallel}^2) \mp (\beta_\phi^p - \beta_{e-\parallel})(1 - \beta_\phi^p \beta_{e-\parallel})} \right) \end{aligned} \quad (2.20)$$

$$= |\beta_\phi^p - \beta_{e-\parallel}| \operatorname{sgn}(\beta_\phi^p - \beta_{e-\parallel}) \quad (2.21)$$

When electron velocity exceeds the plasma-wave phase-velocity, $\beta_\phi^p < \beta_{e-\parallel}$ and $\operatorname{sgn}(\beta_\phi^p - \beta_{e-\parallel}) = -1$. And, when the plasma-wave phase velocity exceeds the electron velocity, $\beta_\phi^p > \beta_{e-\parallel}$ and $\operatorname{sgn}(\beta_\phi^p - \beta_{e-\parallel}) = +1$.

Thus using the known values of $\hat{p}_{e-\perp}$ and $\Delta\psi$ we obtain the condition where the wave breaks and the electron velocity exceeds the plasma-wave phase-velocity.

2.4 Trapping condition - multi-dimensional wake

Trapping occurs when $\beta_\phi^p \gtrapprox \beta_{e-\parallel}$ as the particle slowly drifts in the wave-frame until it reaches the accelerating phase of the wave potential. Since the particle cannot escape the potential well it is localized to the region of accelerating phase in the wave-frame. So, the electrons that are trapped in the plasma-wave gain energy from the fields and $\beta_{e-\parallel} \gtrapprox \beta_\phi^p$.

We refer to a particle being trapped when $\beta_\phi^p = \beta_{e-\parallel}$. Thus under the trapping condition $\mathcal{D} = 4(\gamma_e \beta_\phi^p - \hat{p}_{e-\parallel})^2 = 0$. Under this condition the expression for longitudinal momentum, $\hat{p}_{e-\parallel}$ and the electron Lorentz factor γ_e are,

$$\begin{aligned}\gamma_e &= \frac{1 + \hat{p}_{e-\perp}^2}{\Lambda_0 + \Delta\psi} \\ \hat{p}_{e-\parallel} &= \frac{1 + \hat{p}_{e-\perp}^2 - (\Lambda_0 + \Delta\psi)^2}{\beta_\phi^p(\Lambda_0 + \Delta\psi)}\end{aligned}\quad (2.22)$$

The trapping condition for the Lorentz factor in eq.2.22 is rearranged to obtain, $\Lambda_0 + \Delta\psi = \gamma_0 - \beta_\phi^p p_{e-\parallel}^0 + \Delta\psi = \frac{1 + \hat{p}_{e-\perp}^2}{\gamma_e} = \frac{\gamma_e^2 - \gamma_e^2 \beta_\parallel^2}{\gamma_e} = \gamma_e(1 - \beta_\phi^2) = \frac{1}{\gamma_\phi} \frac{\gamma_e}{\gamma_\phi}$. Thus the condition on the plasma-wave potential to trap the electrons is,

$$\begin{aligned}\Delta\psi &= (\phi - \beta_\phi^p a_\parallel) - \psi_0 = \frac{1}{\gamma_\phi} \frac{\gamma_e}{\gamma_\phi} - \gamma_0 + \beta_\phi^p p_{e-\parallel}^0 \\ \text{If } \gamma_0 = 1, \quad p_{e-\parallel}^0 = \psi_0 = 0, \quad \psi &= \frac{1}{\gamma_\phi} \frac{\gamma_e}{\gamma_\phi} - 1\end{aligned}\quad (2.23)$$

The condition on effective potential ψ for trapping in multi-dimensional wakes is similar to the one derived from simple considerations shown in eq.1.14.

$$\begin{aligned}\text{1D : } \phi_{lab-frame} &< \left(\frac{1}{\gamma_\phi} - 1 \right) \frac{m_e c^2}{e} \\ \text{multi-D : } \psi &< \frac{1}{\gamma_\phi} \frac{\gamma_e}{\gamma_\phi} - 1\end{aligned}\quad (2.24)$$

The factor $\frac{\gamma_e}{\gamma_\phi} = \sqrt{\frac{1-\beta_\phi^p}{1-\beta_{e-\perp}^2-\beta_{e-\parallel}^2}}$ at the trapping condition becomes $\frac{\gamma_e}{\gamma_\phi}|_{(\beta_{e-\parallel}=\beta_\phi^p)} = \sqrt{\frac{1-\beta_\phi^p}{1-\beta_{e-\perp}^2-\beta_\phi^p}} = \sqrt{\frac{1}{1-\gamma_\phi^2\beta_{e-\perp}^2}}.$

In the case where $\beta_{e-\perp} = 0$ we get $\frac{\gamma_e}{\gamma_\phi} = 1$ which gives us the 1-D trapping condition.

It should be noted that this analysis determines an amplitude for the potential ϕ at which $\beta_\phi^p = \beta_{e-\parallel}$ and there is onset of trapping. However, this analysis does not give any estimate on the mixing time over which the electrons that are oscillating accrue enough phase-shift to start experiencing the wave-fields / potential to get trapped.

2.5 Phase-mixing of non-linear plasmons

It is of relevance to study the injection of plasma e^- in a rising density inhomogeneity. The feasibility of the trapping of plasma electron due to phase-mixing in both rising and downward density gradient has been shown in [19]. However, no model of trapping in non-linear plasma structures is presented and no scaling laws have been developed.

An uncontrolled injection of plasma e^- in successive plasmon buckets can increase the energy spread of the accelerated beam. The termination of injection is critical to maintaining nearly equal acceleration lengths at peak field of the stacked trapped beams injected into multiple plasmon-buckets.

Secondly, in beam-driven schemes where the forward longitudinal momenta is smaller in comparison to ultra-short laser pulses (where forward longitudinal ponderomotive force is higher), this mechanism can lead to injection of plasma e^- . The beam-driven plasma does not trap and self-inject because plasma electron longitudinal momenta are lower. These trapped particles may be observed as beam-lets at driving beam energy.

And, an analysis of trapped beams can be used as diagnostics of the beam-plasma interaction and also to study the state of the plasma behind the driver[16].

As the phase-mixing injection mechanism is a 1-D process it is described using 1-D model (seen in the on-axis trapping in Fig.4.2[a]-[c]). The 1-D momentum equation of

longitudinal oscillations of a plasmon (along z) is $\frac{d^2}{d\tau^2} (\beta_\phi p_{ez} - \gamma_e) + \omega_{pe}^2(z) \beta_\phi^2 \frac{p_{ez}}{\beta_\phi \gamma_e - p_{ez}} = 0$, where $d\tau = d(z/\beta_\phi - t)$. By simplifying, $\beta_z^e = p_{ez}/\gamma_e$, $\beta_\phi \sim 1$ and $\mathcal{Z} = \sqrt{(1 - \beta_z^e)/(1 + \beta_z^e)}$, we have, $\frac{d^2}{d\tau^2} \mathcal{Z} + \omega_{pe}^2(\beta_\phi \tau + t) \frac{1}{2}(1/\mathcal{Z}^2 - 1) = 0$. The equation is similar in form to the Hill's equation due to the presence of a function of dependent variable as the coefficient. The momentum solutions have phase-mixing (in Fig.2.2), as the solutions depend upon of plasmon oscillation frequencies and amplitudes ($k_{pe}(z)$ and $\omega_{pe}(z)$).

We can build a physical picture of trapping of plasma e^- by phase mixing of trajectories. The up-ramped density inhomogeneity leads to frequency up-chirped spatial-train of coherently oscillating sheets. The perturbed infinitesimal plasma sheets have different characteristic plasma frequency due to different density, therefore coupled individual sheet oscillators undergo a phase-mixing (see Fig.1)[4]. Following [4]sec.IV-1D model, the displacement, ξ_m from equilibrium, x_0 or the trajectory is $\frac{d^2 \xi}{dt^2} = - \int_{x_0}^{x_0 + \xi} \frac{4\pi e^2}{m_e} n_0(x) dx$. The time for mixing to start is $t_{mix} = \frac{\pi}{2(d\omega_{pe}/dx)\xi_m}$.

The displacement from equilibrium, X depends upon the maximum longitudinal field, $\lambda_{pe}(E_{||}/E_{wb})$. So, in 1-D model $t_{mix} \propto \frac{1}{E_{||}/E_{wb}} \frac{1}{(d\omega_{pe}/dx)}$. The effect of phase-mixing between infinitesimal sheet leads to plasma e^- encountering unbalanced fields that are not experienced during in-phase oscillations, this results in their disruption. The trajectory of first oscillation in the forward direction of propagation of the source do not cross. Because, the driven e^- propagate in the same direction, $\xi_{forward}$. However, during the returning trajectories of the oscillations, $\xi_{returning}$, the faster oscillators (higher in density) encounter the potential well of the slower oscillators. Therefore the trapping of e^- occurs in the second and subsequent buckets and not in the first bucket. Since, the peak fields are in the first bucket this trapping mechanism is not ideal for acceleration.

The disruption of the plasma oscillations also occurs when the e^- trajectories are highly non-linear ($p_e > m_e v_\phi$) resulting in phase-mixing[4] (for instance they cross in the back of the bubble). The plasma e^- that go out-of-phase see unbalanced fields in the wave-frame and get trapped in the accelerating phase of the fields. Therefore in laser excited non-linear

plasmons the trapping also occurs in the first bucket.

1-D Planar geometry Sheet Oscillations in a Rising Density Gradient

To determine the applicability of the simple gradient and amplitude-dependent sheet crossing model in the earlier chapter we use computational methods. It is important and necessary to use computational method because the earlier models assume a freely oscillating set of plasma electron sheet. However, in the wakefields, the sheets are driven by an energy source of arbitrary shape. So the solutions of planar oscillations driven in the wake of a driven in 1-D geometry are hard to model analytically. Thus, we use PIC code to determine the phase-mixing time of the driven planar oscillations.

3.1 Scaling of phase-mixing in 1D beam-driven planar wake

We study the onset of particle trapping using the OSIRIS PIC code [15][21]. Here we study the phase-mixing of plasma oscillations in 1D geometry. Thus spatially we retain only the longitudinal dimension along which the driving energy source propagates. However, to understand the effect of the driving energy source we retain all the 3 components of the electron momentum.

As described earlier in 1D the oscillations are planar with individual electron sheets

following the equation of motion. It was shown that the description of using individual electron sheets as independent oscillator broke down when the amplitude of the oscillations trajectory is higher than a critical amplitude. Secondly, a density gradient was shown to cause phase-mixing due to trajectory crossing of individual oscillators.

We study beam-driven 1D oscillations here. It is important to note an essential difference between the beam-driven and laser-driven longitudinal oscillations. The maximum longitudinal momentum of the oscillators in these two drivers is very different. This can be seen by comparing equations for longitudinal momentum in the two cases.

$$\begin{aligned}
 & \left(\frac{1}{c^2} \frac{\partial^2}{\partial t^2} + k_{pe}^2 \right) [\gamma \beta_{\parallel}] \\
 &= -\frac{1}{c} \frac{\partial}{\partial t} \nabla \frac{a_{\perp}^2}{2} \Big|_{\text{laser}} \\
 &= k_{pe}^2 \int_{-\infty}^{\infty} \frac{1}{c} \frac{\partial}{\partial t} \frac{n_b(z)}{n_0} dz \Big|_{\text{beam}}
 \end{aligned} \tag{3.1}$$

Since, in the laser driven oscillations the longitudinal momentum depends upon the ponderomotive force which depends upon the spatial profile the laser pulse intensity, $\nabla \frac{a_0^2}{2}$ and it can be quite high. In the regime where the peak vector potential $a_0 \gtrsim 1$ the electron longitudinal velocity can approach the plasma wave velocity. Note from earlier discussion that the trapping condition, $\beta_{\parallel}^e \simeq \beta_{\phi}^p$ is then satisfied.

However, in the beam-driven oscillations the longitudinal momentum is dependent upon the time variation of the beam density, $\frac{\partial}{\partial t} \frac{n_b(z)}{n_0}$. However, the beam density is nearly constant, $\frac{\partial}{\partial t} \frac{n_b(z)}{n_0} \ll 1$ over single plasma oscillation and changes much more slowly than the plasma-wave time-scales $\frac{\partial}{\partial t} \frac{n_b(z)}{n_0} \gg \omega_{pe}^{-1}$. This is an essential and good approximation in the plasma wakefield theory, it is referred to as the *quasi-static approximation* or the *frozen-field approximation*. Thus there is no trapping in beam-driven oscillations just behind the beam.

Here, for isolating the effect of the oscillation amplitude on phase-mixing, we simulate

cases where the driven oscillations are expected to be linear. Since, for linearity the condition on the density perturbation in the plasma-wave is $\delta n \ll n_0$. And, from the earlier formulation we known that

$$\delta n \propto n_b < n_0.$$

Thus, in the simulations we beam density less than the background plasma density, $n_b < n_0$.

We analyze the scaling of trapping using the 1D phase-mixing model for phase-mixing time in the rising density gradient,

$$\Delta t_{mix} = \frac{\pi}{2 \frac{\partial \omega_{pe}(x)}{\partial x} \xi_m}.$$

It is noted that the amplitude of the trajectory, $\xi_m \propto n_b$. Thus the scaling of trapping using the 1D phase-mixing model for phase-mixing time in the rising density gradient,

$$\Delta t_{mix} \Big|_{\text{beam-driven}} \propto \frac{\pi}{2 \frac{\partial \omega_{pe}(x)}{\partial x} n_b}.$$

In a general density gradient the plasma frequency along the density gradient varies as

$$\omega_{pe}(x) = \omega_{p0} \sqrt{\frac{n(x)}{n_0}}.$$

Thus, $\frac{\partial \omega_{pe}(x)}{\partial x} = \omega_{p0} \frac{1}{2\sqrt{n_0 n(x)}} \frac{\partial n(x)}{\partial x}$. Substituting this into the phase-mixing time expression for beam-driven planar plasma oscillations, $\Delta t_{mix} \Big|_{\text{beam-driven}} \propto \frac{\pi}{2 \frac{1}{\omega_{p0} \frac{1}{2\sqrt{n_0 n(x)}} \frac{\partial n(x)}{\partial x}} n_b}$.

This can be further simplified as,

$$\Delta t_{mix} \Big|_{\text{beam-driven}} \propto \pi \omega_{p0}^{-1} \frac{\sqrt{n(x)/n_0}}{\frac{\partial n(x)}{\partial x} \frac{n_b}{n_0}} \quad (3.2)$$

Thus the model in eq.3.2 shows that the phase-mixing time, $\Delta t_{mix} \propto \sqrt{n(x)/n_0}$, depends upon the location in the density gradient and increases with rising density. So, it takes longer to accumulate phase-difference between individual oscillations as the density

increases.

The eq.3.2 suggests that the phase-mixing is fastest close to the vacuum-plasma interface and slowest close to where the gradient transitions into homogeneous plasma.

However, since phase-mixing eventually leads to the onset of trapping of plasma electrons, near the vacuum-plasma interface where the density is low, smallest density of electrons is trapped. As we move further up the density gradient a higher density of electrons is trapped but the trapping is slower. Thus there is some optimum density, $n(x)$ at which the density is just high enough and the phase-mixing fast enough to trap a significant density of electrons in the plasma wave.

The eq.3.2 also provides 1D planar scaling laws for the onset trapping in a rising density gradient with the drive-beam density, $\frac{n_b}{n_0}$ and rising density gradient scale length, $\frac{\partial n(x)}{\partial x}$.

$$\begin{aligned} \Delta t_{mix} \Big|_{\text{beam-driven}} &\propto \left(\frac{\partial n(x)}{\partial x} \right)^{-1} \\ &\propto \left(\frac{n_b}{n_0} \right)^{-1} \end{aligned} \quad (3.3)$$

In a linearly rising density gradient with the homogeneous plasma density $\omega_{p0} = \sqrt{\frac{4\pi n_0 e^2}{m_e}}$ and which is taken to rise from $\omega_{pe}(0)|_{n(x=0)} = 0$,

$$n(x) = n_0 \frac{x}{L_\Delta} \mathcal{H}(x) \quad \text{and} \quad \omega_{pe}(x) = \omega_{p0} \sqrt{\frac{x}{L_\Delta}} \mathcal{H}(x).$$

Thus, $\frac{\partial n(x)}{\partial x} = L_\Delta^{-1}$ and $\sqrt{\frac{n(x)}{n_0}} = \sqrt{\frac{x}{L_\Delta}}$. Using these expressions, in a linear rising density gradient,

$$\Delta t_{mix} \Big|_{\text{beam-driven}} \propto \pi \omega_{p0}^{-1} \sqrt{x} \left[\frac{\sqrt{L_\Delta}}{n_b/n_0} \right] \quad (3.4)$$

We simulate the rising density gradient cases where $L_\Delta = 10 \dots 100 \frac{c}{\omega_{pe}}$ and beam-densities $n_b/n_0 = 0.025, 0.05, 0.075, 0.1, 0.2, 0.5$.

3.2 Phase-mixing scaling with drive-beam density, n_b/n_0

We setup the PIC simulations for the 1D with a resolution of 40 simulation cells per plasma skin-depth, $\frac{c}{\omega_{pe}}$. The velocity components are initialized and updated in a 3D space. We initialize plasma electrons with 400 particles per cell with fixed background ions. The plasma electrons have a small thermal velocity of $p_{th} = 0.02m_ec$. We initialize the electron beam with 100 particles per cell with Gaussian profile of $\sigma_z = 1.5 \frac{c}{\omega_{pe}}$ and a relativistic factor $\gamma_b = 38,000$. The beam is assumed to have zero thermal velocity. The particle shape is *quartic*. The particle and field boundaries of the simulation space are open. The electromagnetic field solver uses second-order centered difference approximation. The rising density gradients with different gradients are setup to start from $50 \frac{c}{\omega_{pe}}$, with zero plasma density ahead of the gradient.

In this section we analyze the dependence of the phase-mixing time of the planar longitudinal oscillations on the beam density of the drive electron beam. We simulate beam-densities $n_b/n_0 = 0.025, 0.05, 0.075, 0.1, 0.2, 0.5$ and look for the trapped particles in the longitudinal momentum phase-space. The rising density gradient scale-length is fixed, $L_\Delta = 20 \frac{c}{\omega_{pe}}$.

The longitudinal momentum phase-space are shown in Fig.3.1 and Fig.3.2. As shown in Fig.3.1(a) the drive electron beam is located at $140 \frac{c}{\omega_{pe}}$.

In Fig.3.3 we plot the location of the first trapped particles behind the drive beam. This is equivalent to the phase-mixing time as it indicates the time the phase-offset particles require to get trapped with a phase of the plasma.

From Fig.3.1, Fig.3.2 we observe that for lower beam densities the plasma wave nearly sinusoidal. But as the beam-density approaches, $n_b \rightarrow n_0$ the wave starts *self-steepening*. The phenomenon of self-steepening occurs before the onset of trapping. Self-steepening

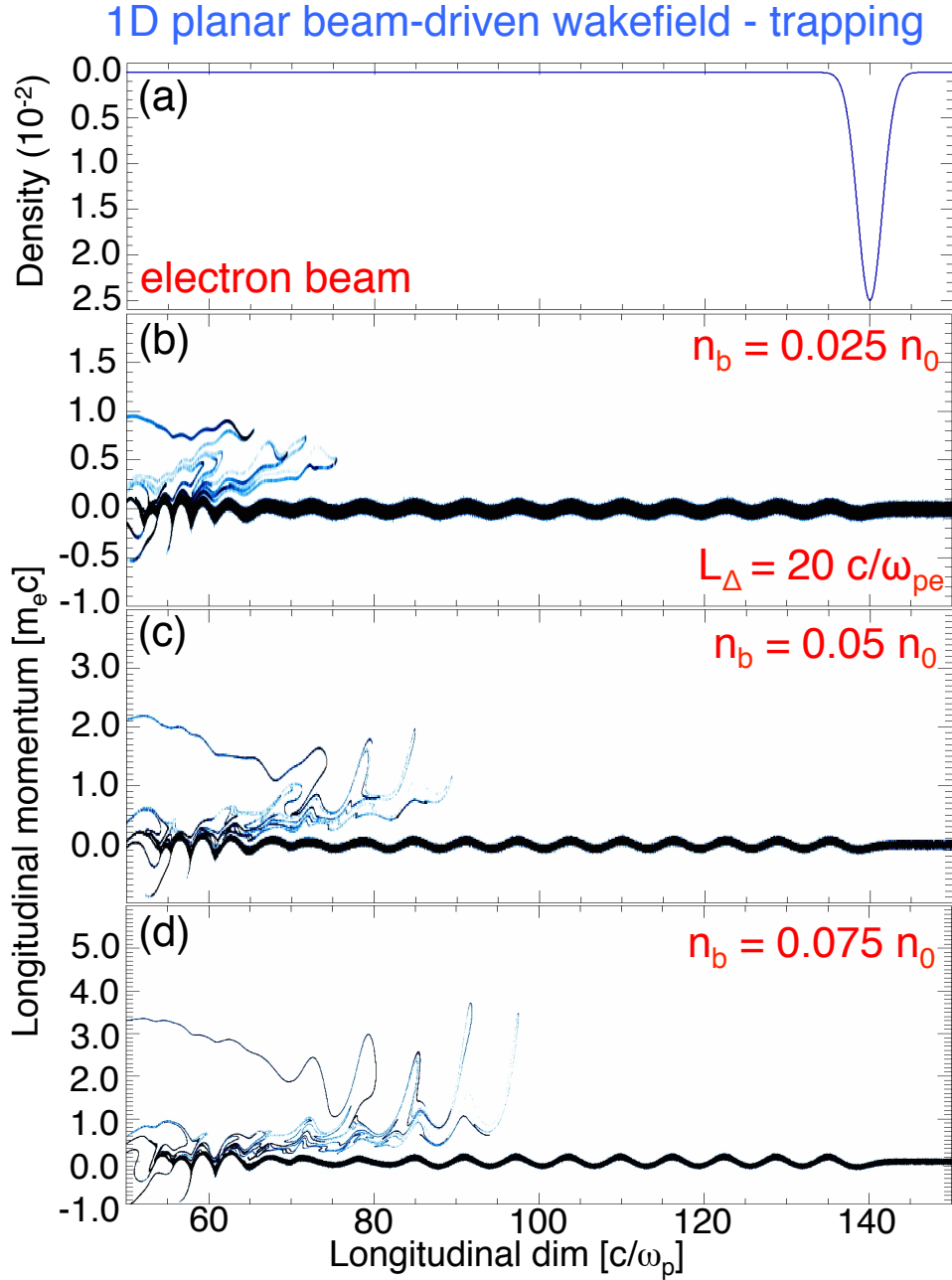


FIGURE 3.1: *Onset of phase-mixing self-injection in a beam-driven 1D planar plasma for different drive beam densities - I.* In this figure we look at the onset of phase-mixing in the wakefields driven in a rising density gradient in a 1D planar plasma. In the simulations here, the plasma density rises from 0 to $1n_0$ over $L_\Delta = 20 \frac{c}{\omega_{pe}}$ between 50 and $70 \frac{c}{\omega_{pe}}$. (a) the beam location and shape is shown for the case of $n_b = 0.025n_0$. (b),(c) and (d) show the longitudinal momentum phase-spaces along the longitudinal dimension for $n_b = 0.025n_0$, $n_b = 0.05n_0$ and $n_b = 0.075n_0$ respectively.

1D beam-driven wakefield – trapping - continued

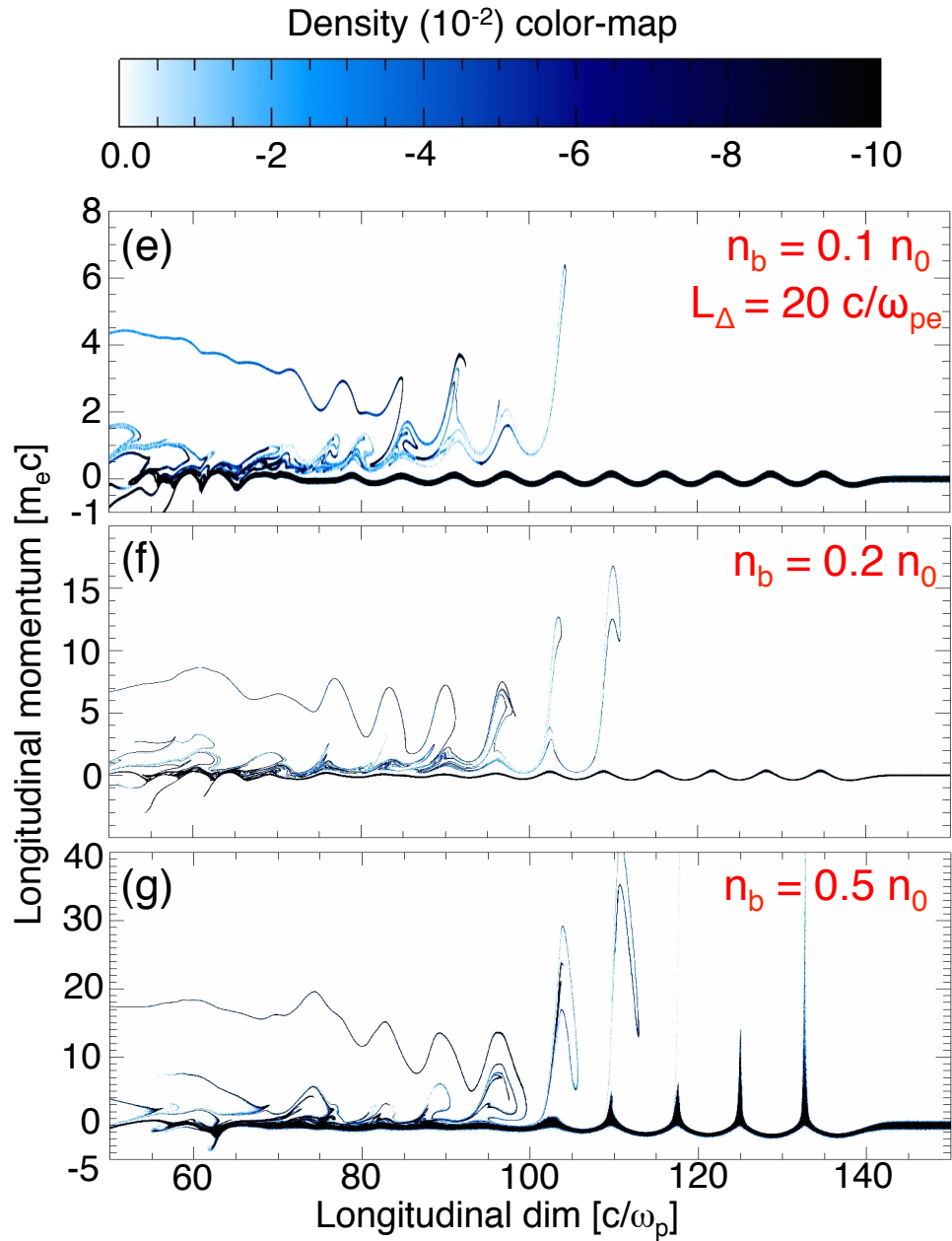


FIGURE 3.2: *Onset of phase-mixing self-injection in a beam-driven 1D planar plasma for different drive beam densities - II.* The longitudinal momentum phase-spaces are shown at the same time as shown in Fig.3.1 with the beam located at $\simeq 140 \frac{c}{\omega_{pe}}$. (e),(f) and (g) show the longitudinal momentum phase-spaces along the longitudinal dimension for $n_b = 0.1n_0$, $n_b = 0.2n_0$ and $n_b = 0.5n_0$ respectively.

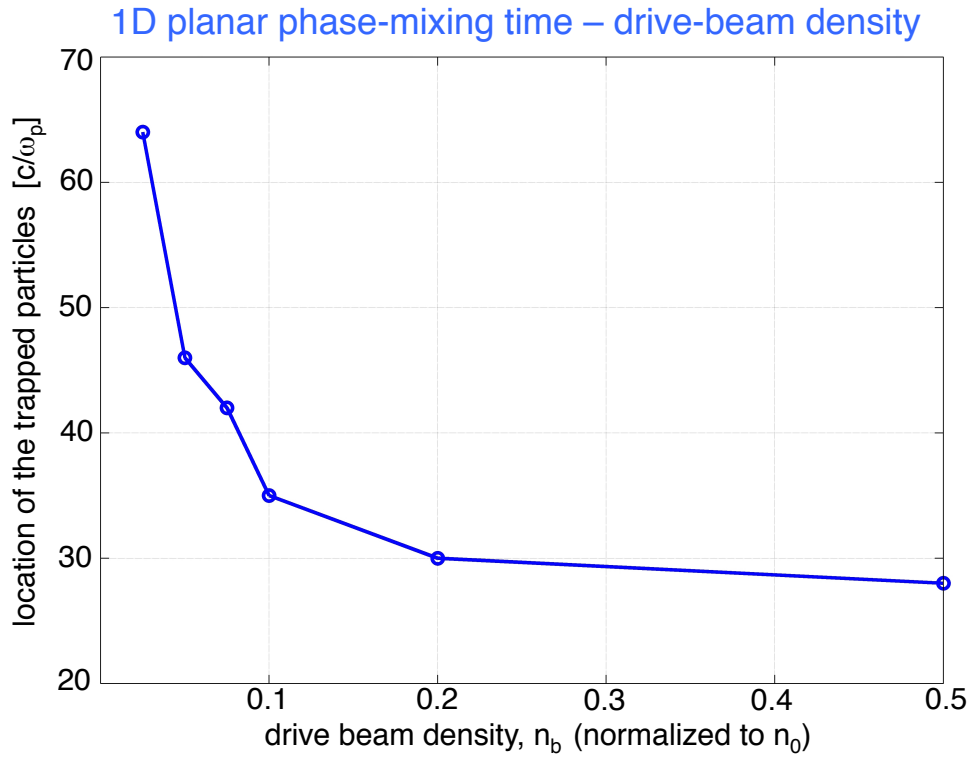


FIGURE 3.3: *Dependence of the phase-mixing time on the drive-beam density.* Dependence of the phase-mixing time on the drive electron beam density. Location of the first trapped particles behind the driver electron beam for different drive beam densities in Fig.3.1 and Fig.3.2 with the beam located at $\simeq 140 \frac{c}{\omega_{pe}}$. Note that from eq.3.4 we know that $\Delta t_{mix} \propto (n_b/n_0)^{-1}$.

occurs when particles get close to the phase-velocity of the wave. The self-steepening of the beam-driven wake is shown in Fig.3.2(g) as the wave potential gets higher the density wave departs from its sinusoidal structure. There are more particles close the the accelerating phase of the wave. Note that self-steepening also leads to trapping.

We also observe trapped particles in each of the simulations. Upon plotting the phase-mixing time leading to trapping we see that the 1D simulations suggest the hyperbolic scaling shown in eq.3.4, $\Delta t_{mix} \propto (n_b/n_0)^{-1}$.

3.3 Phase-mixing scaling with rising gradient scale-length, L_Δ

In this section we analyze the dependence of the phase-mixing time of the planar longitudinal oscillations on the rising gradient scale-length, L_Δ . We simulate rising gradient scale-length, $L_\Delta = 10, 20, 30, 40, 50, 100 \frac{c}{\omega_{pe}}$ and look for the trapped particles in the longitudinal momentum phase-space. The drive-beam density is fixed $n_b/n_0 = 0.1$. As the drive-beam density ensures $\delta = \frac{n-n_0}{n_0} \simeq \frac{n_b}{n_0} \ll 1$ these simulations are in the linear amplitude regime. Thus, we ensure that the observed non-linear effect of phase-mixing and trapping is due to the rising density gradient.

The longitudinal momentum phase-space are shown in Fig.3.4 and Fig.3.5. As shown in Fig.3.1(a) the drive electron beam is located at $140 \frac{c}{\omega_{pe}}$. Plotting the phase-mixing time leading to trapping we see that the 1D simulations suggest the parabolic scaling shown in eq.3.4, $\Delta t_{mix} \propto \sqrt{L_\Delta}$.

1D beam-driven wake – density gradient scaling

Density (10^{-2}) color-map

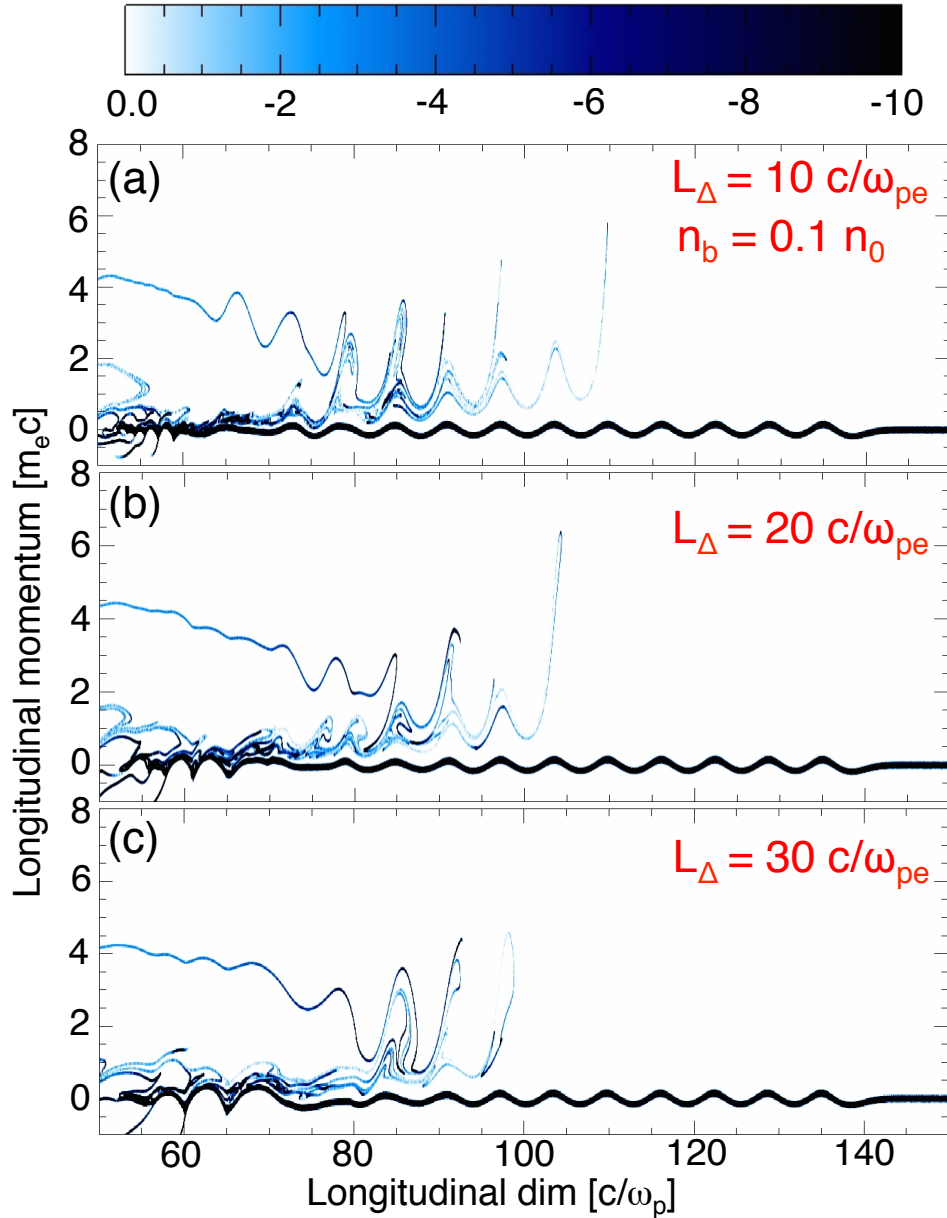


FIGURE 3.4: *Scaling of the onset of 1D planar oscillations phase-mixing with rising gradient length - I.* In the simulations here, the plasma density starts rising from 0 to $1n_0$ from $50\frac{c}{\omega_{pe}}$. The onset of trapping is shown in the longitudinal momentum phase-space of the plasma electrons plotted along the longitudinal dimensions. (a),(b) and (c) show the longitudinal momentum phase-spaces along the longitudinal dimension for $L_\Delta = 10\frac{c}{\omega_{pe}}$, $L_\Delta = 20\frac{c}{\omega_{pe}}$ and $L_\Delta = 30\frac{c}{\omega_{pe}}$ respectively.

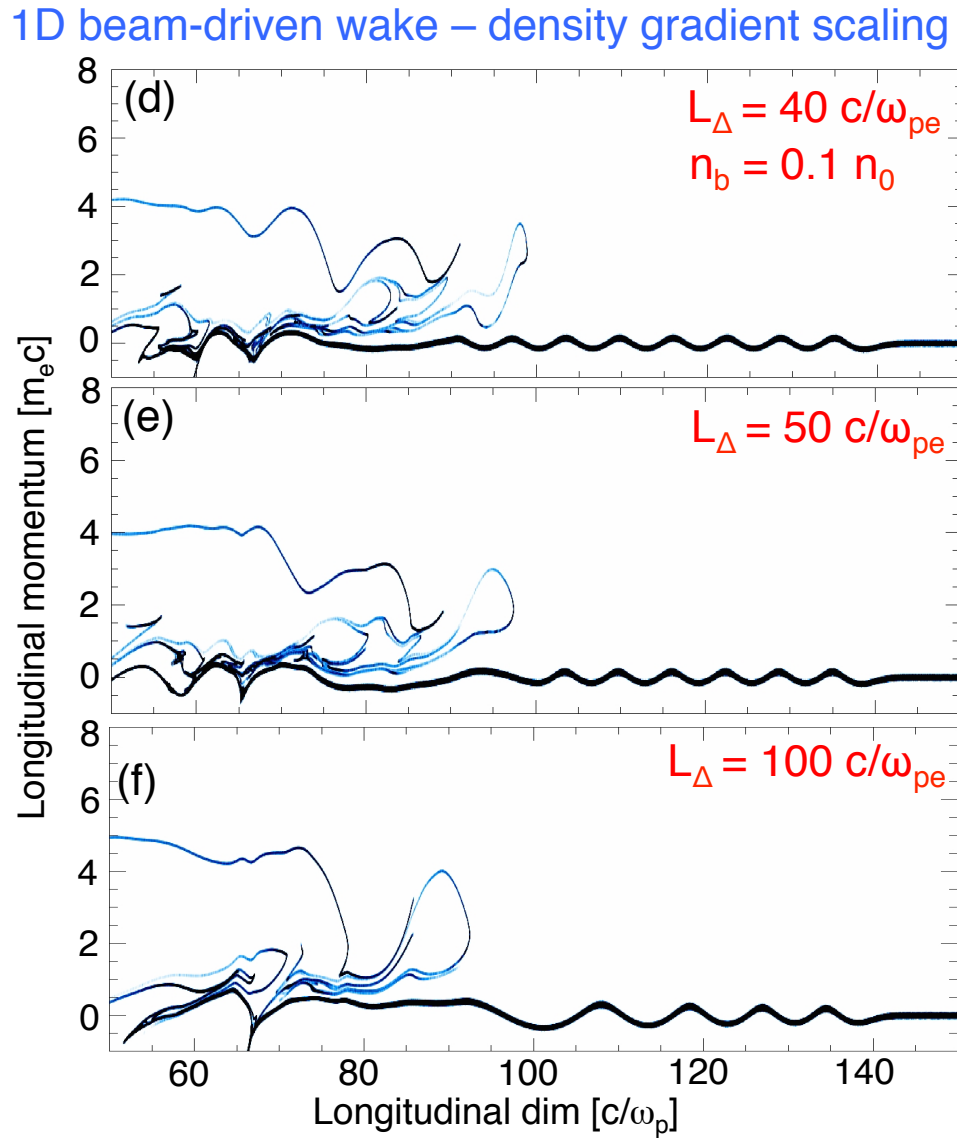


FIGURE 3.5: *Scaling of the onset of phase-mixing in a beam-driven 1D planar plasma with the rising gradient scale-length - II.* The longitudinal momentum phase-spaces are shown at the same time as shown in Fig.3.1 with the beam located at $\simeq 140 \frac{c}{\omega_{pe}}$. (e),(f) and (g) show the longitudinal momentum phase-spaces along the longitudinal dimension for $n_b = 0.1n_0$, $n_b = 0.2n_0$ and $n_b = 0.5n_0$ respectively.

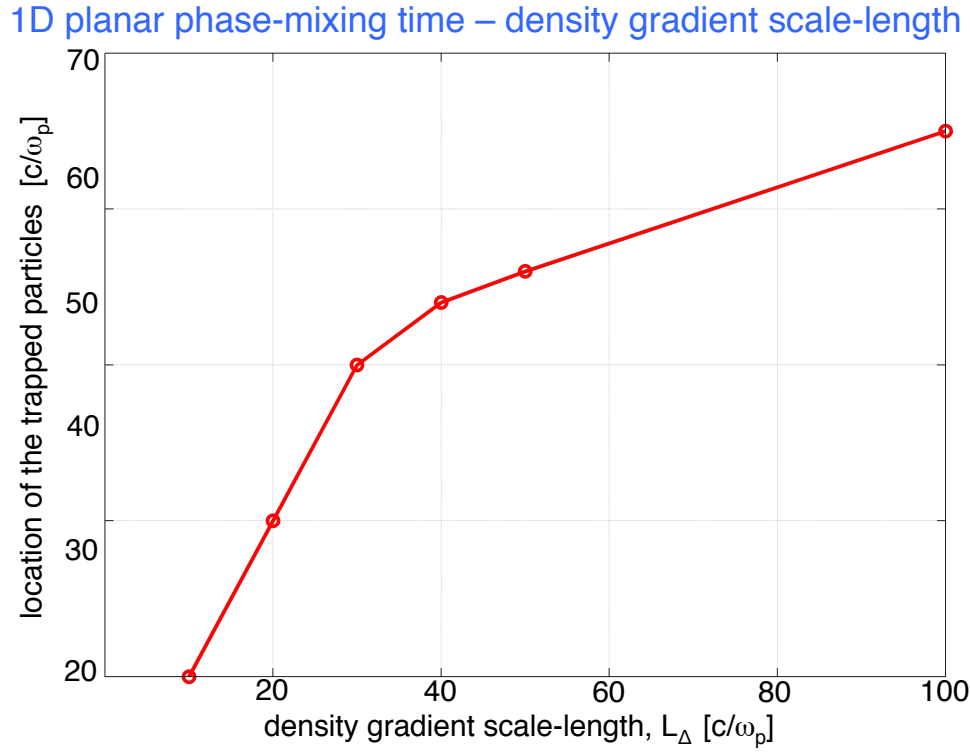


FIGURE 3.6: *Scaling of the onset of phase-mixing in a beam-driven 1D planar plasma with the density gradient scale-length.* Dependence of the phase-mixing time on the density gradient scale-length. Location of the first trapped particles behind the driver electron beam for different density gradient scale-lengths in Fig.3.4 and Fig.3.5 with the beam located at $\simeq 140 \frac{c}{\omega_{pe}}$. Note that from eq.3.4 we know that $\Delta t_{mix} \propto \sqrt{L_\Delta}$.

2-D Cylindrical Geometry Radial Oscillations in a Rising Density Gradient

Here we look at the effect of longitudinal density gradient on radial oscillations in cylindrical geometry. The longitudinal dimension is the direction along which the wave vector of the plasma-wave is oriented and it is also the direction along which the energy-sources propagate. So, it is an important question to ask - how does a longitudinal density gradient affect the radial oscillations.

The electrons are primarily deflected along the radial dimensions when interacting with short-intense energy sources. The oscillations driven in the wake of such drivers are thus along the radial dimensions of a cylindrical geometry, as explored above. A significant radial momentum is induced in the case of *relativistically intense energy sources* which can drive the radial momentum of the plasma electron to be relativistic, $\frac{p_\perp^e}{m_e c} \geq 1$.

A longitudinal component of electron momentum is also forced by the longitudinal force of the short-intense energy sources. In the case of a laser pulse the longitudinal force which is equal to the ponderomotive force shown above, can be significantly high. It is important to analyze the longitudinal momentum of the plasma electrons. Because, it is the relative velocity between the wave phase velocity at which the fields change phase and

the longitudinal velocity of the plasma electrons that decides the fields seen by the electrons with the small relative velocity. It is well known and shown above that the trapping starts if the wave potential is high enough and $\beta_\phi^p \simeq \beta_{\parallel e}^e$.

4.1 Trapping of electrons in 2D cylindrical geometry in a rising density gradient

In this section using PIC simulations we show the effect of a longitudinal density gradient on radial oscillations in a plasma wakefield. We use a density gradient that rises from a vacuum to maximum density in $20c/\omega_{pe}$, with initial vacuum extending out from the edge of the plasma. The profile of the density gradient is shown in Fig.4.1. We excite the density gradient at the vacuum-plasma interface with a laser and an electron beam energy source to determine the effect of trapping due to phase-mixing of oscillations in a rising density gradient.

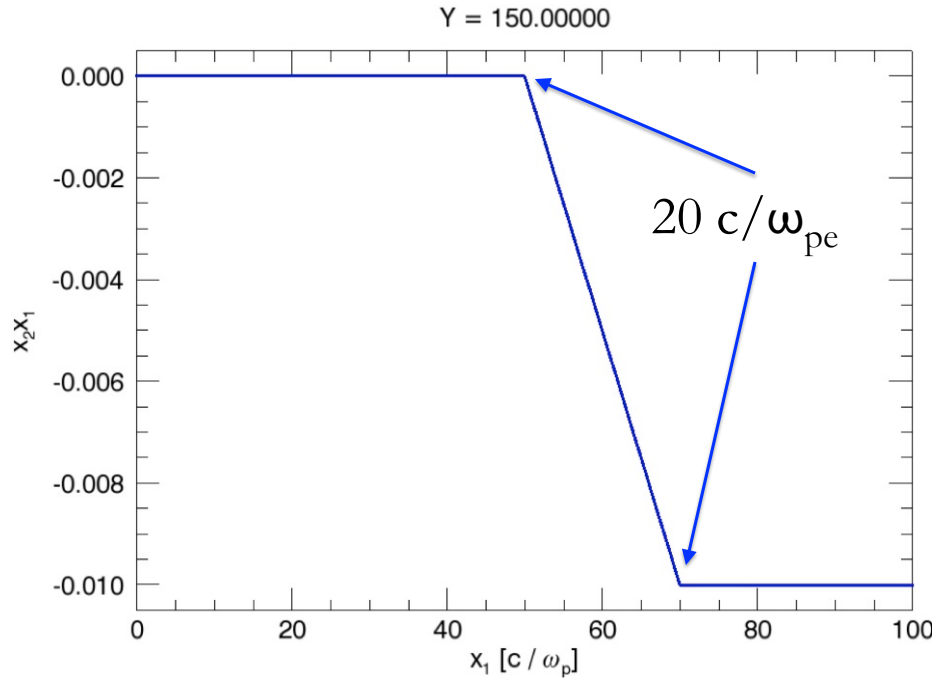


FIGURE 4.1: *Rising plasma density gradient at the vacuum-plasma interface.* The e^- density (negative) rises from 0 to $0.01n_c$ between 50 and $70\frac{c}{\omega_{pe}}$. The homogeneous plasma density is $0.01n_c$.

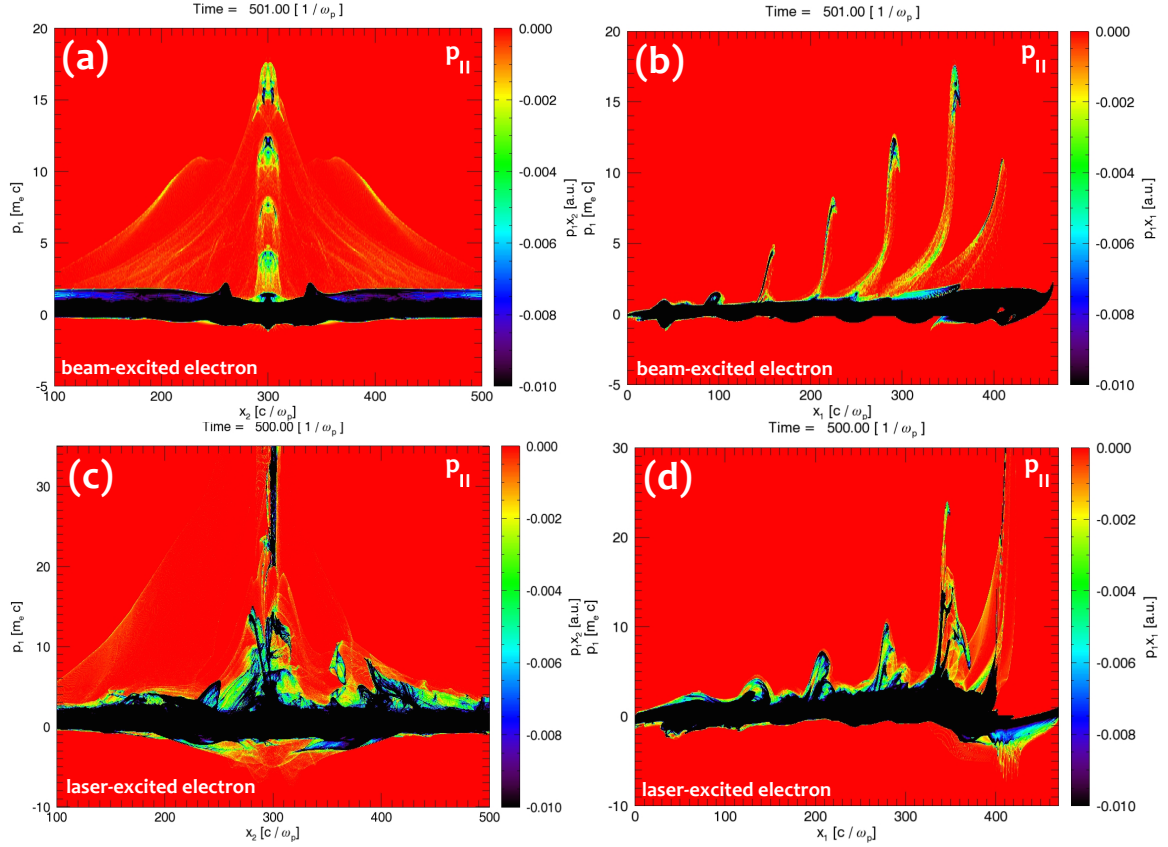


FIGURE 4.2: The 2D plasma e^- longitudinal momentum phase-space showing trapping of plasma electrons. Beam-driven phase-spaces are in (a) with transverse dimension (p_1x_2) and (b) with longitudinal (p_1x_1) dimension. Corresponding Laser-driven phase-space are in (c) and (d). The e^- trapped in first laser-driven bucket gain a peak momentum $\gamma_{\parallel}\beta_{\parallel} > 30$, whereas in both the beam and laser case, the second bucket e^- only gains, $\gamma_{\parallel}\beta_{\parallel} \sim 20$. Also, phase-mixing injection occurs only on the axis.

To show the trapping of plasma e^- oscillating in cylindrical geometry in a longitudinally rising plasma density gradient, we use $2\frac{1}{2}D$ OSIRIS[21] PIC code. We use cartesian coordinates for a laser pulse to setup circular polarization unlike a cylindrical / radial polarization that would be inherent under cylindrical symmetry. For the beam-driven case we use cylindrical coordinates in the PIC simulations. However, to make a fair comparison of trapping, the PIC results we present here are of the beam-driven wakefields in cartesian coordinates.

The simulations are setup with Eulerian specification of the plasma dynamics in a fixed

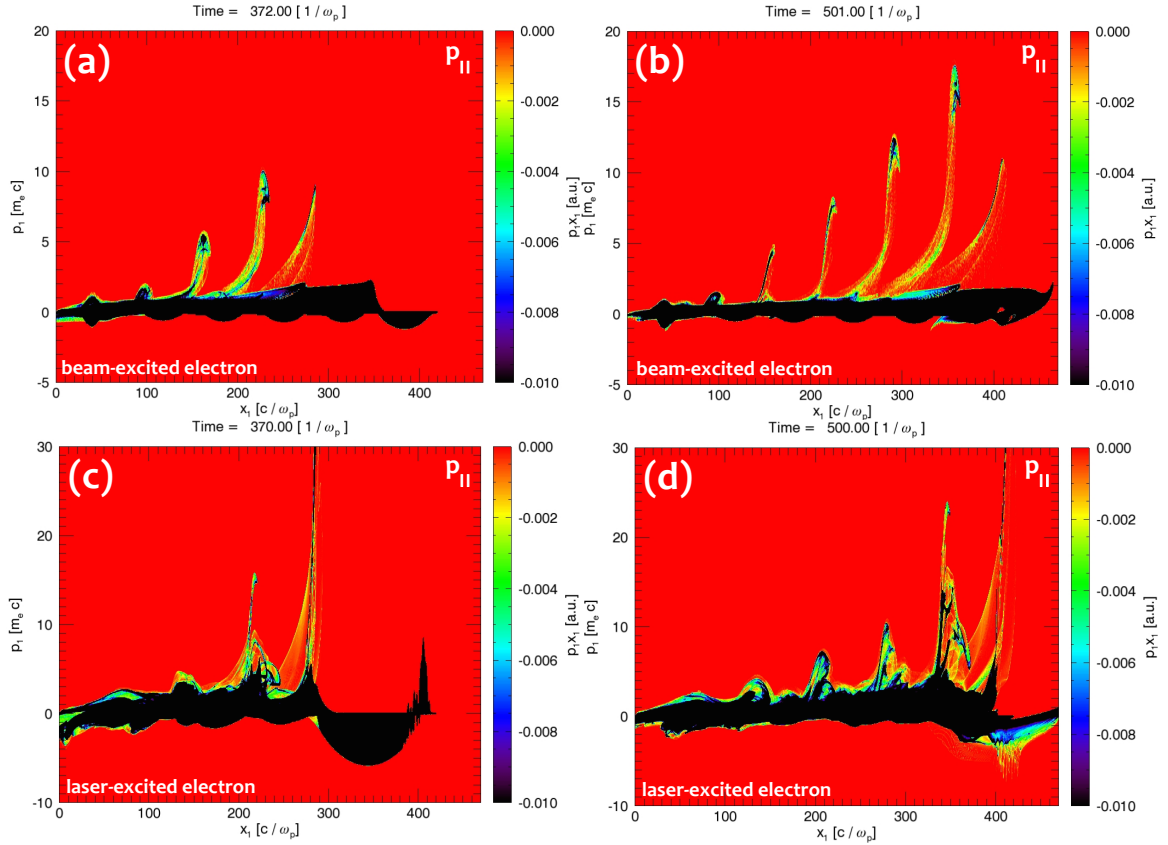


FIGURE 4.3: *Time evolution of plasma e^- longitudinal momentum (p_1x_1)*. The plasma e^- longitudinal momentum phase-space at $t \sim 370\frac{1}{\omega_{pe}}$ and $t \sim 500\frac{1}{\omega_{pe}}$.

frame. We initialize the homogeneous background plasma density to $n_0 = 1$ pre-ionized singly-charged state. The density gradient at the vacuum-plasma interface is in Fig.4.1 starts at $50\frac{c}{\omega_{pe}}$, with vacuum regions in the first and last $50\frac{c}{\omega_{pe}}$ longitudinal space.

For the case of a laser-driven wake we use a $\omega_{pe} = 10\omega_{pe}$. We resolve and reference the real time in simulation to the laser period $2\pi/\omega_0$ thereby the dynamics within a single plasma cycle is simulated in just $\sqrt{n_c/n_e} \sim 10$ laser cycles. We discretize the space with 20 cells per skin-depth (c/ω_{pe}) in the longitudinal and 10 cells per $\frac{c}{\omega_{pe}}$ in the transverse direction. The longitudinal simulation space size is $470\frac{c}{\omega_{pe}}$ and the transverse size is $300\frac{c}{\omega_{pe}}$ for laser-plasma and $600\frac{c}{\omega_{pe}}$ for beam-plasma simulations.

We use absorbing boundary conditions for fields and particles of all species. We use

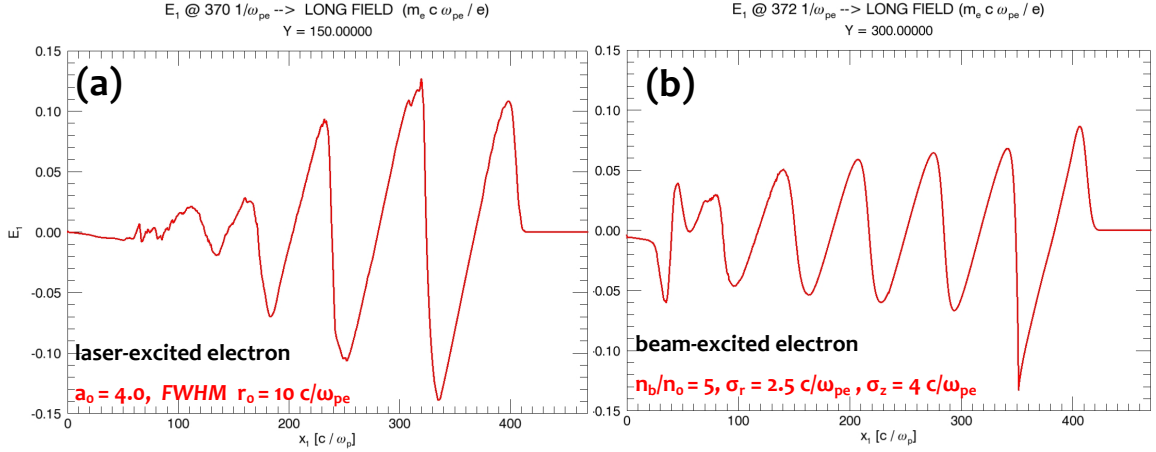


FIGURE 4.4: *On-axis longitudinal electric field (E_1) for the (a)laser and (b)beam excited plasma.* To compare the laser-drive and beam-driven wakefields in 2-D, the driver parameters are chosen such that the on-axis longitudinal accelerating field is nearly equal. A comparison of the longitudinal fields is shown at $370 \frac{1}{\omega_{pe}}$.

cubic or quartic splines to model the particle shapes. The laser pulse is chosen to be a circularly polarized pulse with normalized vector potential $a_0 = 4.0$ with a trapezoidal pulse of Gaussian rise and fall time of $10 \frac{c}{\omega_{pe}}$ and a flat-time of $20 \frac{c}{\omega_{pe}}$. Gaussian- $a(\vec{r})$ with matched[14] FWHM focal radius of $r_0 = 10 \frac{c}{\omega_{pe}}$. The particle beam is initialized with $\gamma \sim 38,000$, $\frac{n_b}{n_0} = 5.0$ and Gaussian-shape with dimensions of $\sigma_r = 2.5 \frac{c}{\omega_{pe}}$ and $\sigma_z = 4.0 \frac{c}{\omega_{pe}}$. These laser and beam driver parameters excite comparable longitudinal fields, in Fig.4.4.

In Fig.4.2, 4.3, the longitudinal momentum phase-space of the plasma e^- is shown. The trapped e^- are seen propagating in longitudinally forward direction, Fig.4.3. The forward propagating e^- are locked to the peak of the wake-plasmon longitudinal fields, this allows the trapped e^- to continuously gain momentum. In 4.2(a) and (b) the *beam-driven* longitudinal momentum of plasma e^- are shown at $t \sim 500 \frac{1}{\omega_{pe}}$ for longitudinal momentum with longitudinal-dimension ($p_1 x_1$) and transverse-dimension ($p_1 x_2$) phase-space respectively. Corresponding snapshot of longitudinal momentum phase-space for *laser-driven* case are shown in (c) and (d) respectively. It is important to note that the forward longitudinal momentum ($p_1 > 0$) in the first bucket for the laser with $a_0 = 4.0$ is

much higher than the beam-driven case with $\frac{n_b}{n_0} = 5$ (in Fig.4.4). The increase (by $\sqrt{\gamma_e} \frac{c}{\omega_{pe}}$) of first-bucket size due to relativistic effects can be observed in Fig.4.4(a),4.5(c). It is also observed that in the beam-driven case, 4.2(a)-(b), there is no plasma e^- trapping in the first bucket behind the beam. The plasma e^- are trapped in the rising density gradient at the vacuum-plasma interface in the second and subsequent buckets. However, in 4.2(c)-(d), plasma e^- are trapped in all the buckets. In the laser-driven case, the plasma oscillations are non-linear due to relativistic effects and larger ponderomotive effect. So, trapping of plasma e^- occurs in the first bucket due to trajectory distortion (trajectories cross in the back of the bubble) as a result of non-linearity of longitudinal trajectories. However, the trapping in the second bucket is due to the rising density gradient at the vacuum-plasma interface.

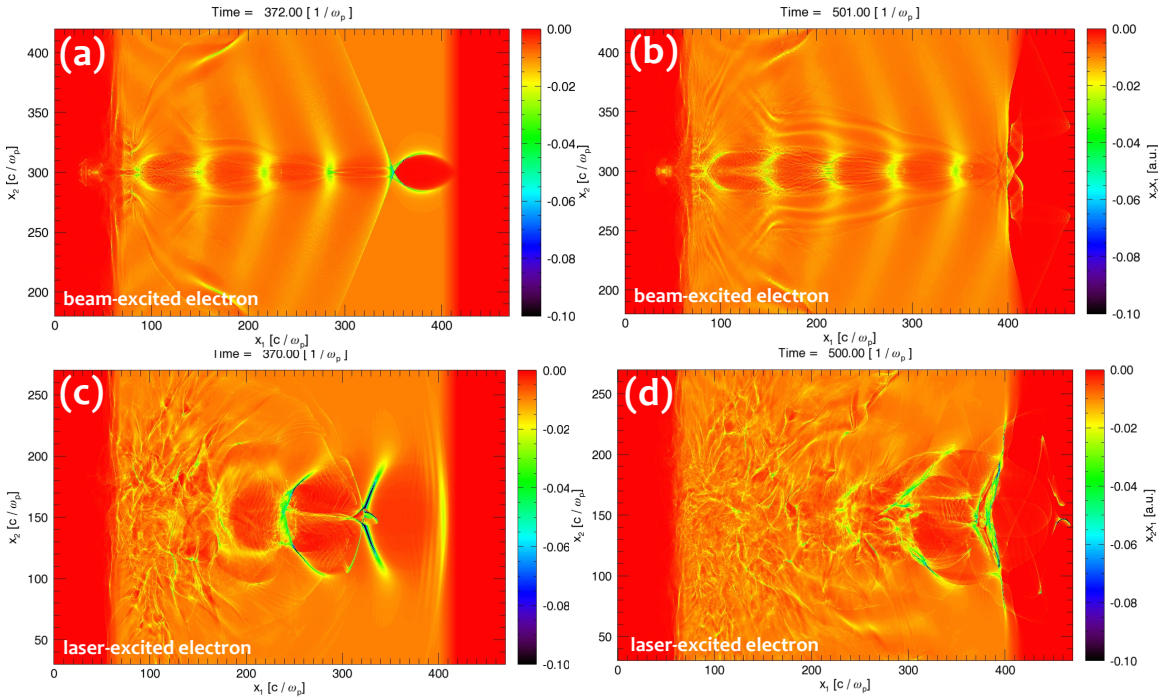


FIGURE 4.5: *Self-injected trapped plasma e^- in plasmon-buckets in real-space from 2-D PIC simulations.* The plasma e^- density is shown in real space. In (a) $t \simeq 370 \frac{1}{\omega_{pe}}$ and (b) $t \simeq 500 \frac{1}{\omega_{pe}}$ the plasma e^- are trapped only in the second and subsequent buckets in the case of beam-driven plasma. Whereas in corresponding snapshots in (c) and (d), the plasma e^- are trapped in all the buckets in laser-driven case.

In Fig.4.5 the plasma e^- density is shown in real-space. In 4.5(a)-(b), the beam-driven plasma is shown in real-space. In laser-driven case in 4.5(c)-(d), the trapped e^- due to trajectory crossing in the back of the first bucket can be observed.

4.2 2D scaling laws - trapping in cylindrical geometry oscillations

We present some preliminary scaling results of the trapping of plasma electrons undergoing radial oscillations in the wakefields driven in a rising density gradient. We show the scaling with the gradient of the rising density at the vacuum-plasma interface in Fig.4.6.

In PIC simulations presented here the particle beam is initialized with $\gamma \simeq 38,000$, $\frac{n_b}{n_0} = 5.0$ and Gaussian-shape with dimensions of $\sigma_r = 2.5 \frac{c}{\omega_{pe}}$ and $\sigma_z = 4.0 \frac{c}{\omega_{pe}}$.

We compare the phase-mixing of radial oscillations using 2-D simulations in three different density gradients with $L_\nabla = 10, 20 \& 100c/\omega_{pe}$.

It can be observed by comparing Fig.fig:2D-trapping-scaling-gradient(d) and (f) corresponding to $L_\nabla = 10c/\omega$ and $100c/\omega$ respectively that the onset of trapping is delayed in a density gradient with large scale-length. This is quite similar to the scaling in the sheet model. Similarly, comparing Fig.fig:2D-trapping-scaling-gradient(d) and (e) in $L_\nabla = 10c/\omega$ and $20c/\omega$, we observe that the bunch trapped in a sharper gradient has gained a higher energy. This occurs because electrons that are trapped earlier have undergone a larger period of acceleration.

We can explain this behavior of the radial oscillations phenomenologically, in lack of a 2-D analytical model. The structure of the radial oscillations is modified due to varying restoring force along the gradient. The envelope of the longitudinal structure formed by the radial oscillations in a density gradient induces phase-mixing.

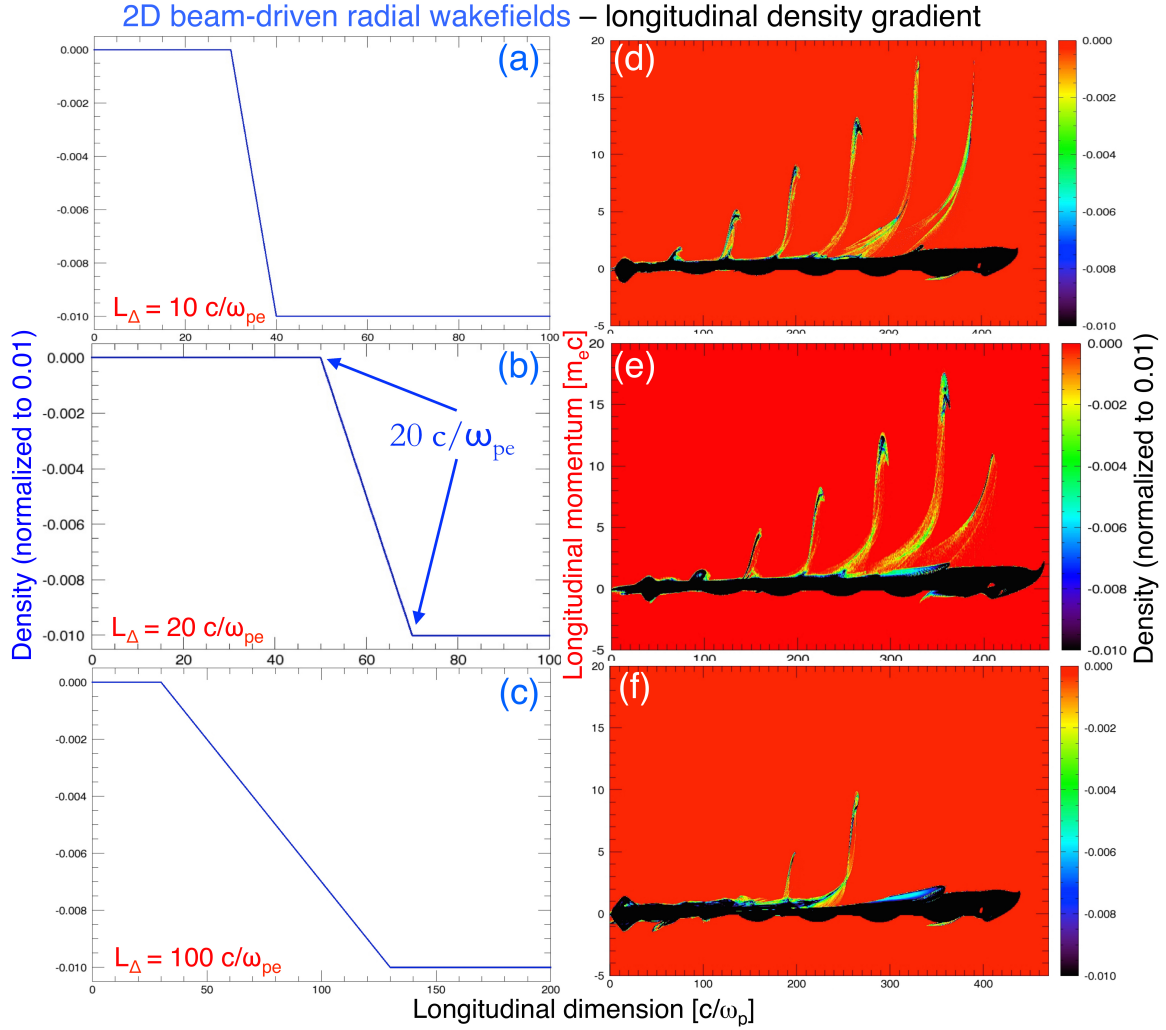


FIGURE 4.6: *Scaling of onset of trapping in radial oscillations with density gradient scale-length - modeled using 2-D PIC simulations - comparison of the longitudinal momentum phase-space.* To show preliminary scaling for the onset of trapping of plasma electrons in the 2D radial oscillations we compare three different rising density gradient scale-lengths. In (a),(b),(c) we show the scale-length for each of the case and in (d),(e),(f) we show the longitudinal momentum phase-space with respect to the longitudinal dimension.

Chapter

5

Conclusions & Future-work Directions

Using the non-linear plasma oscillations model developed by J. M. Dawson [4] for freely oscillating plasma electrons in different geometries, we have tried to model the phase-mixing between individual oscillators driven in a wakefield. More specifically, we try to understand the scaling laws of the phase-mixing time in a rising density gradient.

The onset of trapping is shown to be dependent on either a critical oscillation amplitude or just on geometry, independent of the amplitude. However, the phase-mixing time is not generally considered in the analysis of trapping, as most trapping methods use amplitude threshold crossing as the mechanism for phase-mixing. It is well known that once the space-charge potential is high enough to result in trajectory-crossing, individual oscillators invariably undergo phase-mixing.

We have analyzed driven oscillations in a rising density gradient of planar geometry using 1D PIC simulations and of cylindrical geometry using 2D PIC simulations.

We have shown that the intentional phase-mixing induced in a density gradient leads to trapping and acceleration of electrons in plasma wakefield acceleration structures. We have

developed a model for the mixing time of the oscillations in a linear rising density gradient. Using PIC simulations we have shown that the 1D scaling laws follow the model. In 2D cylindrical oscillations in a plasma wakefield driven by a beam or laser, the oscillations are primarily radial and thus 1D planar model is not adequate. Even though we have not developed a phase-mixing model for cylindrical geometry wakefields that are sustained by radial oscillations, driven in a rising density gradient, we observe that the 1D planar sheet model holds well.

In the future, we wish to develop an analytical model for the phase-mixing of cylindrical geometry electron oscillations in a longitudinal density gradient. Using this model we wish to analyze the onset of trapping in linear & non-linear beam and laser-driven wake-field plasma oscillations. We wish to explore electron and proton beam driven wakefields. We also note that transverse gradients in density can also lead to phase-mixing of radial oscillations of electrons and we wish to explore this further in the future.

There are several experimental designs such as the AWAKE experiment at CERN that excite plasma wave in linear or quasi-linear regime. The plasma oscillations in these wakefields are sub-threshold and thus trapping based self-injection is not possible purely through the amplitude-based wave-breaking. This is especially the case in beam-driven particle accelerators because high-intensity beams from conventional accelerators require significant investment. It is a challenge to inject electrons into these linear wakefields. The phase-mixing based self-injection scheme proposed here presents an alternative to engineer a plasma density gradient in these accelerators and use it for injection of electrons.

Appendix A

Chirp Pulse Amplified Ultra-short Lasers

Intense Lasers are useful tools to study non-linear optical effects and phenomenon in physics of light-matter interactions. Traditionally, laser intensities were increased by compressing the equivalent laser energy into shorter time duration pulses. Laser powers as high as Giga-Watts (GW) were achieved using pulse-compression techniques such as Q-switching and Mode-locking. These techniques could also have been used to generate *Ultra-Fast* laser pulses of Terra-Watt (TW) and Peta-Watt (PW) power with shorter than a pico-second (10^{-12}) pulse duration. However, at such high powers the laser electric fields start being equivalent to the interatomic fields and lead to non-linear ionization processes which can ionize almost any material to plasma. This encouragingly allows observation of many non-linear effects such as harmonics generation, nonlinear Raman and Brillouin scattering, 4-wave mixing, self-focusing etc.

But, the same effects are severely damaging to the amplification medium. The refractive index of the medium depends upon the laser intensity (\simeq irradiance), $n = n_0 + n_2 \times I(\frac{W}{cm^2})$, through the material-dependent non-linear coefficient, n_2 . The propagation of laser electric field in a medium thereby depends upon its own amplitude in addition to the medium property. Laser intensity depends upon space and time, hence, the effect of medium on the propagation of an intense pulse is time and space dependent. Spatial variation of a pulse results in intensity dependent focusing lens (Kerr-lens) for most common spatial (transverse) beam profiles (like Gaussian) with larger intensity at the center, resulting in

beam *self-focusing*. Time variation of the effects of the medium lead to the generation of new frequencies through *self-phase-modulation*. These effects lead to further shortening of the laser pulse (through Kerr-lens-mode-locking) in a medium when the intensities are high enough. In solid crystalline amplifying medium, n_2 is high enough to lead to catastrophic self-focussing, leading to irreversible material damage. This material damage also entirely destroys the laser properties due to its ionization of the medium into a plasma and leading to effects such as mirroring, filametation and other instabilities. Mirroring can damage the ultra-fast oscillator if light couples back into it.

To efficiently couple the energy stored in the laser active medium as population inversion to stimulated emission photons, requires that output fluence (ϕ_{out}) from the medium be of the order of the saturation fluence for the medium (ϕ_{sat}). Typical (ϕ_{sat}) for solid state gain medium ranges between $1 - 10 \frac{J}{cm^2}$, this allows only nanosecond or longer pulses to be amplified without damaging the active medium.

The demonstration of Chirped Pulse Amplification [23] in late 80s was a breakthrough, because at that point the output power was limited to Giga-Watts by non-linearities, primarily self-focussing. Only alternatively available to increase the output power, dictated expanding the focussed beam in space to allow smaller intensities, within the medium. Expansion of a beam meant large, bulky and thereby expensive active medium.

The CPA techniques use three main elements to amplify ultra-short pulses beyond what is possible without CPA. The first element expands ultra-short laser pulse generated by a femtosecond oscillator to a nanosecond pulselwidth (time-spread the energy by a factor of $10^3 - 10^5$), the second element (a gain-bandwidth limited amplifying medium) amplifies (amplification factor of 10^6) is then done at these low intensities (spatial profile is not modified) that are below the active medium damage threshold and the third element compresses the output from the active medium in air or vacuum to a subpicosecond pulselwidth, Fig.A.1. The initial time-domain expansion and post-amplification compression of the laser pulse is achieved by having *time-dependent* frequency (frequency dependent delay in the spectrum) in the laser pulse. Such a pulse is referred to as “*chirped*” pulse. The chirp

parameter ϵ_c is positive if frequency *increases* in time and negative if vice-versa. The pulse expansion element (positive group velocity dispersion (GVD) - high-frequencies take longer to propagate through the dispersive element) positively chirps the pulse resulting in time-expansion of the pulse which is now chirped. After the pulse is amplified by the gain medium, it is processed through a negative chirp element (negative GVD - low-frequencies take longer to propagate through the dispersive element) that tries to exactly invert the positive chirping and restores the pulse to its original ultra-short duration. The pulse compression elements have to be able to withstand the high intensities that are output from the gain medium. The expansion and compression elements are typically a pair of gratings or prisms.

After, the compression stage, the laser pulse is focussed using metallic optical components placed in good quality evacuation chamber (even metals start ionizing for intensities $> 10^{14} \frac{W}{cm^2}$). Evacuation chamber is used after the compression stage because even any low density gas present in the path of the laser beam ionizes and can lead to plasma effects such as filamentation of the beam.

Since, the size of the active medium can be minimized with CPA technique, it allows miniaturization of these lasers leading to Table-Top TeraWatt systems.

Ti:sapphire and Nd:glass, are the active medium for most of the CPA lasers. Ti:sapphire is ideally suited to CPA technique due its excellent mechanical and thermal stress handling properties and the largest bandwidth of the laser transition $\simeq 230\text{nm}$. Using Ti:Sapphire, expanded sub-nanosecond pulselwidth can be efficiently coupled out, because of its high ϕ_{sat} of $0.9 \frac{J}{cm^2}$. The disadvantage of Ti: sapphire is that it needs to be externally pumped using frequency-doubled Nd:YAG, Nd: YLF, and Nd: glass lasers. This is because of the relatively short lifetime of the upper laser level $\simeq 3 \text{ ms}$. High energy 4J Nd:YAG pump lasers that operate at $\lambda = 532\text{nm}$ and repetition rates of 10 Hz are commercially available. Energy from Nd-glass laser can be accumulated over many pulses and used to pump Ti:sapphire at lower repetition rates (or even single-shot). Crystal size places the ultimate limit upon the output energy from the active medium. The bandwidth of the

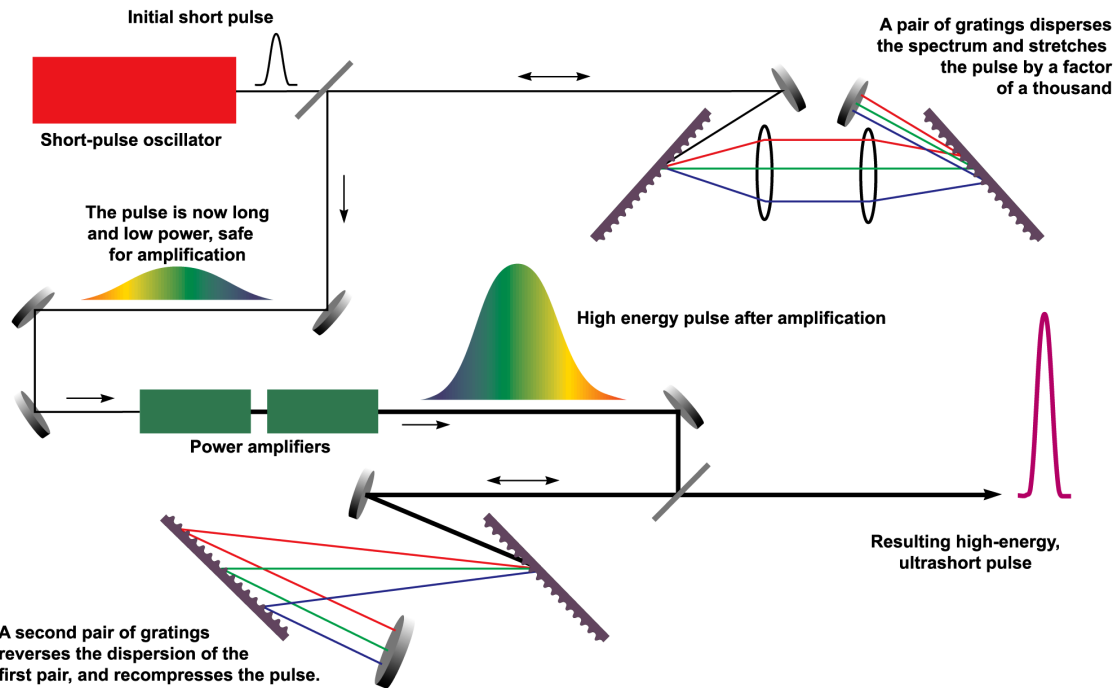


FIGURE A.1: Schematic of Chirped Pulse Amplified laser - from Chirped Pulse Amplification - Wikipedia page

medium is limited by gain narrowing (can be as low as 40-50 nm) but gain-flattening using spectrally selective elements like etalon or bi-refringent filters allow spectrum up to 80 nm and pulse-width < 20fs. Other broadband solid state active medium materials have also been explored with CPA: Cr: LISAF, Cr: forsterite, Yb:glass, Ce:LICAF etc.

Almost all high-intensity sub-nano-second short pulse lasers with output powers > 50 TW use CPA technique. Exception is the set of 500TW lasers at the National Ignition Facility (NIF) at LLNL using purified glass technology which were commissioned before the wide-spread use of CPA. However, CPA technology is still limited to about a kilo-Joule of energy whereas NIF lasers combined to deliver Mega-Watt far-infra-red power on target.

Relativistic laser intensities are high enough to impart relativistic transverse oscillating momentum to the interacting electrons. These intensities were only possible due to the invention of Chirped Pulse Amplification. The invention of the Chirped Pulse Amplification (CPA) technique has led to the development of ultra-intense ($\simeq \frac{TW}{cm^2}$) lasers with ultra-short

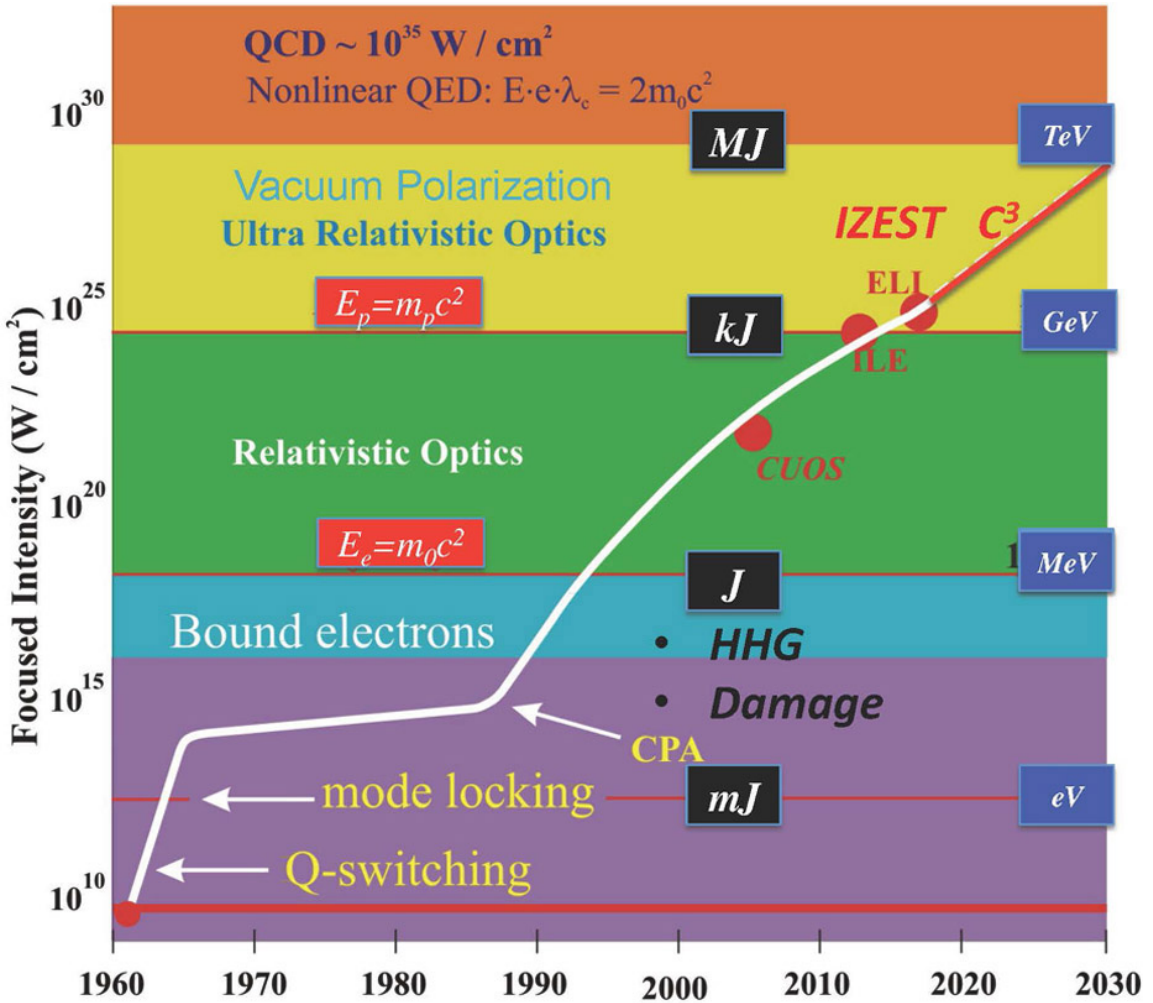


FIGURE A.2: evolution of accessible physics regimes and applications with laser intensities, right hand side axis points to the electron quiver momentum imparted to electrons interacting with the fields [23]

pulse lengths (picoseconds and lesser). Further development of CPA to higher intensities would allow access to physics regimes of higher electric fields, Fig.A.2, that were not possible before and hence high-intensity laser technologies are of immense value to understanding physics.

Bibliography

- [1] Tonks, Lewi and Langmuir, Irving, *Oscillations in Ionized Gases*, Physical Review, **33**, pp.195-210, Feb. (1929). doi:[10.1103/PhysRev.33.195](https://doi.org/10.1103/PhysRev.33.195)
- [2] Vlasov, Anatoly Alexandrovich, *The vibrational properties of an electron gas (Vibratsionnykh svoystvakh elektronnogo gaza)*, Zh. Eksp. Teor. Fitz., **8**, pp.291 (1938). Soviet Physics Uspekhi, **93**, No.3 and 4, May-June (1968). doi:[10.1070/PU1968v010n06ABEH003709](https://doi.org/10.1070/PU1968v010n06ABEH003709)
- [3] Akhiezer, Aleksander Ilyich and Polovin, R. V. *Theory of wave motion of an electron plasma*, Zh. Eksp. Teor. Fiz., 30, 915 (1956) [Sov. Phys. JETP 3, 696 (1956)].
- [4] Dawson, John Myrick, *Nonlinear Electron Oscillations in a Cold Plasma*, Phys. Rev. **113**, iss.2, pp.383-387, (1959) doi:[10.1103/PhysRev.113.383](https://doi.org/10.1103/PhysRev.113.383)
- [5] Tajima, T., Dawson, J. M., *Laser Electron Accelerator*, Phys. Rev. Lett. **43**, pp.267-270 (1979), doi:[10.1103/PhysRevLett.43.267](https://doi.org/10.1103/PhysRevLett.43.267)
- [6] Chen, P., Dawson, J. M., Huff, R. W., Katsouleas, T., *Acceleration of electrons by the interaction of a bunched electron beam with a plasma*, Phys. Rev. Lett. **54** (7), 693-696 (1985), doi:[10.1103/PhysRevLett.54.693](https://doi.org/10.1103/PhysRevLett.54.693)
- [7] Esarey, E. H., Schroeder, C. P., Leemans, W. P., *Physics of laser-driven plasma-based electron accelerators*, Reviews of Modern Physics, Vol.81, Iss.3, pp.1229-1285, Jul-Sep 2009, doi:[10.1103/RevModPhys.81.1229](https://doi.org/10.1103/RevModPhys.81.1229) doi:[10.1103/RevModPhys.81.1229](https://doi.org/10.1103/RevModPhys.81.1229)
- [8] Kruer, W. L., *The Physics of Laser Plasma Interactions*, (Frontiers in Physics), Westview Press (2003). ISBN-13:978-0813340838
- [9] Geddes, CGR; Toth, C; van Tilborg, J; et al. *High-quality electron beams from a laser wakefield accelerator using plasma-channel guiding*, Nature, **431**, (7008), pp.538-541, Sep. 30 (2004), doi:[10.1038/nature02900](https://doi.org/10.1038/nature02900).
Mangles, SPD; Murphy, CD; Najmudin, Z; et al. *Monoenergetic beams of relativistic electrons from intense laser-plasma interactions*, Nature, **431**, (7008), pp.535-538, Sep. 30 (2004). doi:[10.1038/nature02939](https://doi.org/10.1038/nature02939)

- Faure, J; Glinec, Y; Pukhov, A; et al. *A laser-plasma accelerator producing monoenergetic electron beams*, Nature, **431** (7008), pp.541-544, Sep. 30 (2004). doi: 10.1038/nature02963
- [10] Blumenfeld, Ian; Clayton, Christopher E.; Decker, Franz-Josef; et al. *Energy doubling of 42 GeV electrons in a metre-scale plasma wakefield accelerator*, Nature, **445**, (7129), pp.741-744, Feb. 15 (2007). doi:10.1038/nature05538
- [11] Litos, M., et. al., *High-efficiency acceleration of an electron beam in a plasma wakefield accelerator*, Nature, **92**, 515, (2014). doi:10.1038/nature13882
- [12] Katsouleas, T. and Mori, W. B., *Wave-Breaking Amplitude of Relativistic Oscillations in a Thermal Plasma*, Phys. Rev. Lett. 61, 90, (1988). doi:10.1103/PhysRevLett.61.90
- [13] Hora, H., *Nonlinear Confining and Deconfining Forces Associated with the Interaction of Laser Radiation with Plasma*, Physics of Fluids **12**, 182 (1969), doi:10.1063/1.1692262
 Lindl, J. D. and Kaw, P. K., *Ponderomotive force on laser-produced plasmas*, Phys. Fluids 14, 371 (1971), doi:10.1063/1.1693437.
 Silva, L. O., Bingham, R., Dawson, J. M., Mori, W. B., *Ponderomotive force of quasi-particles in a plasma*, Phys. Rev. E **59**, 2273 (1999), doi:10.1103/PhysRevE.59.2273
- [14] Lu, W., *Nonlinear Plasma Wakefield Theory and Optimum Scaling for Laser Wakefield Acceleration in the Blowout Regime*, Ph.D. thesis, submitted to the Physics department at the University of California, Los Angeles, CA.
- [15] Hemker, R., *Particle-In-Cell Modeling of Plasma-Based Accelerators in Two and Three Dimensions*, Ph.D. thesis, submitted to the Physics department, University of California at Los Angeles, CA.
- [16] Sahai, A. A., Katsouleas, T. C., et. al., *Long-term evolution of plasma wake fields*, Proc of NA-PAC 2013, **MOPAC10**, pp. 90-92, Oct. 2013, ISBN: 978-3-95450-138-0, <http://accelconf.web.cern.ch/accelconf/pac2013/papers/mopac10.pdf>
- [17] Sahai, A. A., *FDTD simulations of Radio-wave propagation in wireless channels with guiding effects*, Master of Science report, Submitted to the Department of Electrical Engineering, Stanford University, CA.
- [18] Suk, H., Esarey, E. et. al., *Plasma electron trapping and acceleration in a plasma wake field using a density transition*, Phys.Rev.Lett. **86** (2001) 1011-1014, doi:10.1103/PhysRevLett.86.1011
- [19] Brantov, A.V, Esirkepov, T. Zh., Kando, M., Kotaki, H., Bychenkov, V. Yu., Bulanov, S.V., *Controlled electron injection into the wake wave using plasma density inhomogeneity*, Physics of Plasmas, **15**, 073111 (2008), doi:10.1063/1.2956989

- [20] Gonsalves, A. J., Nakamura, K., et. al., *Tunable laser plasma accelerator based on longitudinal density tailoring*, Nature Physics 7, 862?866 (2011) doi:10.1038/nphys2071
- [21] Fonseca, R. A., et al., *OSIRIS, a three-dimensional fully relativistic particle in cell code for modeling plasma based accelerators*, Lect. Note Comput. Sci. **2331**, 342-351 (2002). doi:10.1007/3-540-47789-6_36
- [22] Birdsall, C. K. and Langdon, A. B., *Plasma Physics via Computer Simulation*, Plasma Physics Series, Philadelphia, PA: Institute of Physics Publishing, 1991. The Adam Hilger Series on Plasma Physics, 1991
- [23] Strickland, D. and Mourou, G., *Compression of amplified chirped optical pulses*, Optics Communications, Volume 56, Issue 3, pp.219-221, 1985 doi:10.1016/0030-4018(85)90120-8
Mourou, Gerard A., Tajima, Toshiki and Bulanov, Sergei V., *Optics in the relativistic regime*, Rev. Mod. Phys. **78**, p.309, (2006) doi:10.1103/RevModPhys.78.309
Mourou, Gerard A., Tajima, Toshiki *Exploring fundamental physics at the highest-intensity-laser frontier*,

Biography

2003	BACHELOR OF TECHNOLOGY, Electrical Engineering, Pondicherry Engineering College, Pondicherry University, India
2005	MASTER OF SCIENCE, Electrical Engineering, Stanford University, Stanford, CA, USA
2005-10	RESEARCH & DEVELOPMENT ENGINEER, Radio-frequency high-power & board-level systems, Laser & optics, Digital communication physical layer, USA [Qualcomm Inc., San Diego, CA; Silicon Valley / Stanford startups]
2015	MASTER OF SCIENCE, Accelerator Physics, Indiana University, IN & United States Particle Accelerator School, USA
2015	DOCTOR OF PHILOSOPHY, Electric Engineering, Duke University, NC, USA